

**NASA
Reference
Publication
1360
1995**

**Spectral Analyses, Climatology,
and Interannual Variability of
Nimbus-7 TOMS Version 6
Total Column Ozone**

J. L. Stanford

*Department of Physics and Astronomy
Iowa State University
Ames, Iowa*

J. R. Ziemke

*National Research Council
Goddard Space Flight Center
Greenbelt, Maryland*

R. D. McPeters

A. J. Krueger

P. K. Bhartia

*Goddard Space Flight Center
Greenbelt, Maryland*



National Aeronautics and
Space Administration

Scientific and Technical
Information Branch

This publication is available from the NASA Center for AeroSpace Information,
800 Elkridge Landing Road, Linthicum Heights, MD 21090-2934, (301) 621-0390.

ABSTRACT

This reference publication presents selected results from space-time spectral analyses of 13 years of version 6 daily global ozone fields from the Total Ozone Mapping Spectrometer (TOMS). One purpose is to illustrate more quantitatively the well-known richness of structure and variation in total ozone. A second purpose is to provide, for use by modelers and for comparison with other analysts' work, quantitative measures of zonal waves 1, 2, 3, and medium-scale waves 4-7 in total ozone. Their variations throughout the year and at a variety of latitudes are presented, from equatorial to polar regions. The 13-year averages are given, along with selected individual years which illustrate year-to-year variability.

The largest long wave amplitudes occur in the polar winters and early springs of each hemisphere, and are related to strong wave amplification during major warming events. In low latitudes total ozone wave amplitudes are an order of magnitude smaller than at high latitudes. However, TOMS fields contain a number of equatorial dynamical features, including Rossby-gravity and Kelvin waves.

TABLE OF CONTENTS

Section	Page
1. INTRODUCTION	1
2. NIMBUS-7 TOMS VERSION 6 DATA	1
2.1 Gridding Process and Missing Data	1
2.2 Potential Data Problems	2
2.2.1 <i>Clouds</i>	2
2.2.2 <i>Gridding Artifact Revealed by Spectral Analysis</i>	2
3. THIRTEEN-YEAR CLIMATOLOGY	3
4. MONTHLY MEAN FIELDS AND INTERANNUAL VARIABILITY	4
5. VARIABILITY ON SHORTER TIME SCALES	4
6. ON THE DYNAMICAL FORCING OF TOTAL OZONE WAVES	7
8. REFERENCES	79

1. INTRODUCTION

Both the general Fast Fourier Transform (FFT) computing technique and the extensive Nimbus-7 TOMS (Total Ozone Mapping Spectrometer) instrument data are widely accessible, the latter on Compact Disk-Read Only Memory (CD-ROM). In the present reference publication, we illustrate the rich structure in TOMS data through the application of FFT space-time spectral analysis. To reduce space, we have given only selected detailed results aimed at illustrating major phenomena.

The results in this publication are intended to provide modelers with quantitative measures of the zonal means and asymmetries in total ozone for long waves 1, 2, and 3, and for medium-scale waves 4–7. Thirteen-year averages (climatologies) for 1979–1991 are given, along with monthly mean component fields to illustrate interannual variability. In addition, global space-time spectra covering latitudes 60° S to 60° N are provided for locating and identifying fastest waves. We also include an example of the use of this same space-time spectral method to find and describe a data processing artifact.

Acknowledgments. We thank Ms. Patricia T. Guimaraes and the members of the NASA TOMS NIMBUS Experiment and Information Processing Teams, and the National Space Science Data Center for providing the TOMS data on CD-ROM disc. We also thank the British Meteorological Office for supplying the geopotential height data used in the report. This work was supported by National Aeronautics and Space Administration Grant NAG 5–1519.

2. NIMBUS-7 TOMS VERSION 6 DATA

The TOMS satellite provided daily global measurements of total column ozone from 31 October 1978 until 6 May 1993. Version 6 data (see *NASA Reference Publication RP-1323*, November, 1993) has been processed to include several improvements, among these being a long-term calibration correction for instrument degradation (beginning in April 1984) and a redefinition of B-pair wavelengths used in the retrieval scheme. The data used in this technical note come from daily asynoptic fields on CD-ROM derived by the Goddard Ozone Processing Team (OPT) at NASA's Goddard Space Flight Center (GSFC) in Greenbelt, Maryland. Coverage on CD-ROM extends from 1 November 1978 through 31 January 1992 (total of 4840 days) and is conveniently gridded into 1° latitude by 1.25° longitude bins.

2.1. Gridding Process and Missing Data

Because the relatively long horizontal scales investigated in this report did not require the full TOMS data set, the CD-ROM data were compacted by regridding onto a 5° × 5° latitude-longitude field, extending from latitudes 85° S to 85° N. Zonally averaged monthly mean percentages of missing 5° × 5° data were found to be less than about 2–3% at all latitudes (excluding polar night) and all months from June 1980 to January 1992. The worst month is June 1979 for which ~30%–40% of data is missing at latitudes not in polar night. (No TOMS measurements were available for 14–19 June 1979 because of a

relay malfunction.) Similarly, July 1979 through May 1980 have roughly 5%–10% missing data. All missing data in this report were replaced using linear interpolation in time.

2.2. Potential Data Problems

2.2.1. Clouds

A primary improvement in version 6 TOMS over previous versions was correction of the instrument degradation problem (*Herman et al.*, 1991), but there still exist other problems that could be improved in future versions. One problem relates to an assumed climatological cloud top height (a function only of latitude) in the retrieval process. It was shown by *Thompson et al.* (1993) that low marine stratus clouds, occurring lower in altitude than the climatological cloud heights used in the algorithms, induce a small positive bias in TOMS version 6 values; largest daily and monthly mean biases west of Africa around 5–25° S during August–October months were found in that study to be $\sim +20$ and $+5$ Dobson Units (DU), respectively. This result underscores the care needed if using TOMS version 6 data in such regions to estimate tropospheric ozone. Other oceanic regions in which low marine stratus clouds are a common occurrence is west of South America and west of North America.

Another potential problem with version 6 TOMS relates to Polar Stratospheric Clouds (PSCs) and episodic (life spans ~ 2 –5 days) “miniholes” that appear in the high latitudes of both hemispheres around winter months. As discussed by *Rood et al.* (1992), wintertime miniholes can be generated dynamically by the uplifting of ozone-poor tropospheric air during the passage of an anticyclone. This uplifting of air contributes to colder than normal lower stratospheric temperatures, and can result in formation of PSCs. In these much more rare cases involving PSCs, it is not uncommon for TOMS measurements inside miniholes to be significantly smaller than ground based measurements. One event in February 1990 indicated TOMS measurements inside a Northern Hemisphere minihole to be around 100 DU less than estimated ground-based measurements. (*Hofmann and Deshler*, 1990; *Fiedler et al.*, 1993).

2.2.2. Gridding Artifact Revealed by Spectral Analysis

As one illustration of the usefulness and sensitivity of space-time analysis of TOMS, we briefly describe a data processing artifact found in the analyses. Figure 1a shows eastward/westward spectral amplitudes for zonal wave 14 covering years 1979–1991. Seen in this figure is a peculiar spectral feature with period near 6 days. While there is a known westward propagating wave 1 atmospheric global normal mode with period around 5 days, the feature seen here is not related to it. Reasons for this assertion are first, that the spectral peak in Figure 1a is exceptionally sharp, having a period that is always very close to 5.7 days, throughout the entire 13-year TOMS; this is too sharp for a wave mode in the real atmosphere. Second, the main contribution was found to occur at wave 14, suspiciously close to the number of orbits per day, with respect to the Earth grid, made by the Sun-synchronous Nimbus-7 satellite. This feature is an artifact caused by cross-track bias. The effect is strongest in low latitudes where orbital scans do not overlap.

Moreover, largest amplitudes in Figure 1 are directly related to aerosol loading of the stratosphere, being strongest after two major volcanic eruptions that occurred during the TOMS record, the Mexican El Chichon in early 1982 and Mt. Pinatubo in the Philippines in mid-1991. These artifacts are strongest at 20° N after El Chichon and at 10° S after Pinatubo (Figures 1a and 1b, respectively). In years of more normal aerosol loading in the stratosphere, errors are seen to be much reduced in magnitude. In conclusion, original gridding used in version 6 CD-ROM TOMS results in ~1–5 DU errors in low latitudes. Space-time spectral analysis thus provides a sensitive tool for detection of data processing artifacts.

3. THIRTEEN-YEAR CLIMATOLOGY

Thirteen-year climatologies of TOMS ozone are shown in Figure 2. Because of polar night, latitudes poleward of 65° are not included. (TOMS data requires backscattered sunlight for its measurements.) The time mean and RMS amplitudes in the left half of Figure 2 can be compared with the earlier version TOMS 4-year (October 1978–September 1982) calculations of *Bowman and Krueger* (1985). The most significant differences between the results in Figure 2 and those of *Bowman and Krueger* are the slightly larger amplitudes in version 6 TOMS for the time mean field. Time mean values in Figure 2 are ~5–20 DU larger (largest biases in high latitudes) than values shown in Figure 3 of *Bowman and Krueger*.

The two right-half frames in Figure 2 show RMS amplitudes for planetary scale waves 1–3 and medium-scale waves 4–7. Prior to computing RMS amplitudes in time for these latter two cases, an inverse FFT was used to select only waves 1–3 or waves 4–7, respectively. Waves 1–3 are seen to be strongest in high latitudes, primarily because of planetary scale fluctuations of total ozone during stratospheric sudden warmings in Northern Hemisphere winter and the winter vortex breakup in spring in both hemispheres. Medium-scale waves 4–7 are strongest in total ozone in middle latitudes because of forcing from strong midlatitude medium-scale baroclinic instabilities. This can be seen from the continuity equation for ozone volume mixing ratio X :

$$X_t = -uX_x - vX_y - wX_z + S. \quad (1)$$

Here subscripts denote partial differentiation, S represents ozone sources or sinks, and u, v and w are the eastward, northward and vertical velocity components, respectively. All other symbols are standard. Atmospheric wind velocity (u, v, w) therefore induces waves in the ozone mixing ratio field X subject to the gradients of X . Wave perturbations (denoted by prime symbol) in total column ozone measured by TOMS are given by

$$\Omega' = 0.772 \times 10^5 \cdot \int_0^\infty dz \cdot \rho \cdot X' \approx 10^5 \cdot \int_0^\infty dz \cdot e^{-z/H} \cdot X', \quad (2)$$

where units are DU, z is altitude (units meters), X' represents perturbations in mixing ratio, H is scale height (7 km here), and ρ (units $\text{kg}\cdot\text{m}^{-3}$) is the total atmospheric mass density approximated by $1.3 \cdot e^{-z/H}$. Strong baroclinic waves in the upper troposphere and lower stratosphere can thus induce sizeable waves in total ozone.

Tabulated values of the fields in Figure 2 are provided in Table 1 on the following page. Included in this table (and several following tables) are values at the equator. TOMS values corresponding to latitudes in polar night are flagged with the value 999 in all tables provided in this technical report.

Figure 3 shows climatological monthly mean TOMS ozone, averaged using November 1978 through January 1992 fields. Tabulated data (Table 2) are included in the immediate following pages.

4. MONTHLY MEAN FIELDS AND INTERANNUAL VARIABILITY

Shown in Figure 4 are monthly mean polar stereographic TOMS ozone fields for years 1978-1992 in both hemispheres for seasonal months January, April, July, and October. Also shown for completeness are climatology fields (denoted "CL") for each month, computed by averaging TOMS over the years shown on each page.

Monthly mean TOMS ozone data for zonal waves 0-7 are also given in this report, shown in Table 3 in the following pages. With time coverage November 1978 through January 1992, these tables provide a detailed account of interannual and interseasonal variability in monthly mean wave components. Amplitudes (units DU) are given in these tables for zonal wavenumbers 0, 1, 2, 3, and combined medium-scale waves 4-7. Zonal phases (units degrees) are included for waves 1, 2, and 3. The expression needed to reconstruct a specific wave component (fixed zonal wavenumber k) monthly series from these tables is given by

$$\Omega(x = 0, 1, \dots, 71; t = 1, 2, \dots, 159) = AMP(k, t) \cdot \cos\left[\frac{2\pi k x}{72} - \Phi(k, t)\right] \quad (3)$$

where t is now a month index, beginning with November 1978, and $AMP(k, t)$ and $\Phi(k, t)$ are the tabulated amplitudes and phases. Longitude (in units degrees) is given by $-180 + 5x$.

5. VARIABILITY ON SHORTER TIME SCALES

To illustrate temporal variability at time scales shorter than, say a month, no temporal filtering was applied to the data used in any of the figures shown in this section. The only filtering employed was along longitude (using an FFT) to select fields for zonal wave 0 (zonal mean), 1, 2, 3, and 4-7.

Figure 5 shows selected (1979, 1980, 1991, and climatology) latitude vs. time plots of TOMS total ozone for waves 0, 1, 2, 3, and 4-7. Values shown for waves 1, 2, and 3 are RMS amplitudes. Values involving waves 4-7 are also RMS amplitudes, but were computed from $[\sum_{k=4}^7 AMP^2(k, t)]^{1/2}$. All of the 13-year climatological fields shown in Figure 5 were calculated by averaging equivalent days of similar months. (Example: the 1 January values were calculated by averaging 1 January 1979, 1 January 1980, ..., 1 January 1991.)

Pre-ozone hole years 1979 and 1980 are given, together with 1991, a deep ozone hole year. The 13-year mean is also given. In considering the 13-year mean, both here and in

the figures to follow, it is worth remembering that the ozone hole was especially deepening from the mid-1980s onwards. Thus, in Antarctic latitudes the 13-year means will show more ozone than the latter years and less than the first few years of the 13-year record.

Figure 5 reveals more variability, and more ozone, in the Northern Hemisphere (NH) winters than in Southern Hemisphere (SH) winters. The ozone hole is perspicuous during October in high Southern latitudes. A quasi-biennial oscillation in ozone hole strength (*Lait et al.*, 1989) is apparent in the yearly analyses (not all shown here). In addition, even at non-Antarctic latitudes, there is significant year-to-year variability. Nevertheless, the 13-year means are useful to give some indication of recurring features. A prominent example of this is the major buildup of total ozone in high latitudes in late winter/early spring that is caused by residual mass transport from summer to winter hemispheres. Related to this mean residual circulation are large wave activities discussed next. .

Figure 5 (c)–(j) demonstrates wave activity in total ozone as a function of latitude and time. Planetary wave activity during stratospheric warmings and spring final breakdowns of the polar night vortex are especially prominent during winter/early spring, in both the NH and SH. Strong amplitude vacillations are revealed in waves 1 and 2 in total ozone, primarily during late winter and early spring when the winter polar vortex (both NH and SH) is disturbed by large wave amplification events during sudden stratospheric warmings and final spring warmings, respectively.

Amplitudes of wave 3 and medium-scale waves 4–7 are seen to have relatively sizeable amplitudes on the majority of days in winter/spring in both hemispheres. The medium-scale ozone perturbations (waves 4–7) are primarily induced by strong baroclinic disturbances in the upper troposphere; the latter are dynamically forced by large-scale temperature gradients rather continuously throughout the winter and spring. This can be compared with the strong amplitude long waves in ozone that are manifestations in total ozone of midwinter and final spring warming events. The wave amplitudes can be read from the plots with values for individual years typically exceeding 100, 60, 50, and 25 DU for waves 1, 2, 3, and 4–7, respectively. During October and early November 1991, especially large amplitudes are seen in the pronounced contortions of the spring breakup of the Antarctic polar vortex. That year's Southern ozone hole was the deepest observed in zonal means, and its morphology was exceptionally elongated (nonzonal) at times (*Krueger et al.*, 1992).

In the 13-year mean, waves 1 and 2 are seen to be more pronounced in the Antarctic spring (starting in the last half of September) and in the NH high latitudes in the last part of January through most of March; medium-scale waves 4–7 are more uniformly distributed throughout both winter and spring in both hemispheres.

Figure 6 shows time vs. longitude plots of TOMS ozone at selected latitudes for years 1979, 1985, and 1991. In high Southern latitudes, pronounced amplitudes and eastward phase propagation of wave 2 is evident around the time of the ozone hole and breakup of the stratospheric polar vortex. The perturbations in total ozone at middle and high latitudes can be understood on the basis of the approximate conservation of potential vorticity (*Vaughan and Price*, 1991). Stationary wave behavior is a characteristic in the tropics and subtropics for longest waves 1–2. *Shiotani* (1992) suggested that the dominant stationary wave 1 in total ozone along the equator could be due to smaller total column

ozone associated with a higher tropopause from strong tropical convection in the western Pacific. Note that lowest total ozone along the equator for wave 1 occurs near the dateline for each of the three years shown here in Figure 6. A portion of this stationary wave 1 in TOMS has been shown to be a retrieval artifact, related to the presence of persistent low marine stratus clouds (see section 2.2.1). In addition, there is evidence that there may also be a contribution from tropospheric ozone originating from biomass burning. For example, *Shiotani and Hasebe* (1994) analyzed Stratospheric Aerosol and Gas Experiment (SAGE) data by integrating ozone mixing ratio from 16 to 60 km, forming a “stratospheric only” ozone column. Their results with SAGE data indicated an absence along the equator of a dominant wave 1 in stratospheric only column ozone (zonal wave 2 was instead dominant). This suggests that the observed wave 1 in TOMS may have contributions from tropospheric ozone.

The equatorial wave 4–7 analyses at times indicate possible coherent pulses of medium-scale wave activity: see, for example, August–October 1985 in Figure 6 (1985, EQU). Careful examination of tropical TOMS data has resulted in the identification of both Rossby-gravity waves (*Stanford and Ziemke*, 1993) and Kelvin waves (*Ziemke and Stanford*, 1994a) in total ozone. (Kelvin waves in ozone mixing ratio were previously shown by *Hirota et al.*, 1991, and *Randel*, 1991.) In addition, *Ziemke and Stanford* (1994b) show and describe the synchronization between these fast tropical waves in total ozone and the quasi-biennial oscillation of the equatorial zonal wind.

Figure 7 shows space-time spectra for January 1979 through December 1991 at latitudes 60° S to 60° N (15° increment). Each 1979–1991 frame shows spectra at a fixed latitude for a distinct zonal wavenumber, or combination of wavenumbers in cases involving waves 4–7. These plots are best described as monthly series of TOMS westward/eastward spectral amplitudes at fixed latitude and zonal wavenumber(s). These monthly spectra were computed using a 90-day window stepped forward in time with a 1-month increment. During each 90-day calculation, time series averages were removed and a 10%–10% cosine taper window was applied to reduce leakage. (Ten percent, or 9 days, of each end of every 90-day series was tapered smoothly to zero with a half-cosine bell.) These spectra calculations used an exact method to separate space-time series into eastward and westward components (see, for example, the Appendix of *Ziemke and Stanford*, 1990). Harmonic coefficients $A(k, p)$ and $B(k, p)$ for the 90-day running window were calculated by applying an FFT in both time and space under the following zonal space-time harmonic expansion for total column ozone Ω :

$$\Omega_{\pm}(x = 0, 1, \dots, 71; t = 0, 1, \dots, 89) = \sum_{k=0}^{36} \sum_{p=0}^{45} \left[A_{\pm}(k, p) \cdot \cos(\kappa x \pm \omega t) + B_{\pm}(k, p) \cdot \sin(\kappa x \pm \omega t) \right]. \quad (4)$$

Here, t (x) is the day (longitude) index, $\kappa = 2\pi kx/72$, $\omega = 2\pi pt/90$, and $+$ ($-$) denotes the westward (eastward) propagating component of Ω . Longitude (in units degrees) is given by $-180 + 5x$.

Spectral amplitude in Figure 7, whether computed for a single zonal wavenumber ($k_1 = k_2$) or for combined wavenumbers ($k_2 > k_1$), was derived from $\langle \sum_{k=k_1}^{k=k_2} [A^2(k, p) +$

$B^2(k, p)]^{1/2} >$, where the angle brackets denote one application of a 0.25–0.5–0.25 smoothing along frequency index p .

The spectra in Figure 7 are potentially useful for identifying fast wave events in total ozone for selected zonal wavenumber(s). Examples include high-latitude planetary waves 1–3 during winter and spring, and baroclinic disturbances (seen in waves 4–7) in midlatitudes. By using Figure 7, important characteristics of such disturbances can be identified, including time of the occurrence, approximate latitude domain, oscillation period, effective amplitude (over the 90-day window used), and direction of zonal propagation. Interhemispheric comparison of high-latitude waves can also be deduced. For example, large amplitude waves occur during polar vortex breakup in late winter in both polar regions. In the North, the activity is primarily in winter (November through March), which often includes major midwinter stratospheric warming events. Activity is relatively weak in other seasons at 60° N. At 60° S, in addition to the obvious strong wave developments during vortex breakdown in the Antarctic spring, note the considerable activity of waves 1 and 2 during the Antarctic autumn, April–May and at times lasting into early winter, June. This bimodal distribution of autumn and spring longwave activity in total ozone may be related to the double maximum in wave 1 amplitude found in geopotential analyses by Randel (1988).

6. ON THE DYNAMICAL FORCING OF TOTAL OZONE WAVES

Insight into the dynamical forcing of TOMS zonal waves 1–7 examined in this reference publication is provided in Figure 8, which shows seasonal correlations between TOMS ozone and British Meteorological Office (BMO) geopotential heights for planetary scale waves 1–3 and medium-scale waves 4–7. These calculations used 12 years (1 January 1980 through 31 December 1991) of daily BMO geopotential heights. These datasets (with the same horizontal gridding as 5° × 5° TOMS) extend from the low troposphere up to the stratopause on the following eleven pressure surfaces: 850, 500, 300, 200, 100, 50, 20, 10, 5, 2, and 1 hPa. Up to 100 hPa the BMO data are NMC analyses; Stratospheric Sounding Unit (SSU) radiance temperatures are used to obtain stratospheric geopotential heights. It should be noted that this same correlation procedure was applied using the full NMC data extending from 1 to 850 hPa for 1980–1991. No observable differences were found between results in Figure 8 and correlation fields derived from the full NMC data.

The seasonal correlation plots in Figure 8 were computed from daily measurements of 3D (latitude, longitude, pressure) BMO and 2D (latitude, longitude) TOMS data by first computing their cross-field correlations for each month of each particular year. In this first step (following zonal wavenumber truncation in these data for either waves 1–3 or 4–7 via a Fast Fourier Transform), at each fixed latitude and longitude, the monthly series of TOMS was cross-correlated with that of geopotential heights at each of the eleven vertical pressure levels (850 to 1 hPa); this resulted in 144 monthly (January 1980–December 1991) 3D (latitude, longitude, pressure) correlation fields. The next step was to average these 3D correlation fields over equivalent months. (For example, the January correlation field was derived by averaging fields for January 1980, January 1981, ..., January 1991.) The final step was to average these 3D correlation fields zonally, resulting in the 2D (latitude, pressure) fields shown in Figure 8. Monte Carlo statistical significance tests for various

significance levels are noted in the figure caption. Because of the large amount of BMO and TOMS data involved, the Monte Carlo method used a simplified approach incorporating a red-noise model each month for both random time series $x(t)$ used in the cross-correlation calculations: $x(t) = a \cdot x(t-1) + Z(t)$, where $Z(t)$ is a randomly generated standard normal series and the constant parameter a was set equal to 0.99 as a reasonable upper bound for the redness of monthly sequences of both TOMS ozone and BMO heights. Correlations were calculated monthly and then averaged over 12 similar months, just as was done with the TOMS and BMO data. (This process was repeated 100,000 times to establish the significance level values stated in the Figure 8 caption.)

Results in Figure 8 show that both planetary and medium-scale waves in TOMS ozone are highly anticorrelated with lower atmospheric geopotential heights around 200–300 hPa at latitudes 35° – 60° in both hemispheres. The strong anticorrelations are indicative of the “tropopause effect” in total ozone whereby a higher than average tropopause altitude, in principal, yields a smaller than average amount of vertically integrated total column ozone above. This effect can also be understood on the basis of potential vorticity conservation.

Figure 8 also shows that these strong negative correlations tend to follow seasonal migration of the tropospheric eastward wind jet that maximizes (in both hemispheres) near 200 hPa around latitudes 30° in winter and 45° in summer. This latter observation suggests that horizontal advection of ozone associated with the tropospheric jet is a primary source for observed midlatitude zonal waves 1–7 in TOMS ozone in all seasons. This appears most evident for medium-scale waves 4–7.

In addition, planetary waves 1–3 in TOMS ozone show strong positive correlations with midstratospheric geopotential heights at high latitudes in Figure 8. This effect dominates during Southern springtime (October shown) when large stratospheric waves 1–3 in temperature occur in association with the zonal variations and ultimate breakup of the polar stratospheric wind jet. Large midstratospheric geopotential height perturbations are indicative of perturbed lower stratospheric thicknesses (i.e., temperatures).

In summary, medium-scale waves 4–7 in TOMS, particularly in midlatitudes, appear to be forced by a combination of tropopause effects related to height changes and horizontal advection associated with the eastward tropospheric wind jet. As noted earlier, medium-scale waves are primarily caused by baroclinic instability processes. Planetary waves 1–3 appear similarly affected by the tropospheric jet, but less so. Largest correspondence between TOMS ozone and lower stratospheric thicknesses at planetary scales occur in the high latitudes during Southern springtime in association with the breakdown of the Southern polar vortex.

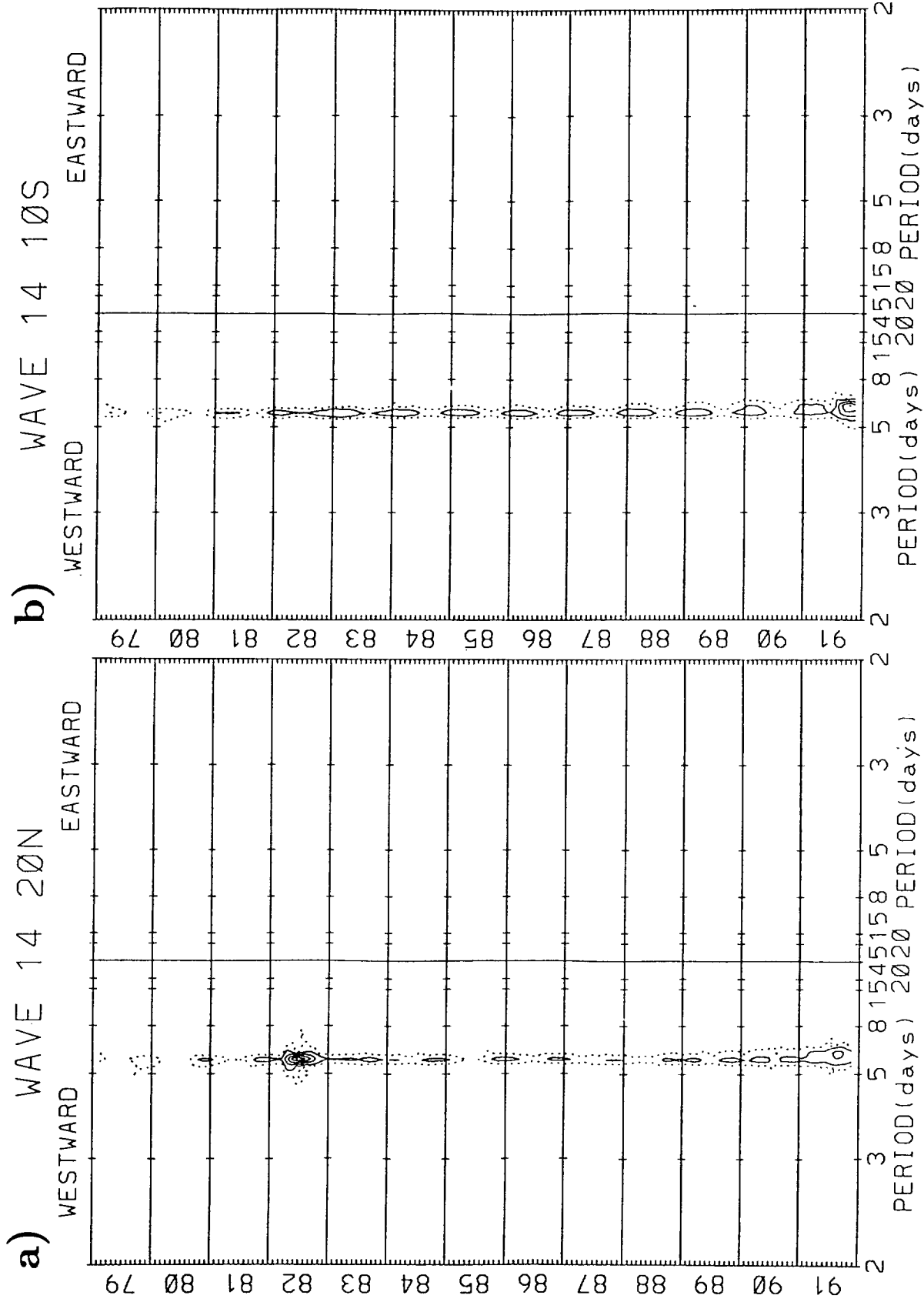


Figure 1. Time vs. frequency (periods in days shown) TOMS eastward/westward spectral amplitudes for zonal wave 14 computed using a 90-day window with a one month step. Days: 1 January 1979-31 December 1991. Units: DU. Dashed (solid) contours 0.5 (1, 2, 3,...). (a) Latitude 20°N. (b) 10°S.

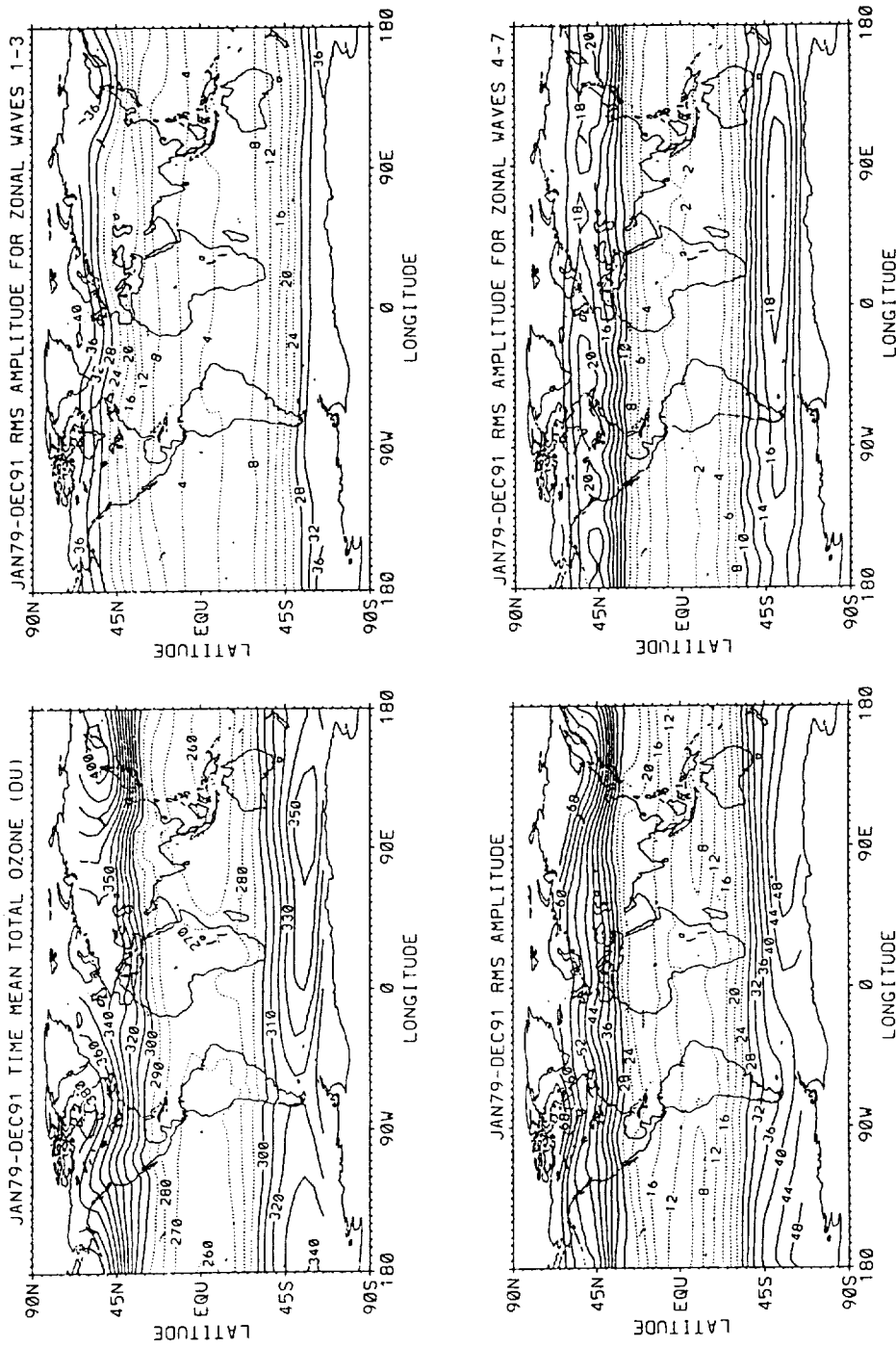


Figure 2. TOMS total ozone time mean and RMS amplitudes computed using daily data from 1 January 1979 through 31 December 1991. All units: DU. Upper Left: Time mean. Dashed (solid) contours begin at 290 (300) and decrement (increment) by 10. Lower left: RMS amplitudes for all zonal wavenumbers. Dashed (solid) contours begin at 24 (28) and decrement (increment) by 4. Upper right: RMS amplitudes for zonal waves 1-3. Dashed (solid) contours begin at 24 (28) and decrement (increment) by 4. Lower right: RMS amplitudes for zonal waves 4-7. Dashed (solid) contours begin at 8 (10) and decrement (increment) by 2. Tabulated values are provided on the following page.

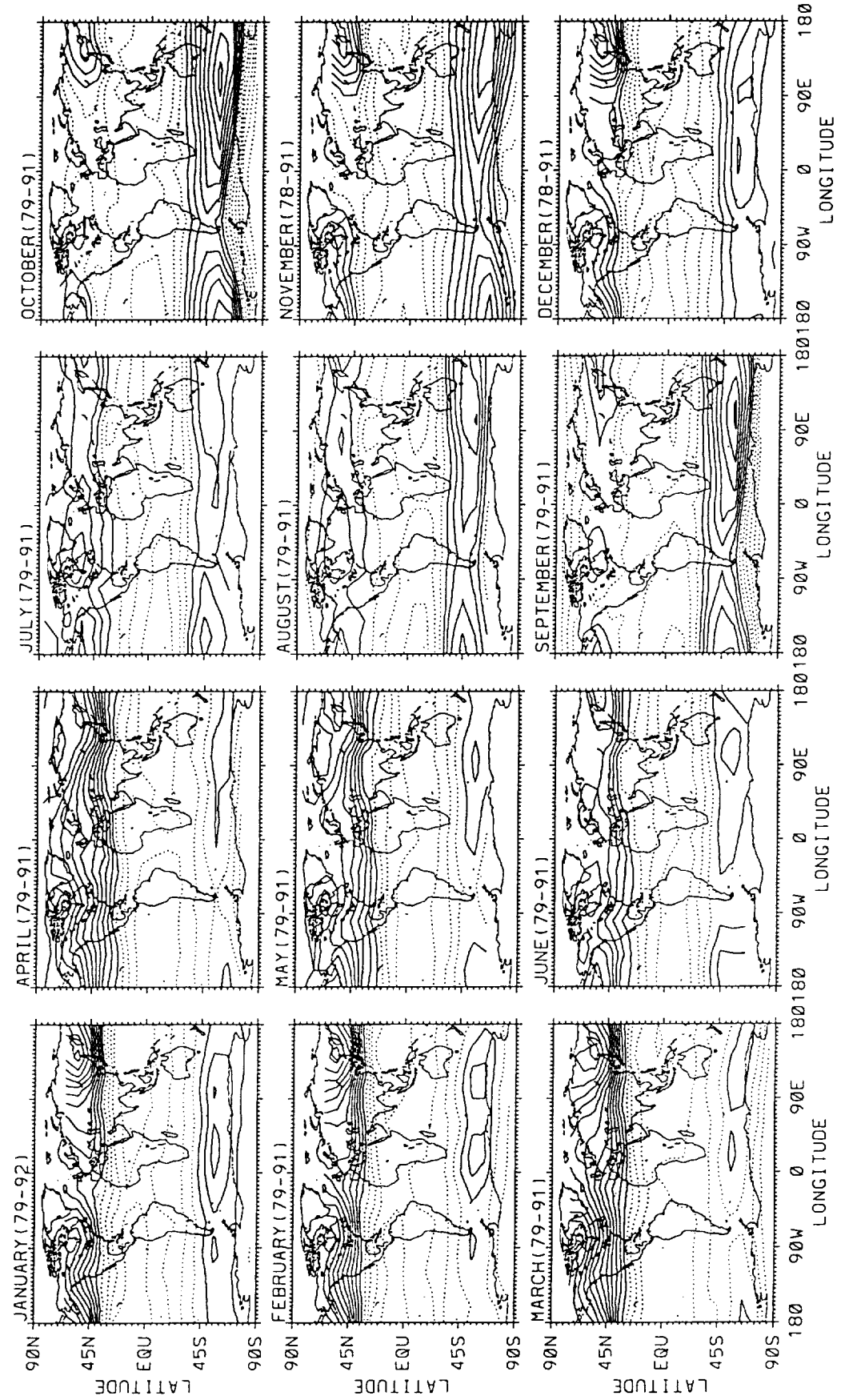


Figure 3. Climatological monthly mean TOMS ozone (units DU) computed using November 1978 through January 1992 monthly fields. Dashed (solid) contour values begin at 300 (315) and decrement (increment) by 15. Tabulated values are included in following pages.

NH JANUARY MONTHS

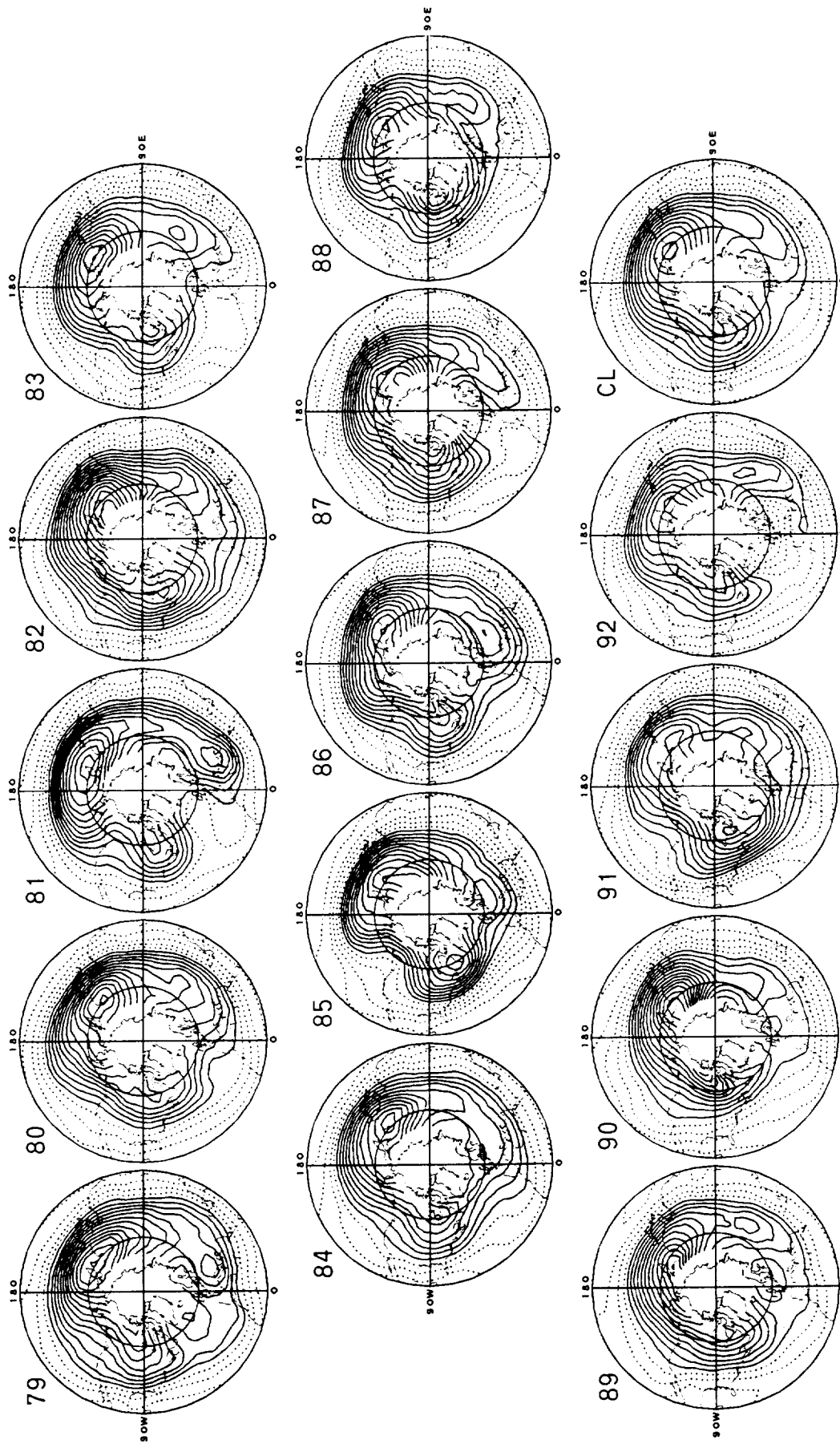


Figure 4. Monthly mean polar stereographic TOMS ozone (units DU) for seasonal months indicated [January, April, July, October] and in hemisphere indicated [Northern Hemisphere (NH), Southern Hemisphere (SH)]. Concentric circles: latitudes 20 and 55°. Dashed (solid) contours begin at 300 (315) and decrement (increment) by 15. Climatology fields for each month, denoted "CL", were computed by averaging TOMS over the years shown.

NH APRIL MONTHS

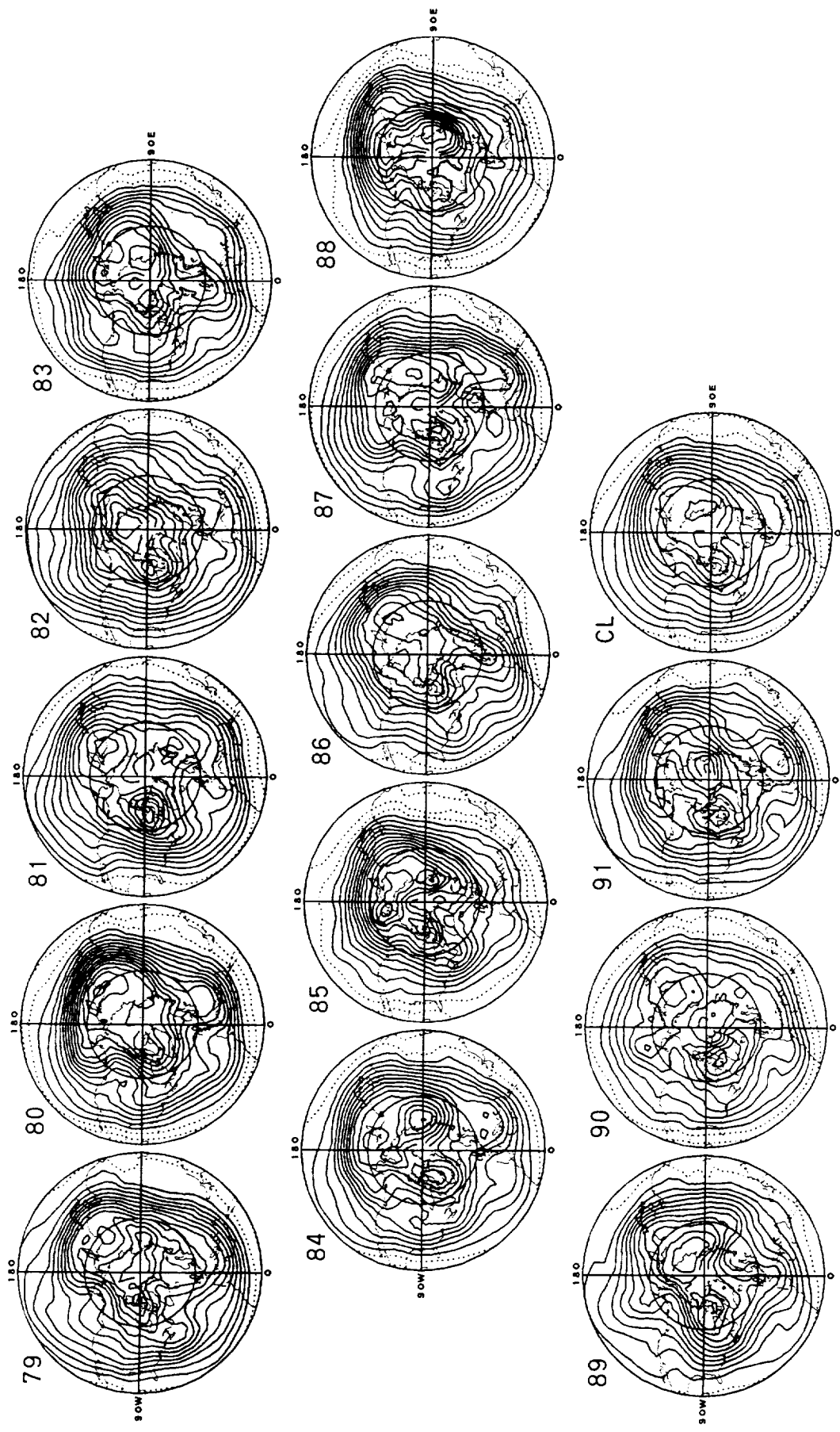


Figure 4. (continued)

NH JULY MONTHS

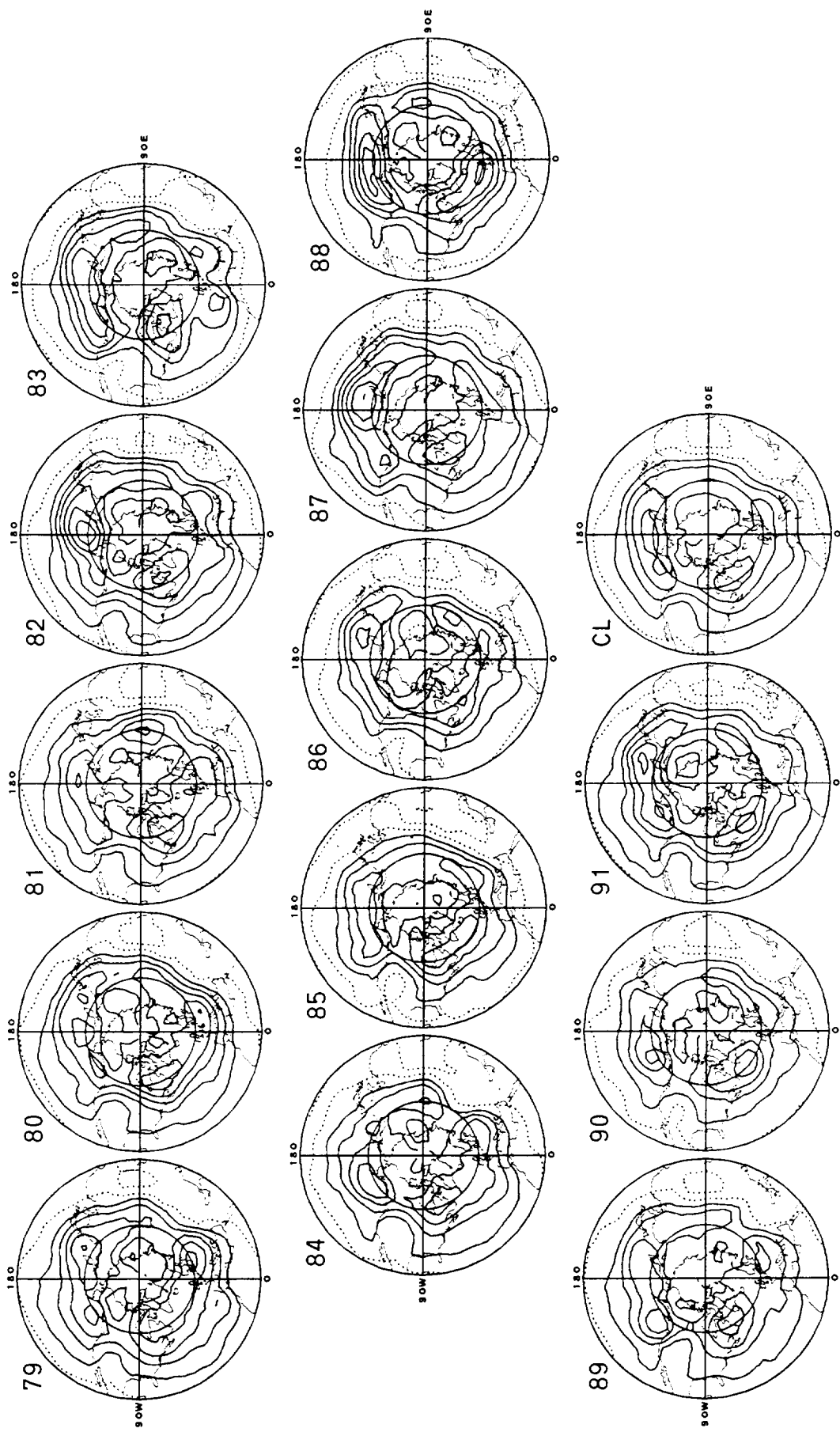


Figure 4. (continued)

NH OCTOBER MONTHS

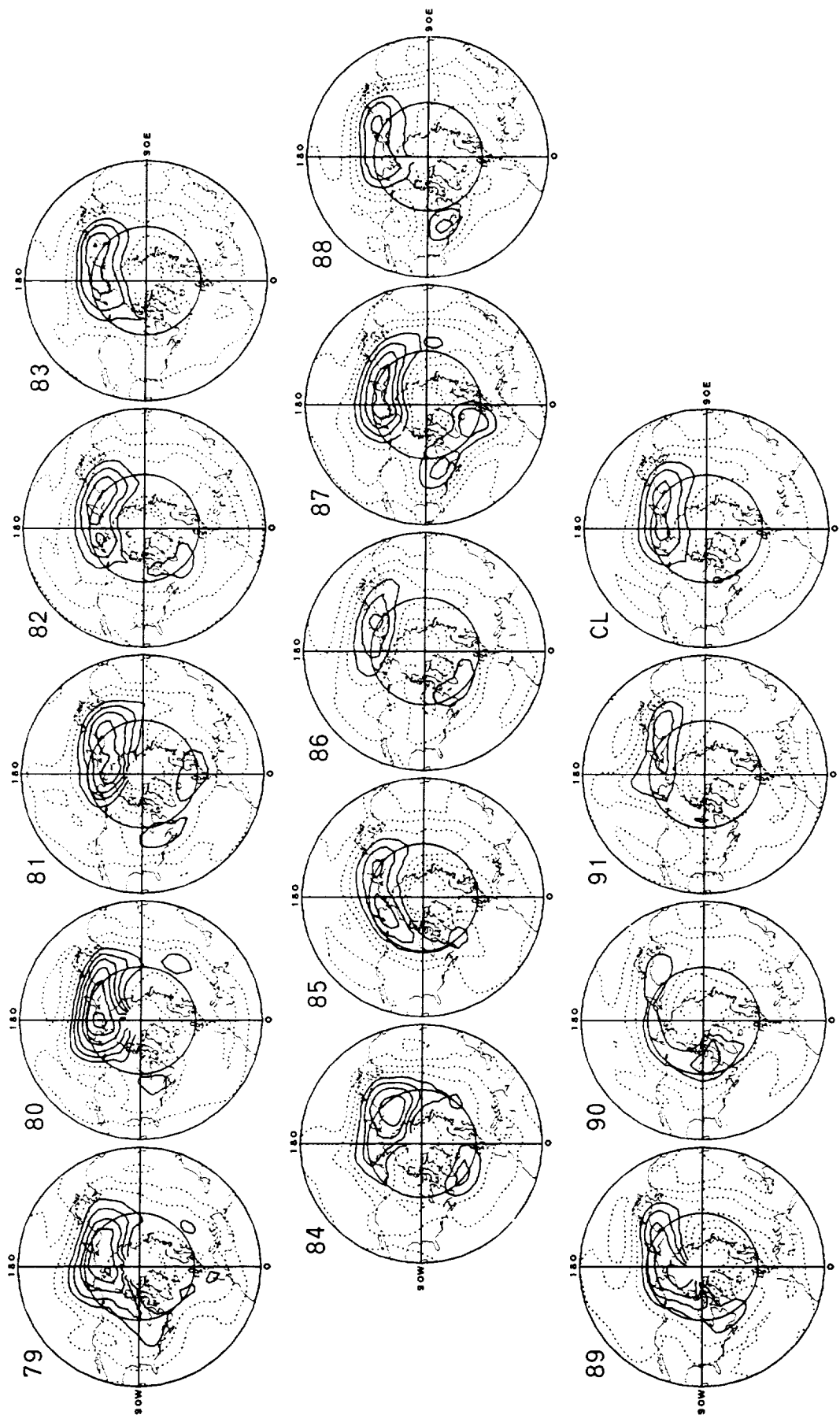


Figure 4. (continued)

SH JANUARY MONTHS

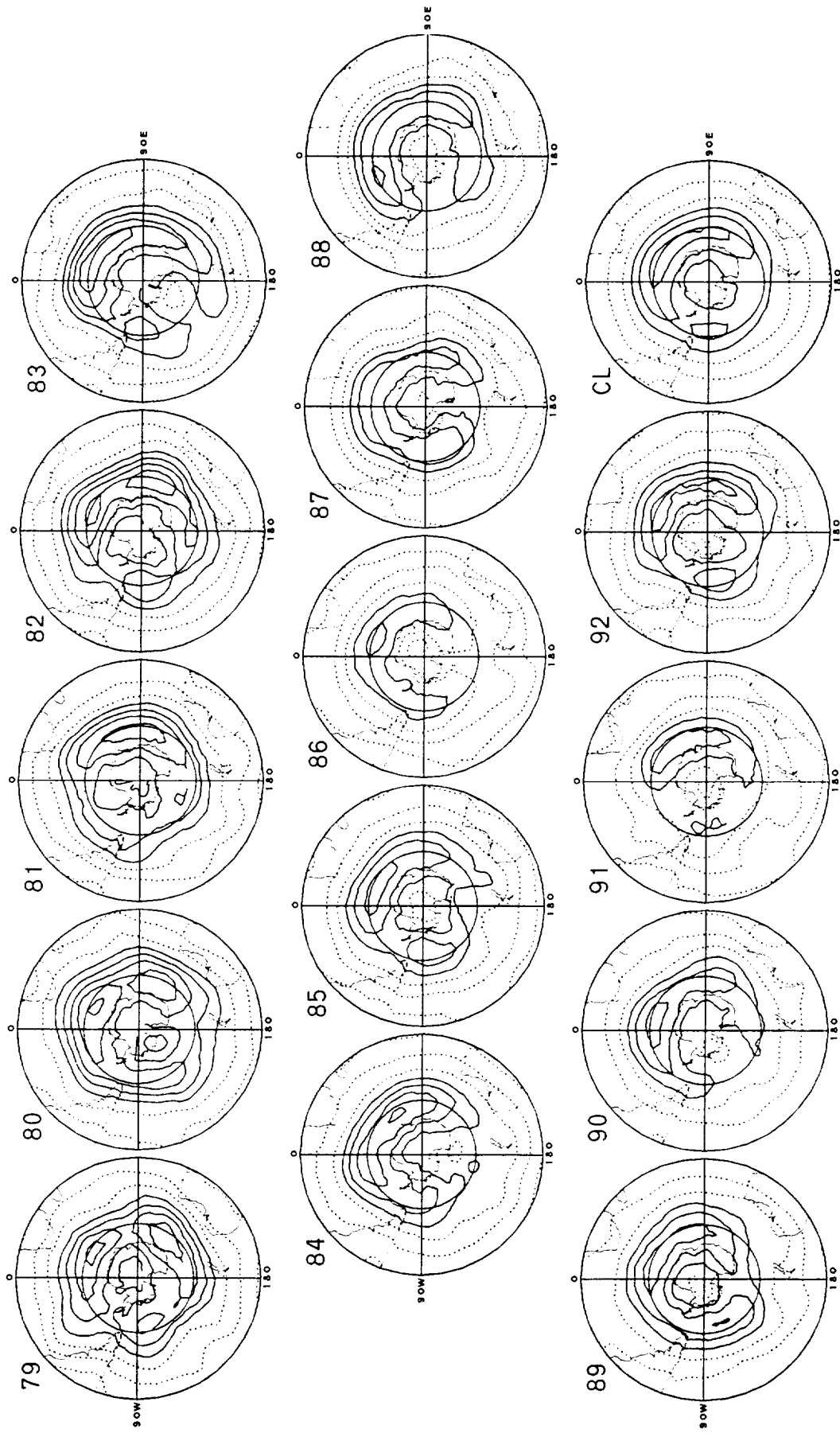


Figure 4. (continued)

SH APRIL MONTHS

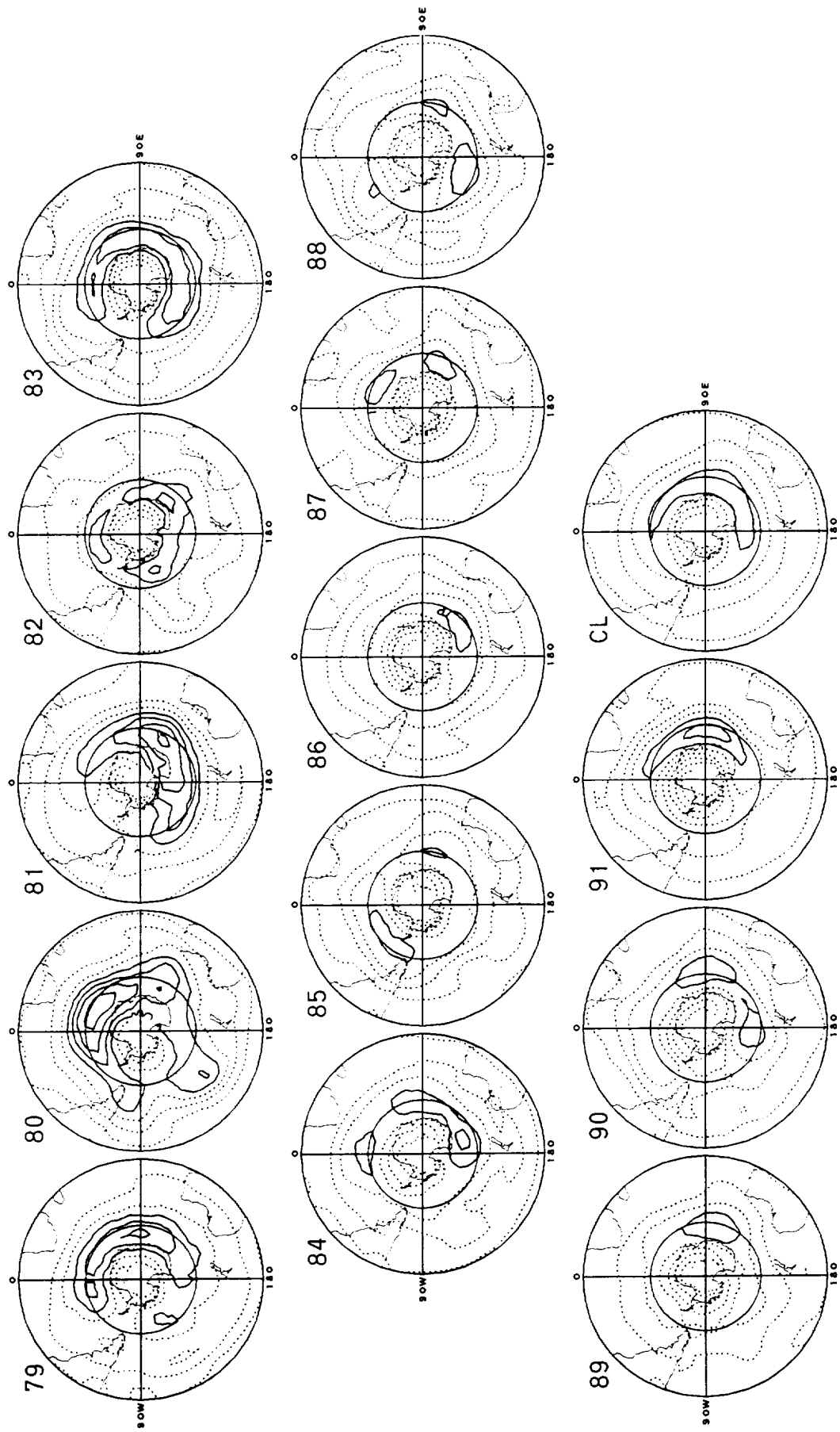


Figure 4. (continued)

SH JULY MONTHS

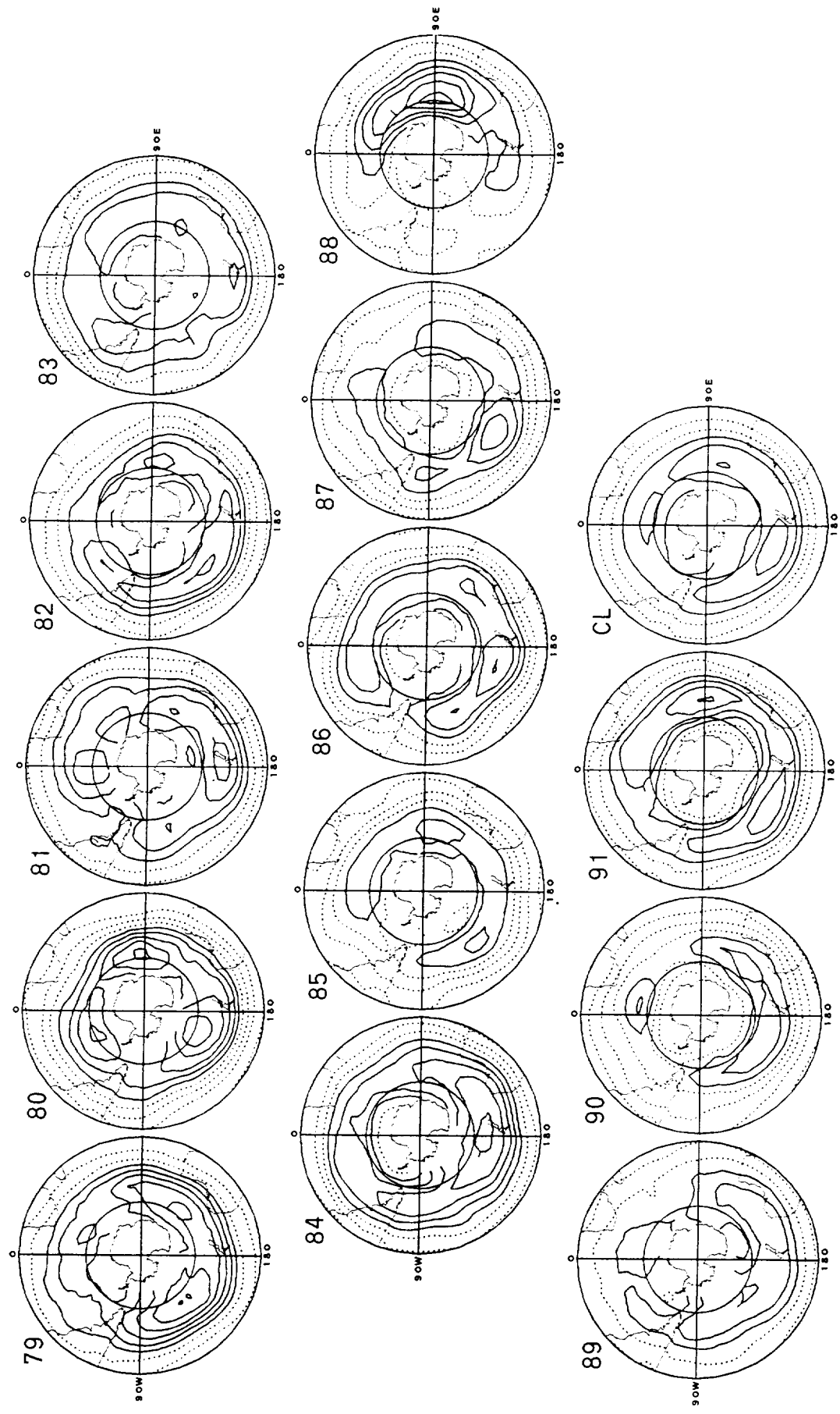


Figure 4. (continued)

SH OCTOBER MONTHS

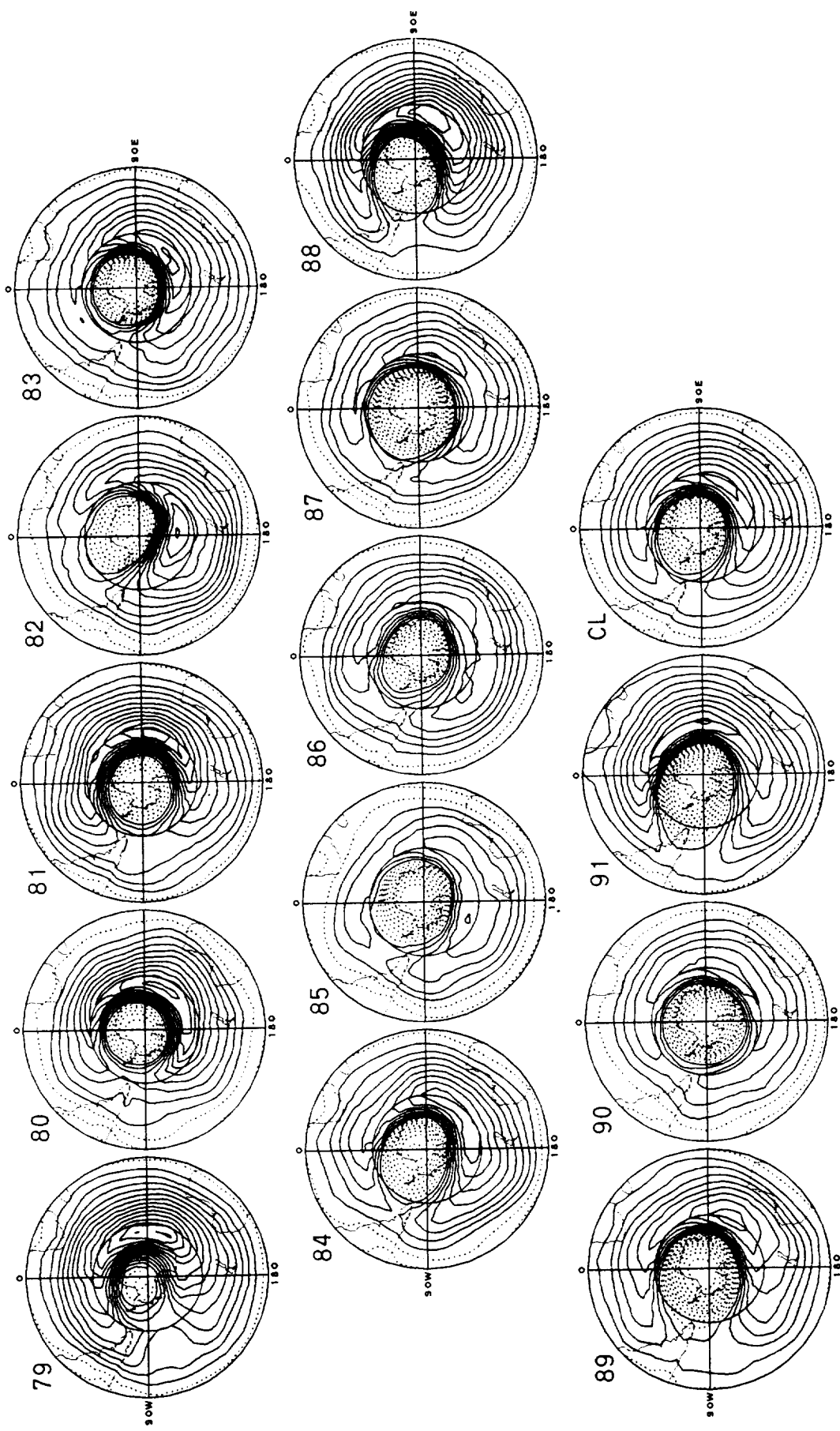


Figure 4. (continued)

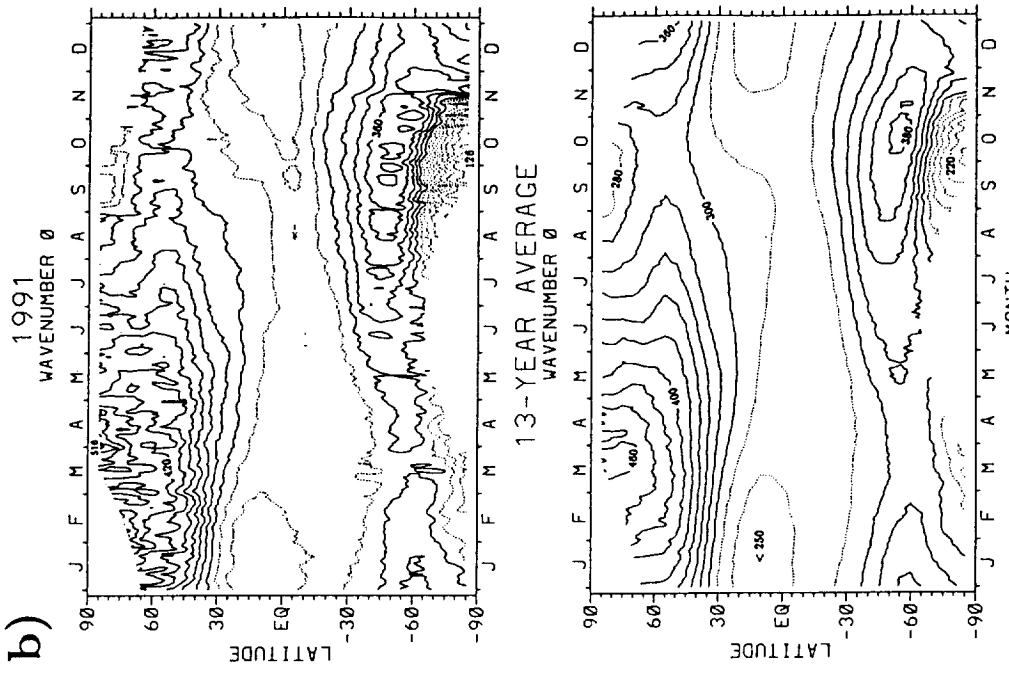
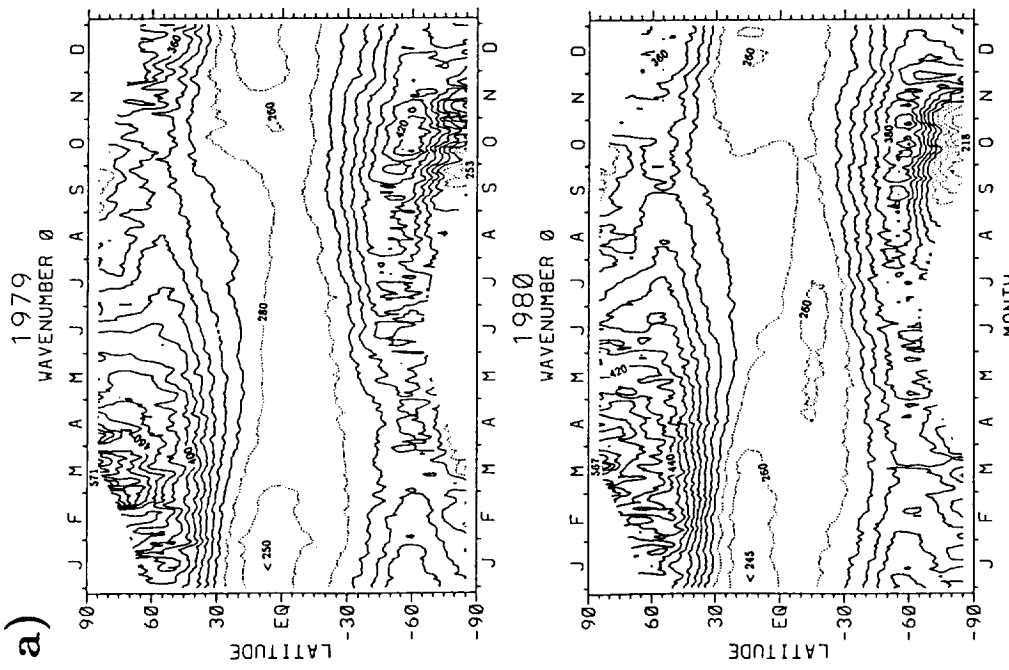


Figure 5. (a)-(b): Zonal mean TOMS total ozone (units DU) plotted latitude vs. time (months indicated). No temporal filtering employed. Dashed (solid) contours begin at 280 (300) and decrement (increment) by 20. (a): Years 1979 (top) and 1980 (bottom). (b): Year 1991 (top) and 13-year (1979–1991) average (bottom). [13-year means formed by averaging similar days of each year.] (c)–(d): Same as (a) and (b), except for zonal wave 1 RMS amplitudes. For all but 13-year average plot, dashed contours are 20; solid contours begin at 40, incrementing by 20. For 13-year average plot, dashed (solid) contours are 8 (16, 24, 32,...). (e)–(f): Wave 2, with all dashed (solid) contours 15 (30, 45, 60,...). (g)–(h): Wave 3, with all dashed (solid) contours 5 (15, 25, 35,...). (i)–(j): Waves 4–7, with all dashed (solid) contours 10 (20, 30, 40,...).

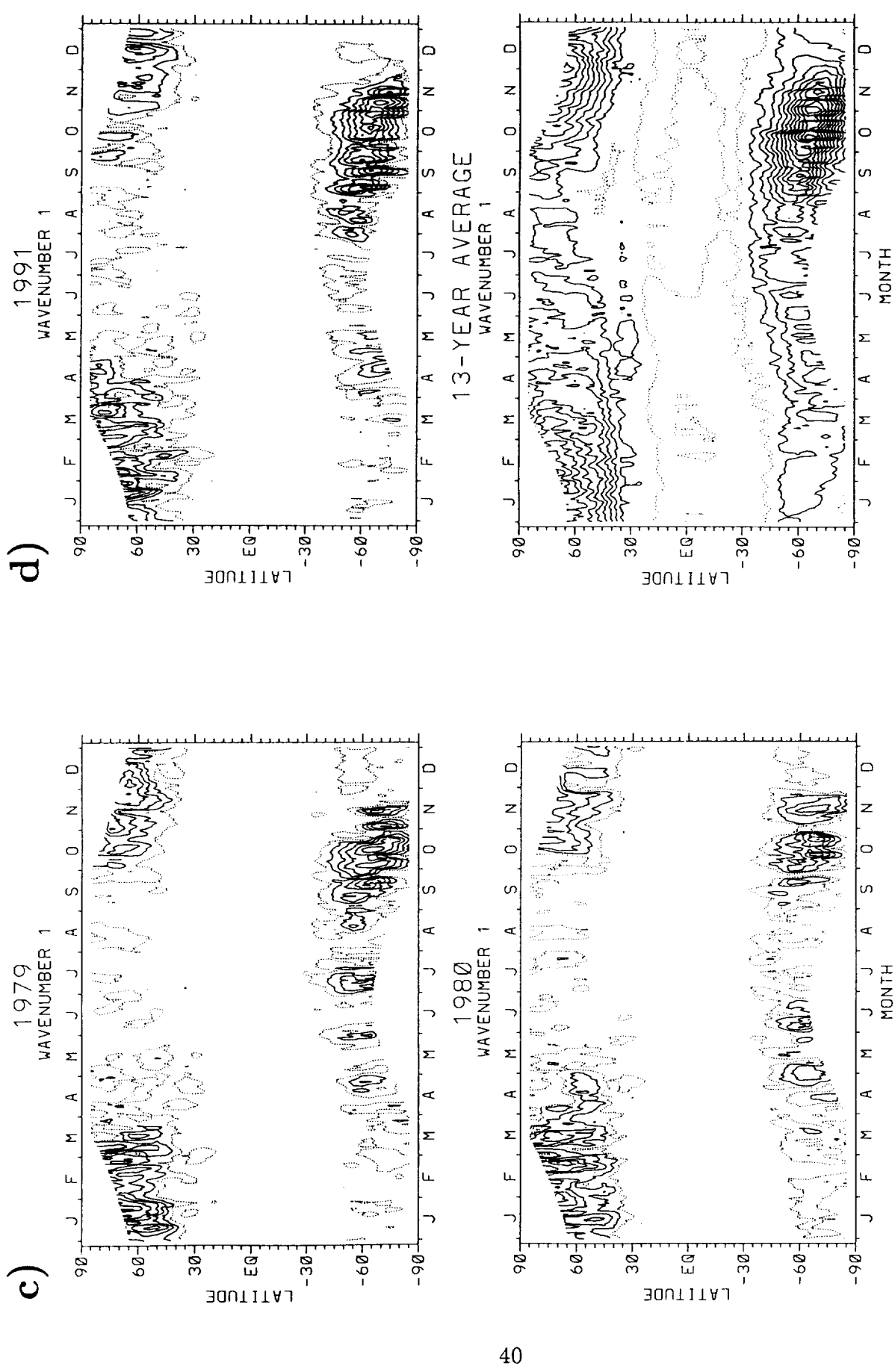


Figure 5. (continued)

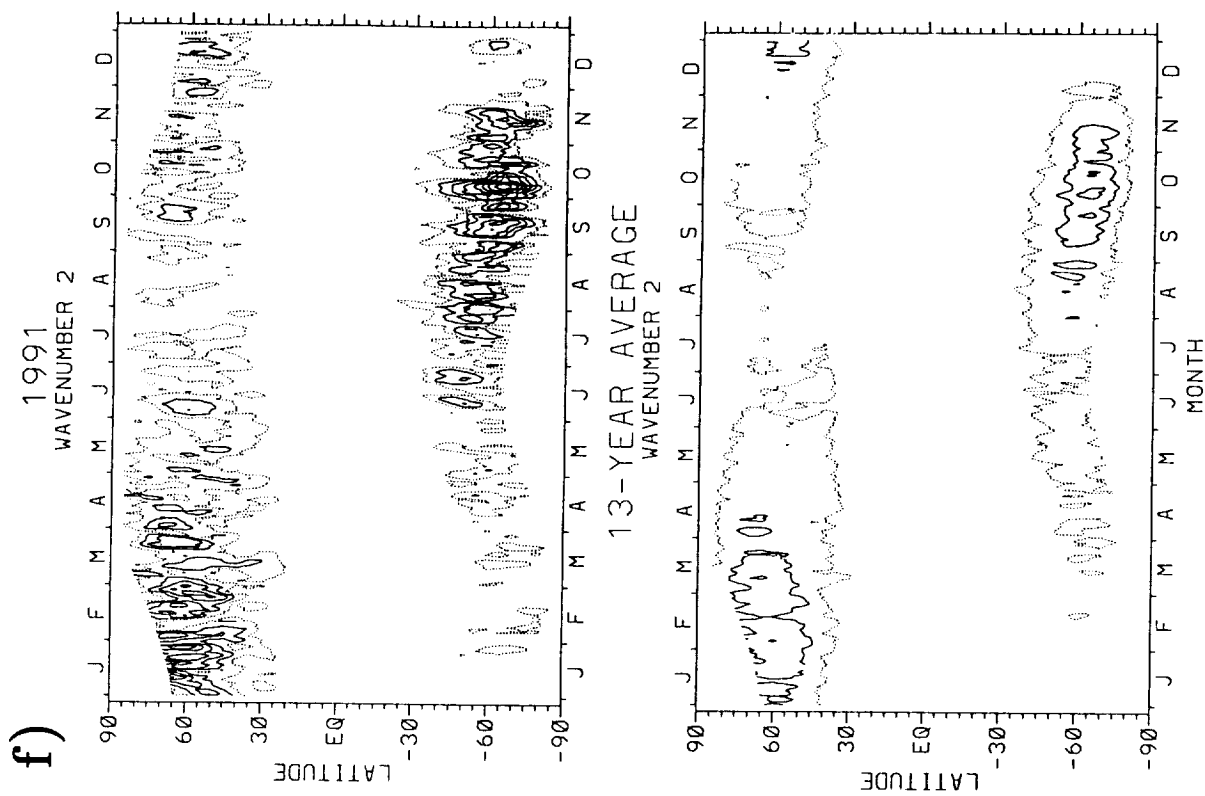
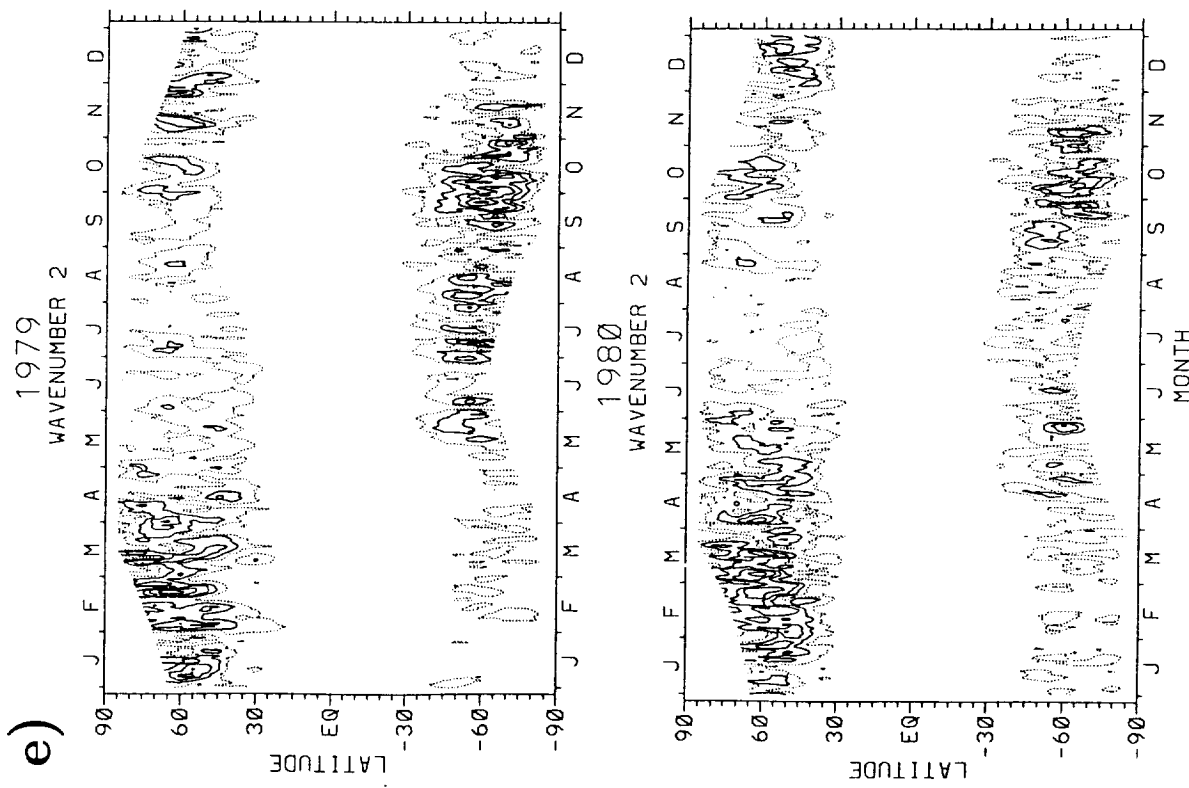


Figure 5. (continued)

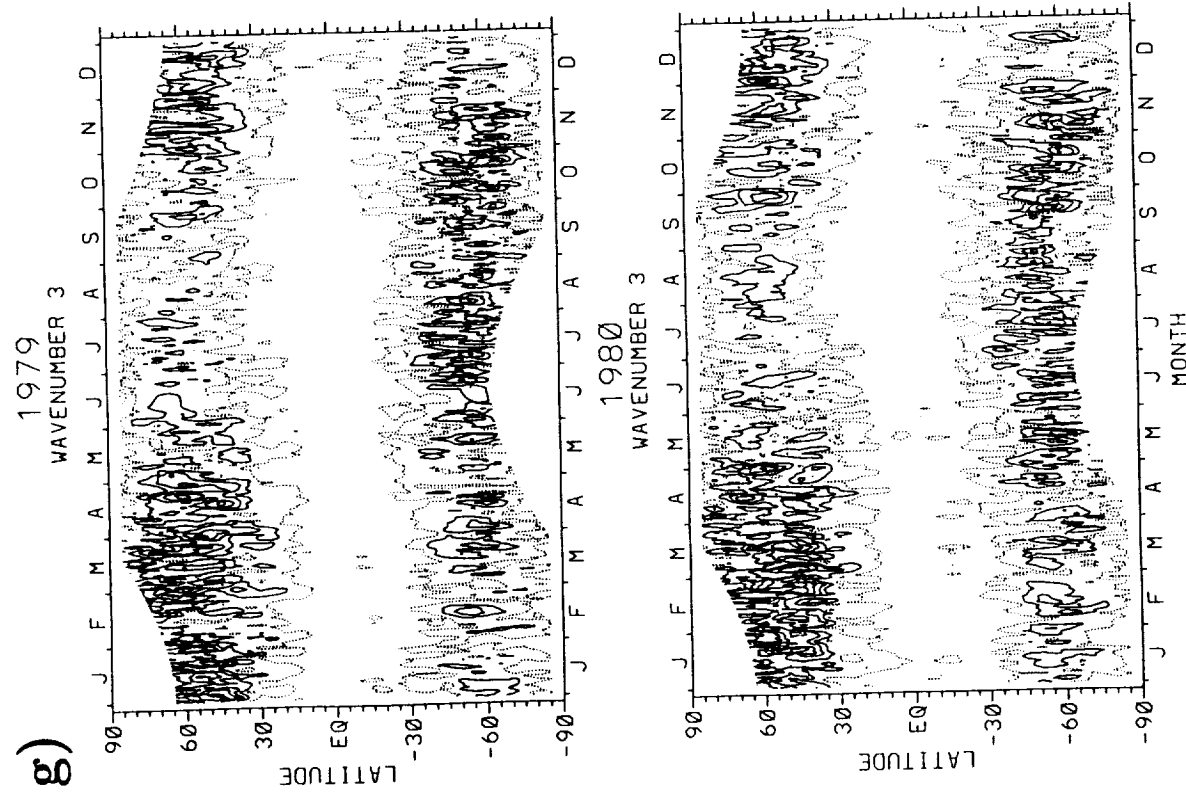


Figure 5. (continued)

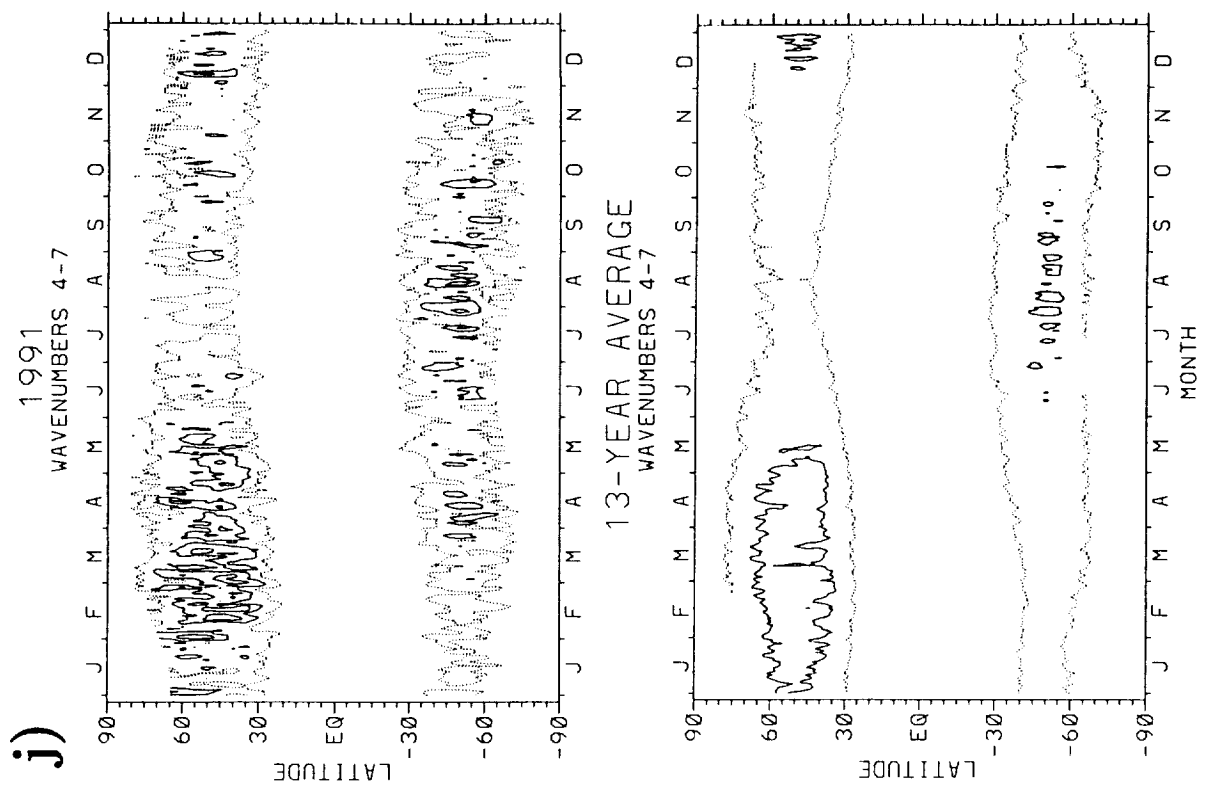
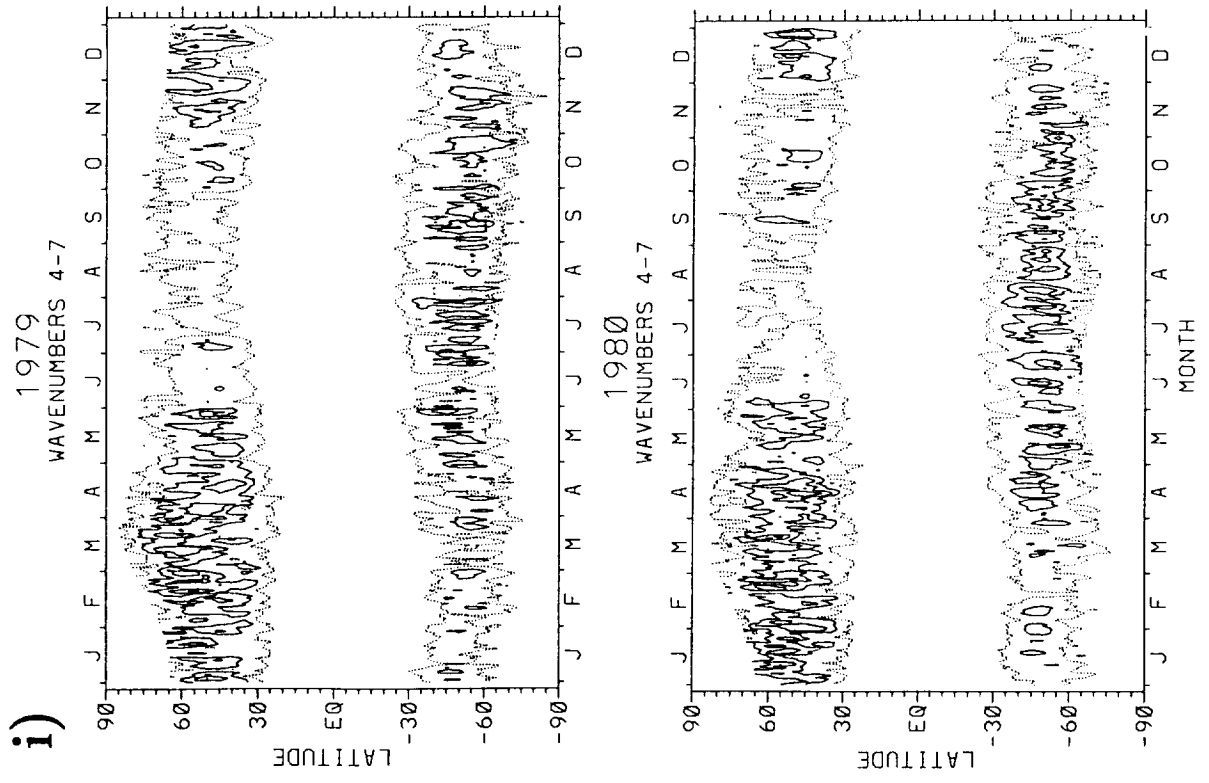
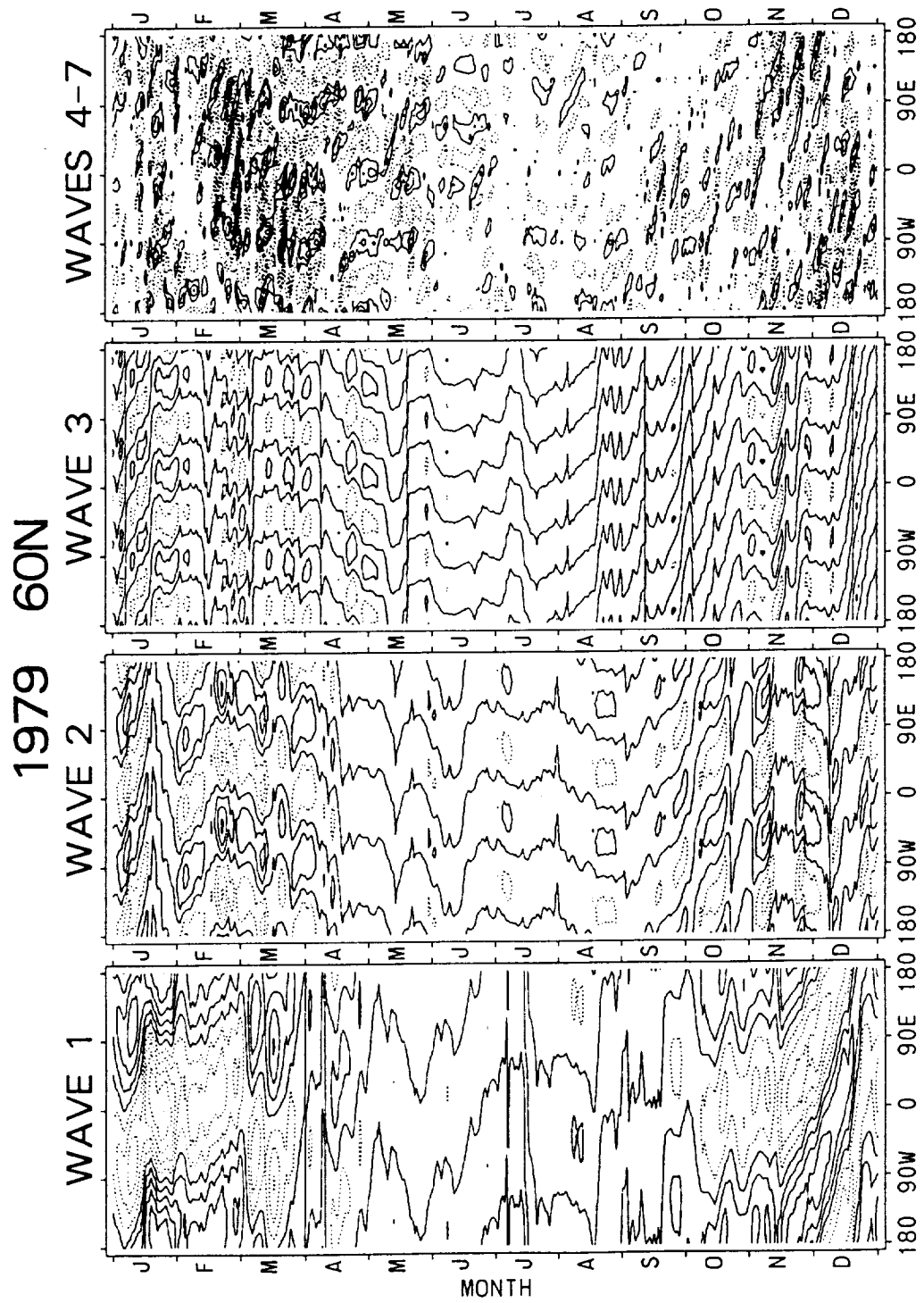


Figure 5. (continued)



Waves 1-3 (Units:DU) : Dashed: -25, -50, ... Solid: 0, 25, 50, ...

 Waves 4-7 (Units:DU) : Dashed: -15, -30, ... Solid: 15, 30, ...

Figure 6. Hovmöller time (months shown) vs. longitude diagrams of TOMS ozone (units DU) at latitudes indicated on each page. Years shown: 1979, 1985, and 1991. No temporal filtering employed. Contour values indicated on each page.

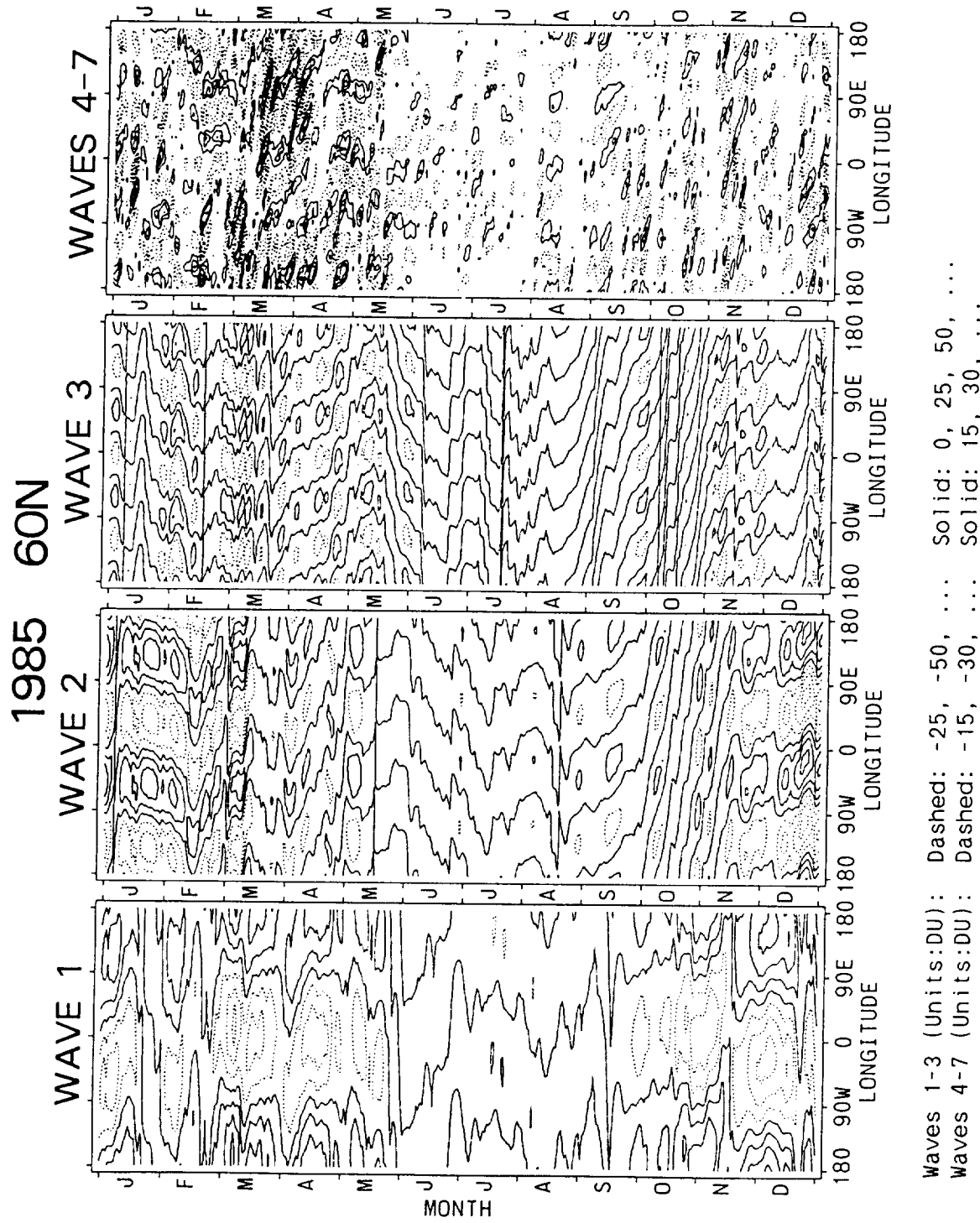


Figure 6. (continued)

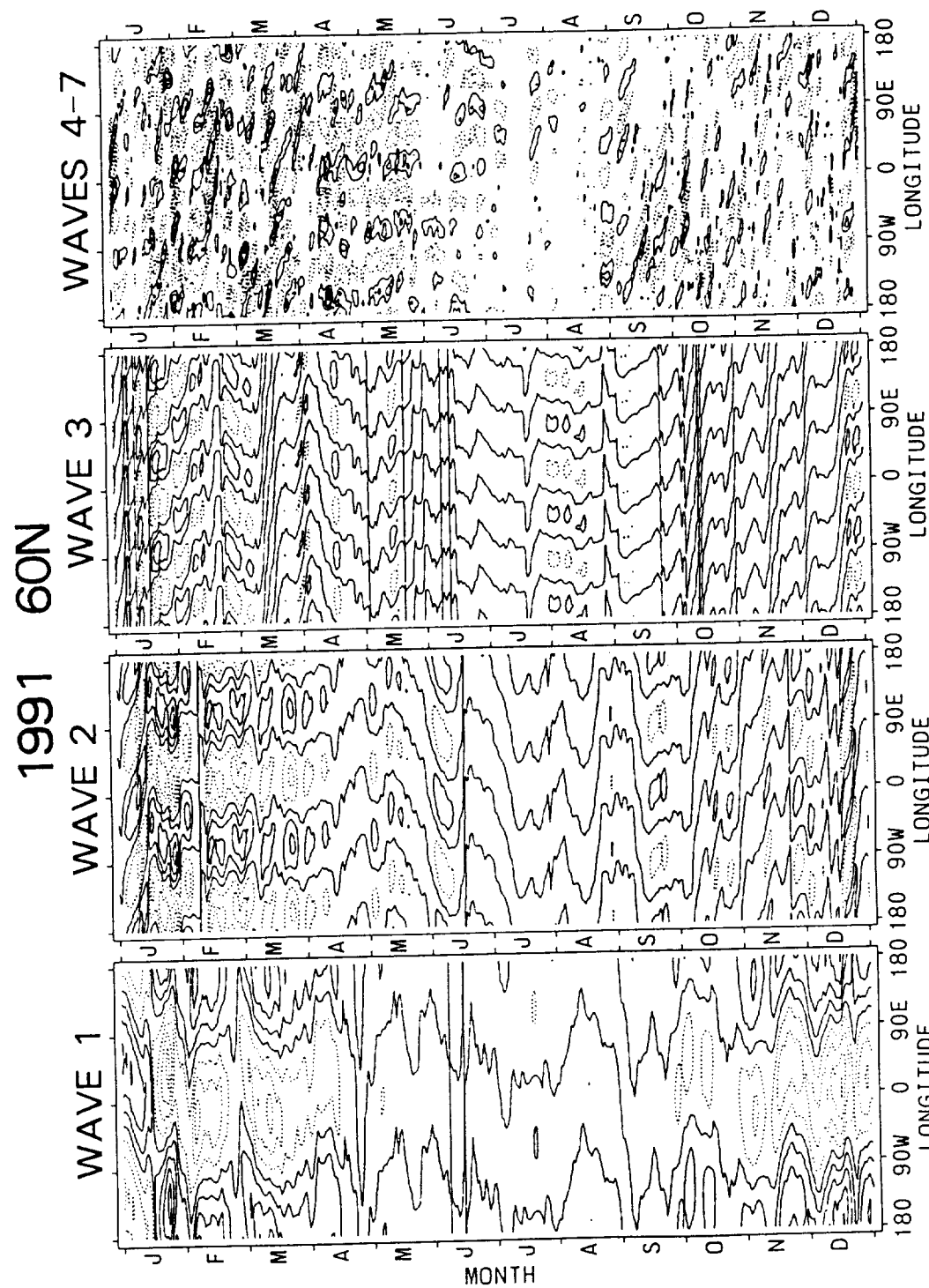


Figure 6. (continued)

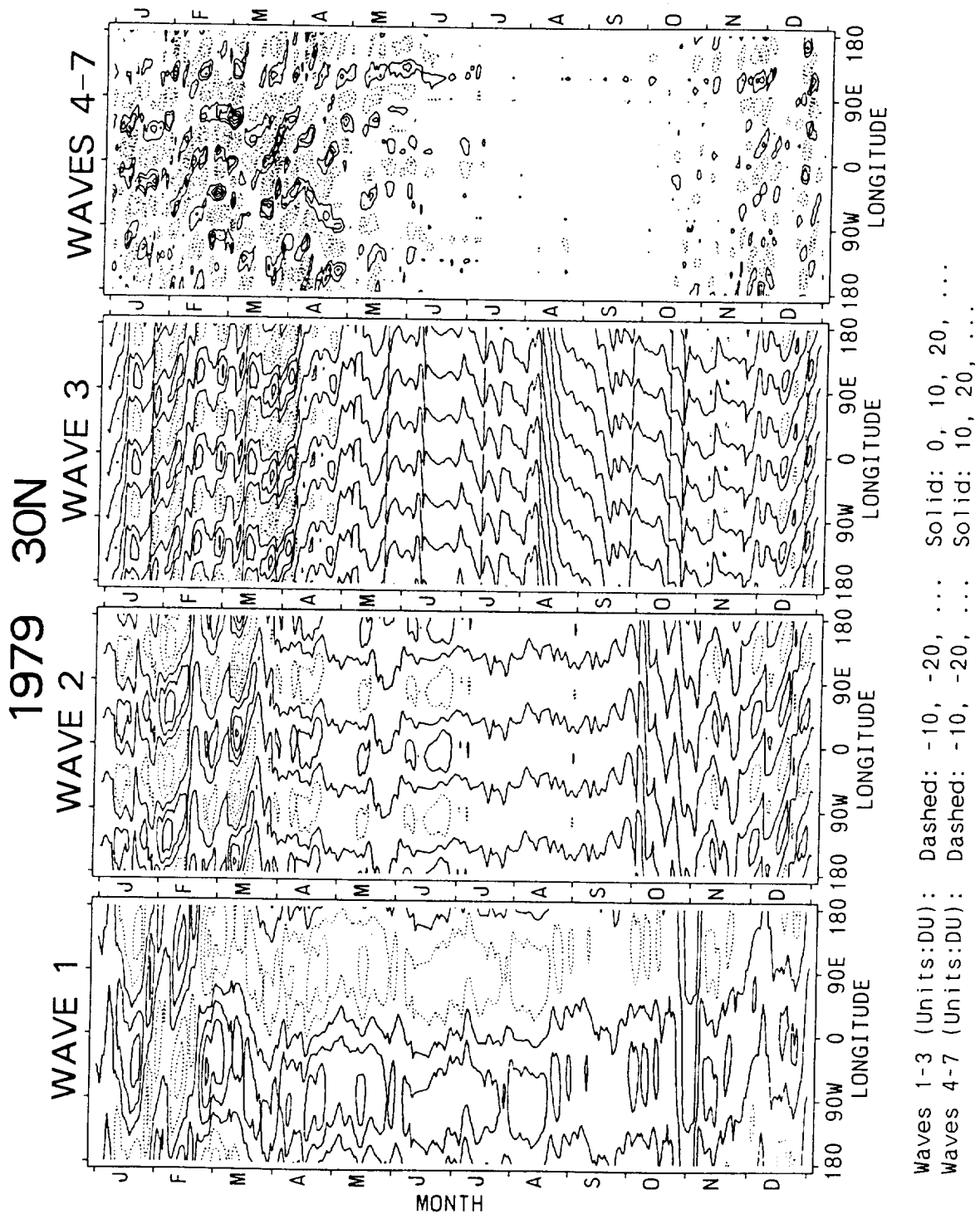
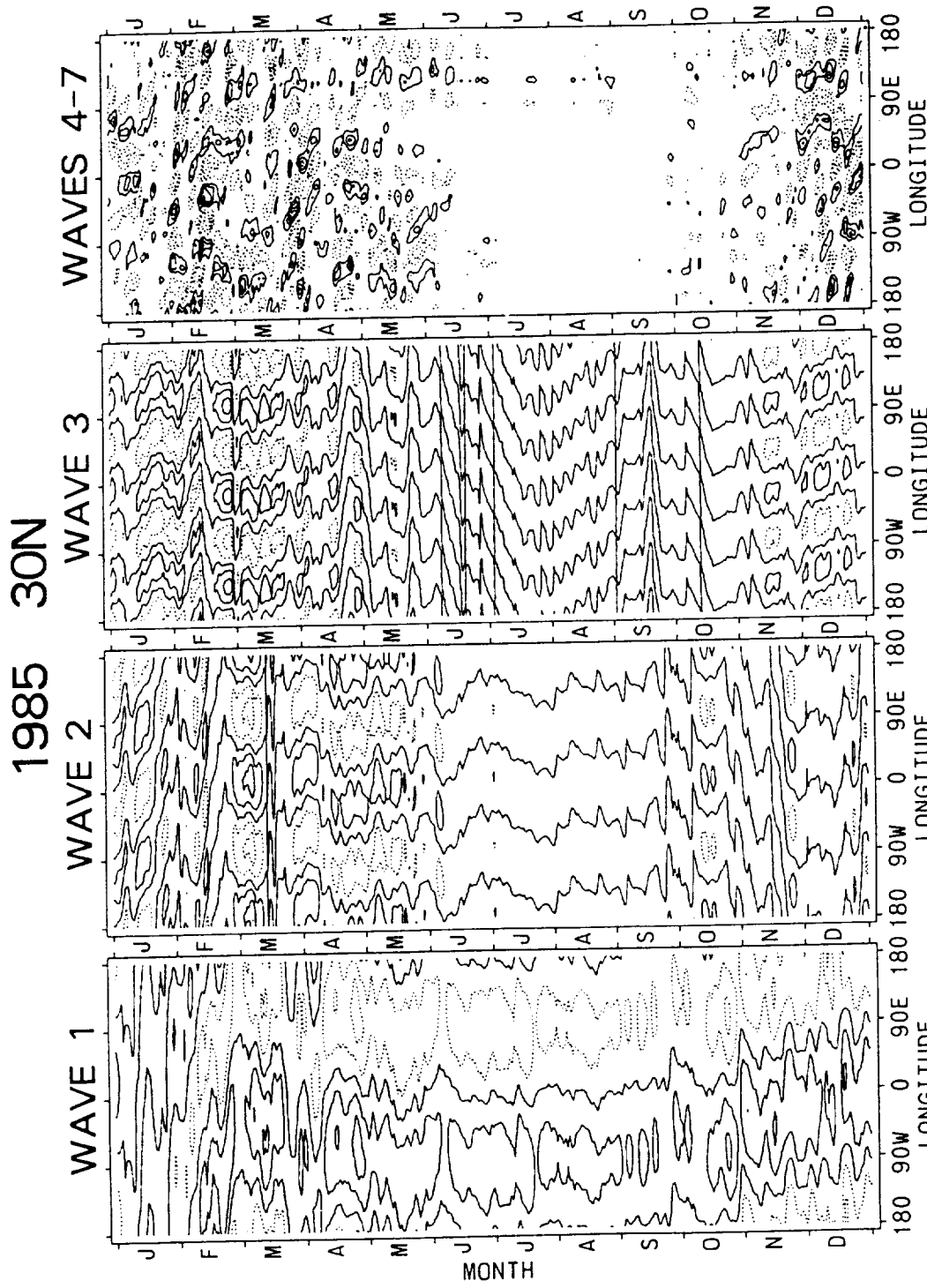


Figure 6. (continued)



Waves 1-3 (Units:DU) : Dashed: -10, -20, Solid: 0, 10, 20, ...
 Waves 4-7 (Units:DU) : Dashed: -10, -20, Solid: 10, 20, ...

Figure 6. (continued)

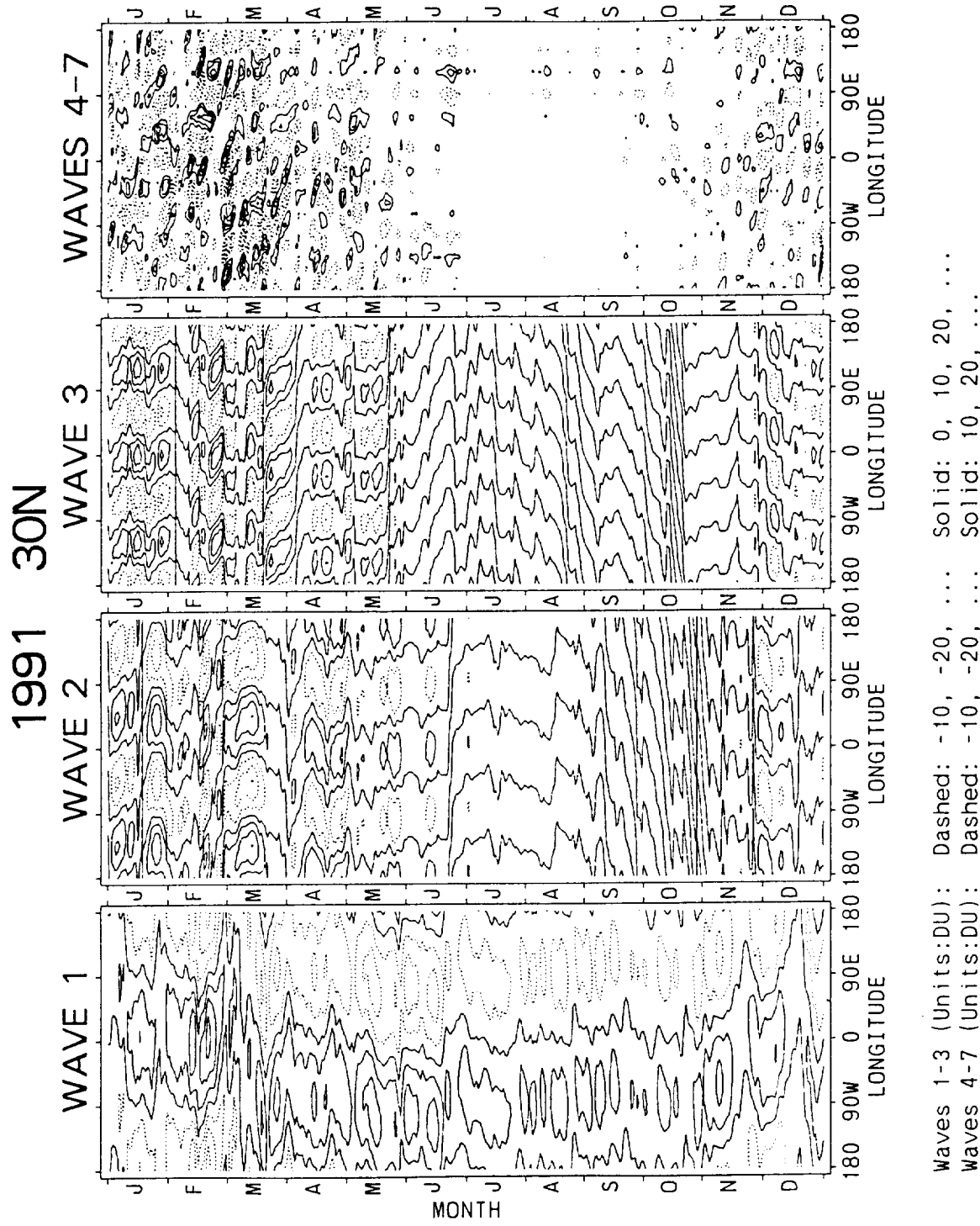


Figure 6. (continued)

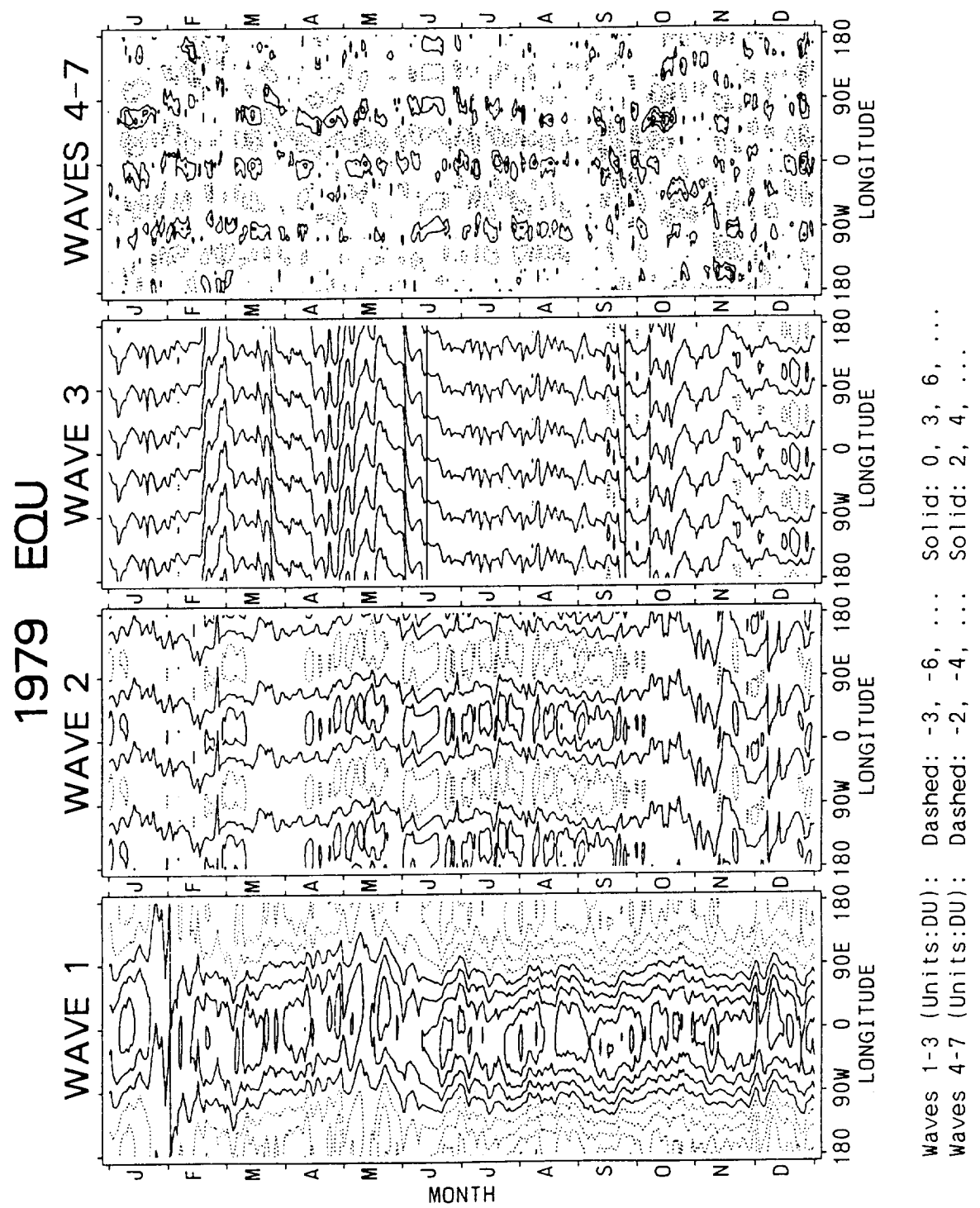


Figure 6. (continued)

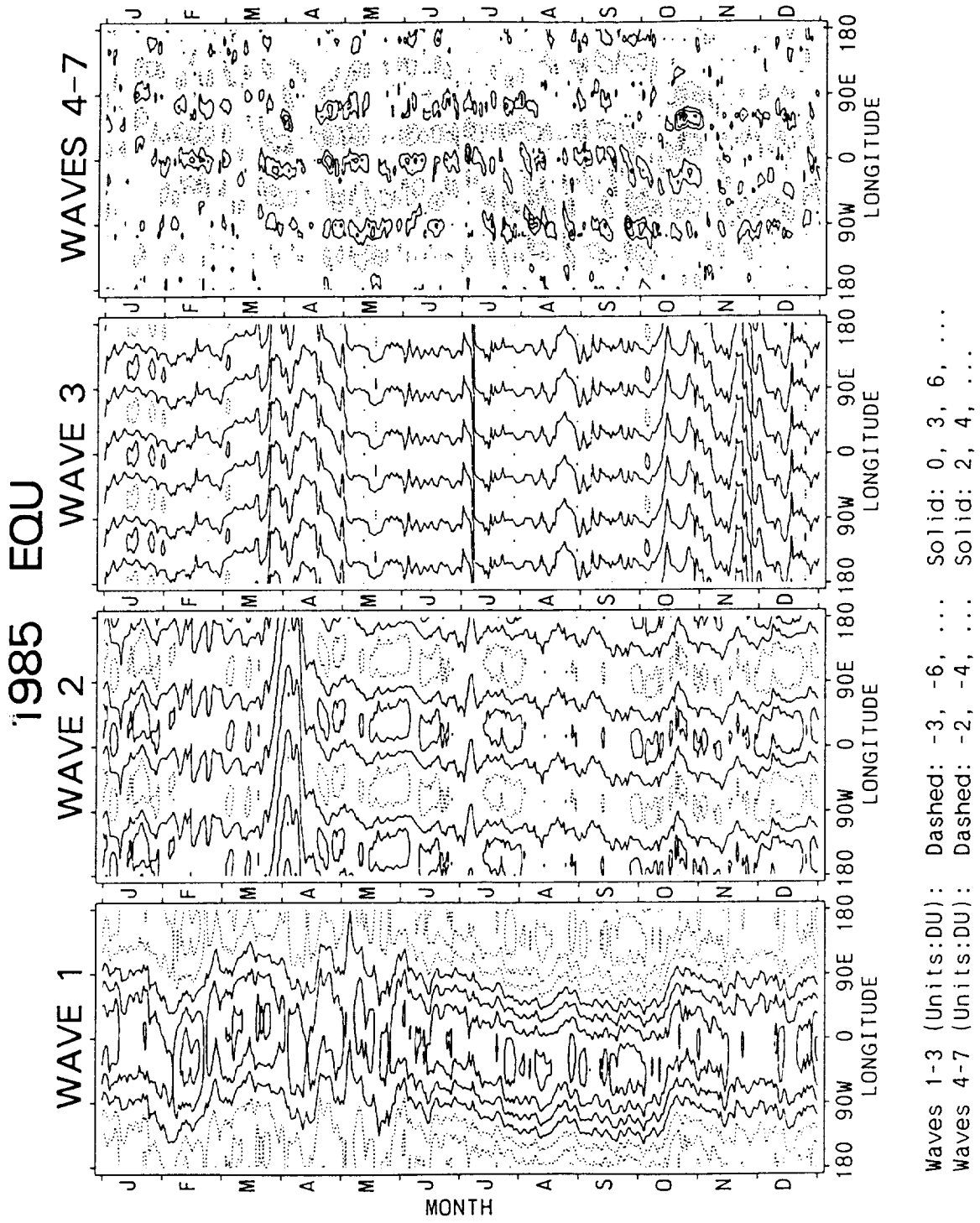


Figure 6. (continued)

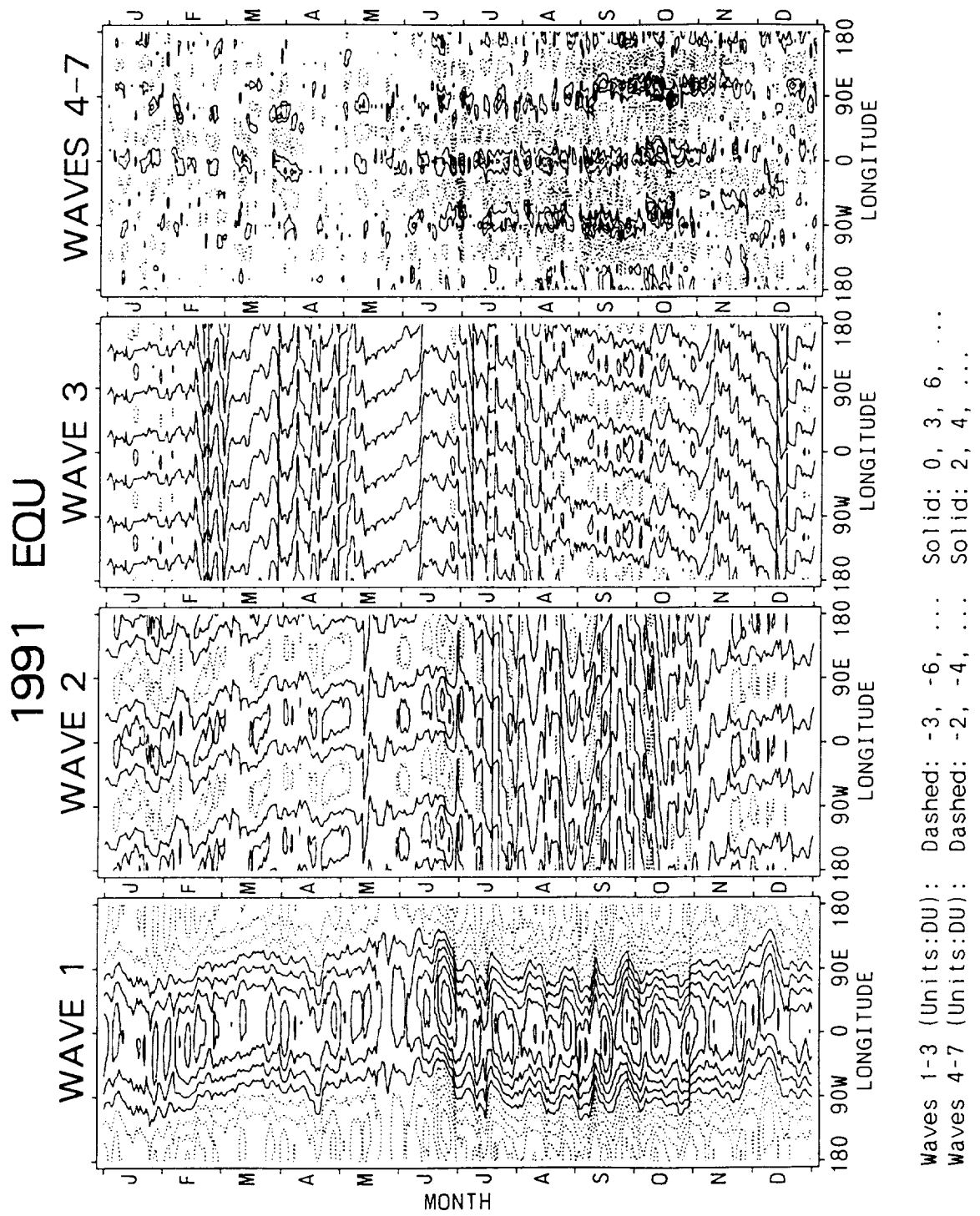


Figure 6. (continued)

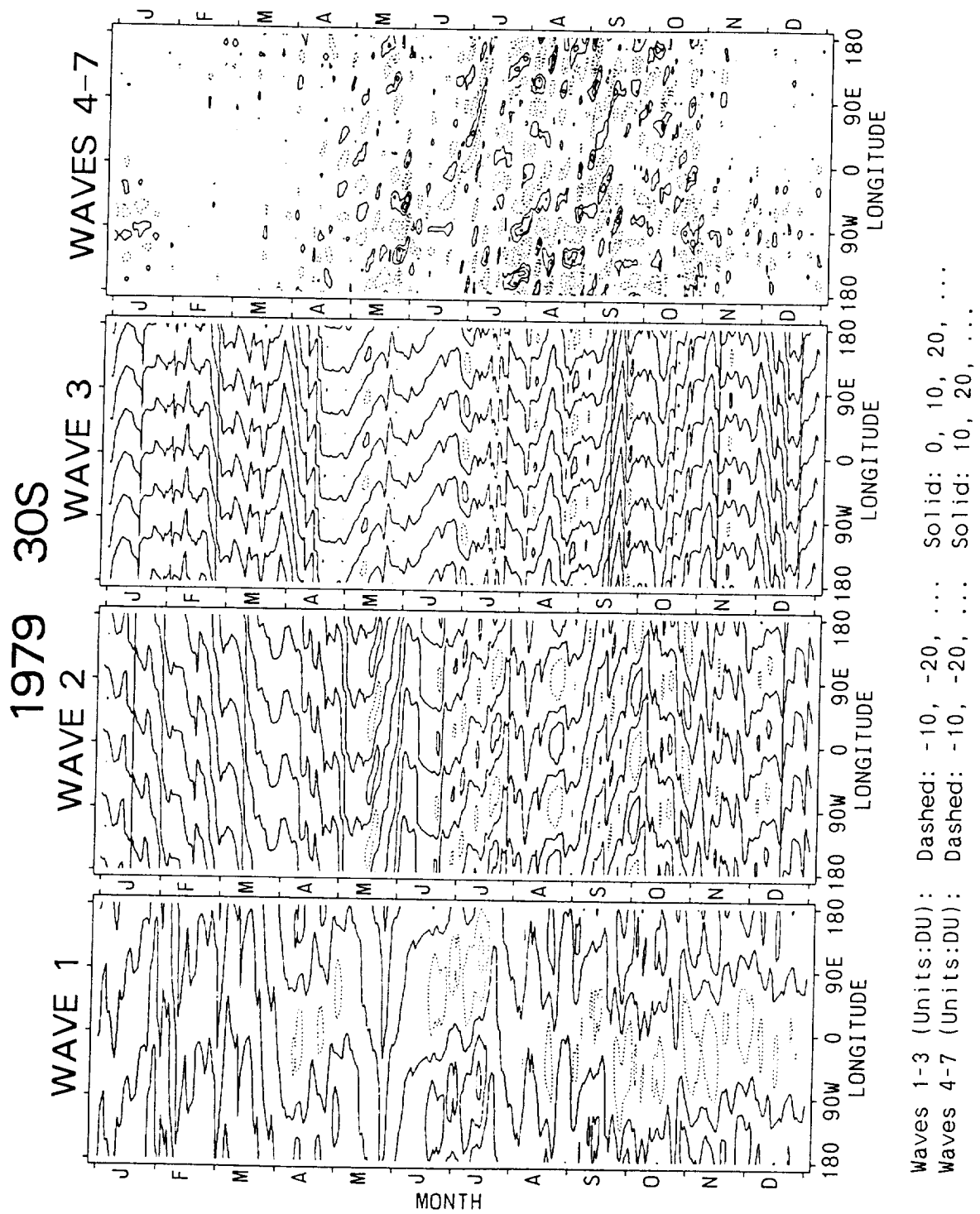


Figure 6. (continued)

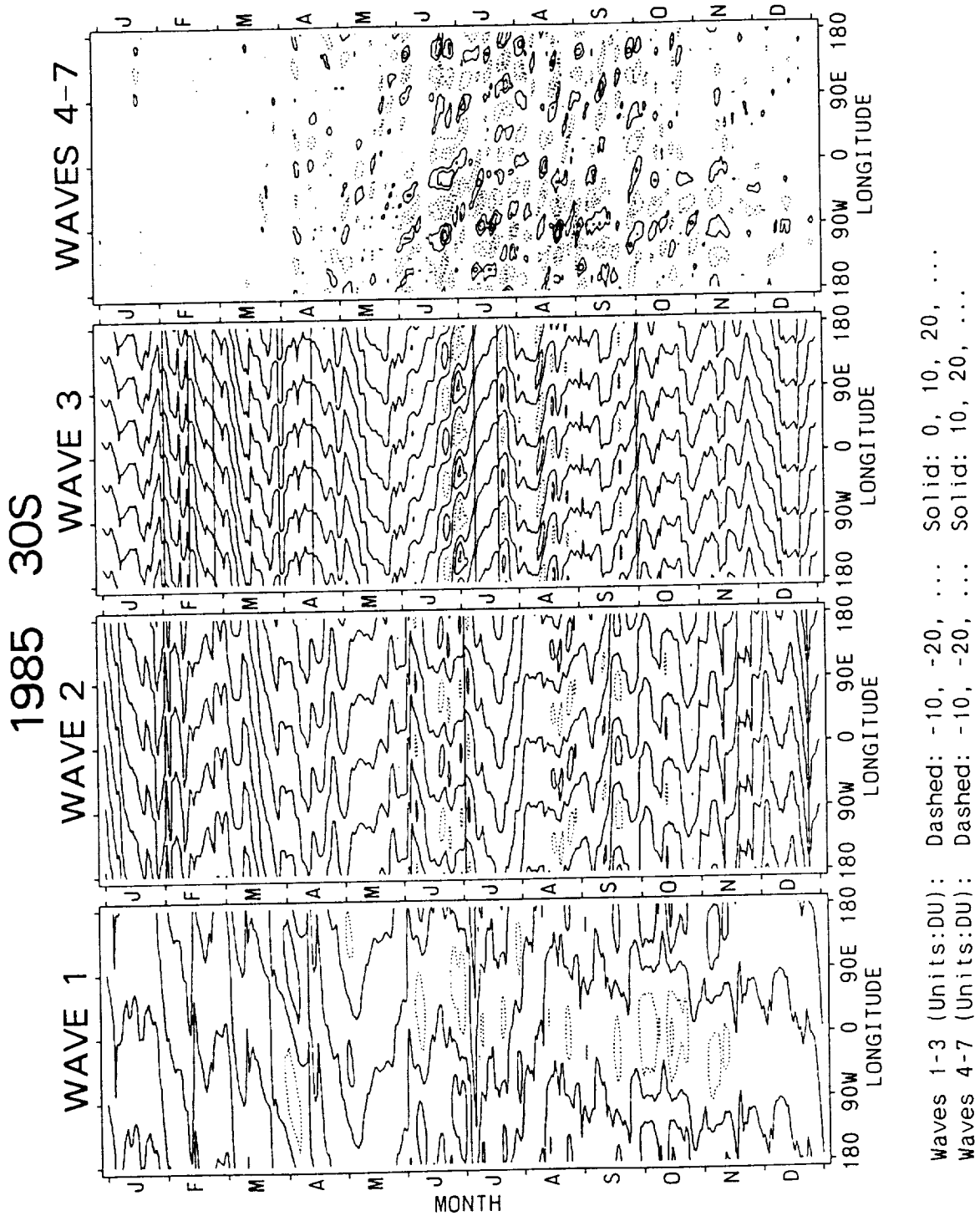


Figure 6. (continued)

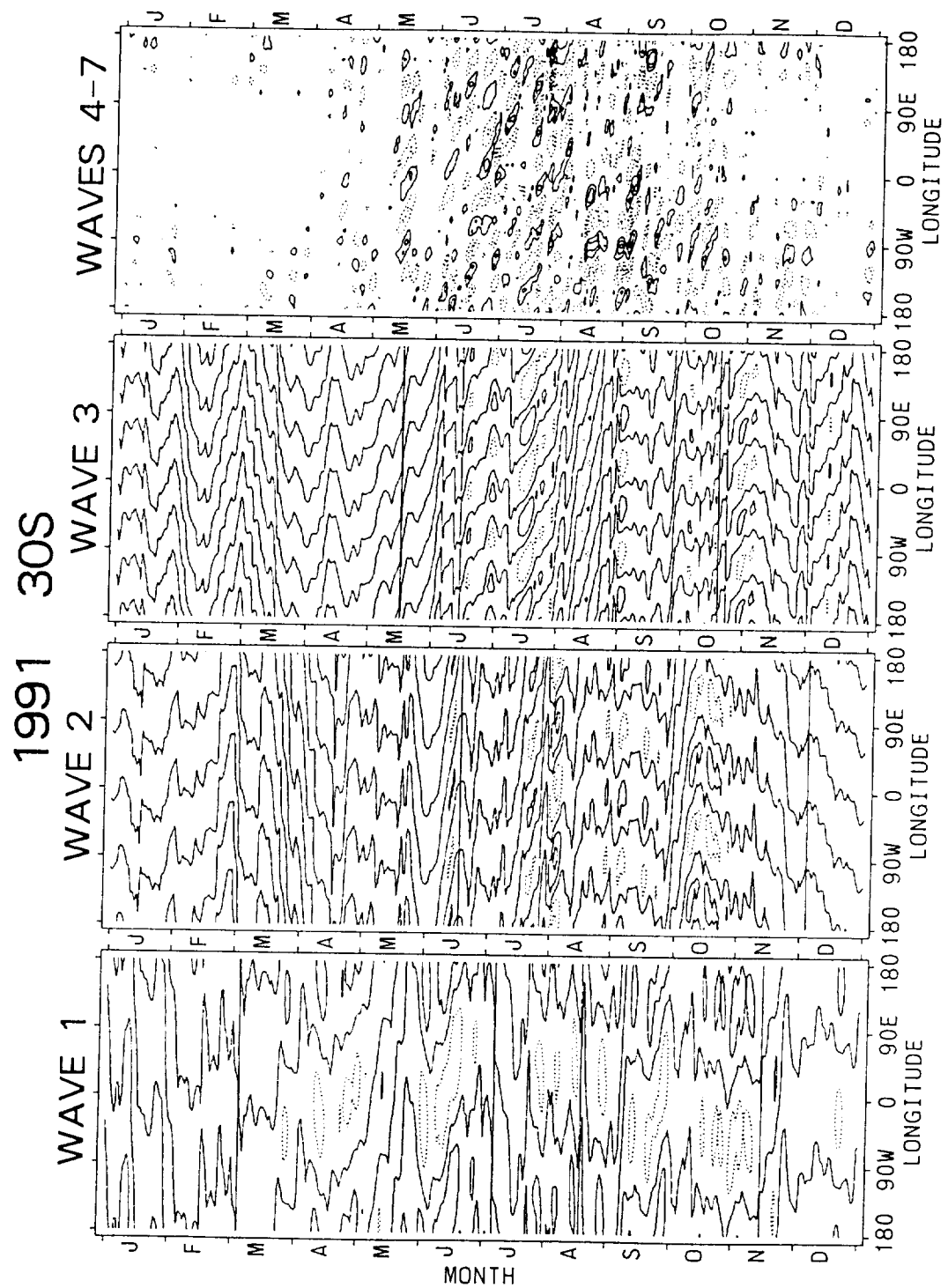


Figure 6. (continued)

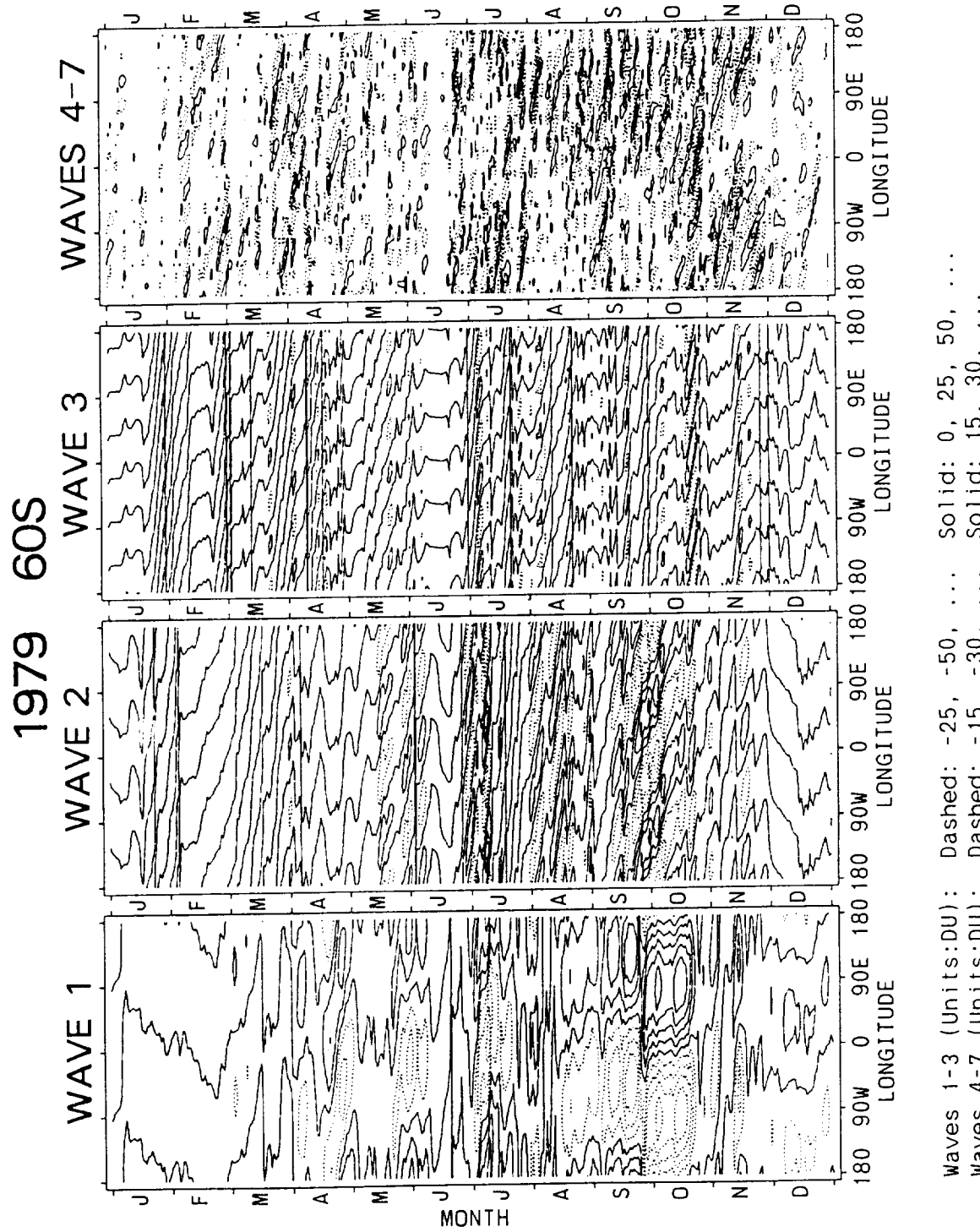


Figure 6. (continued)

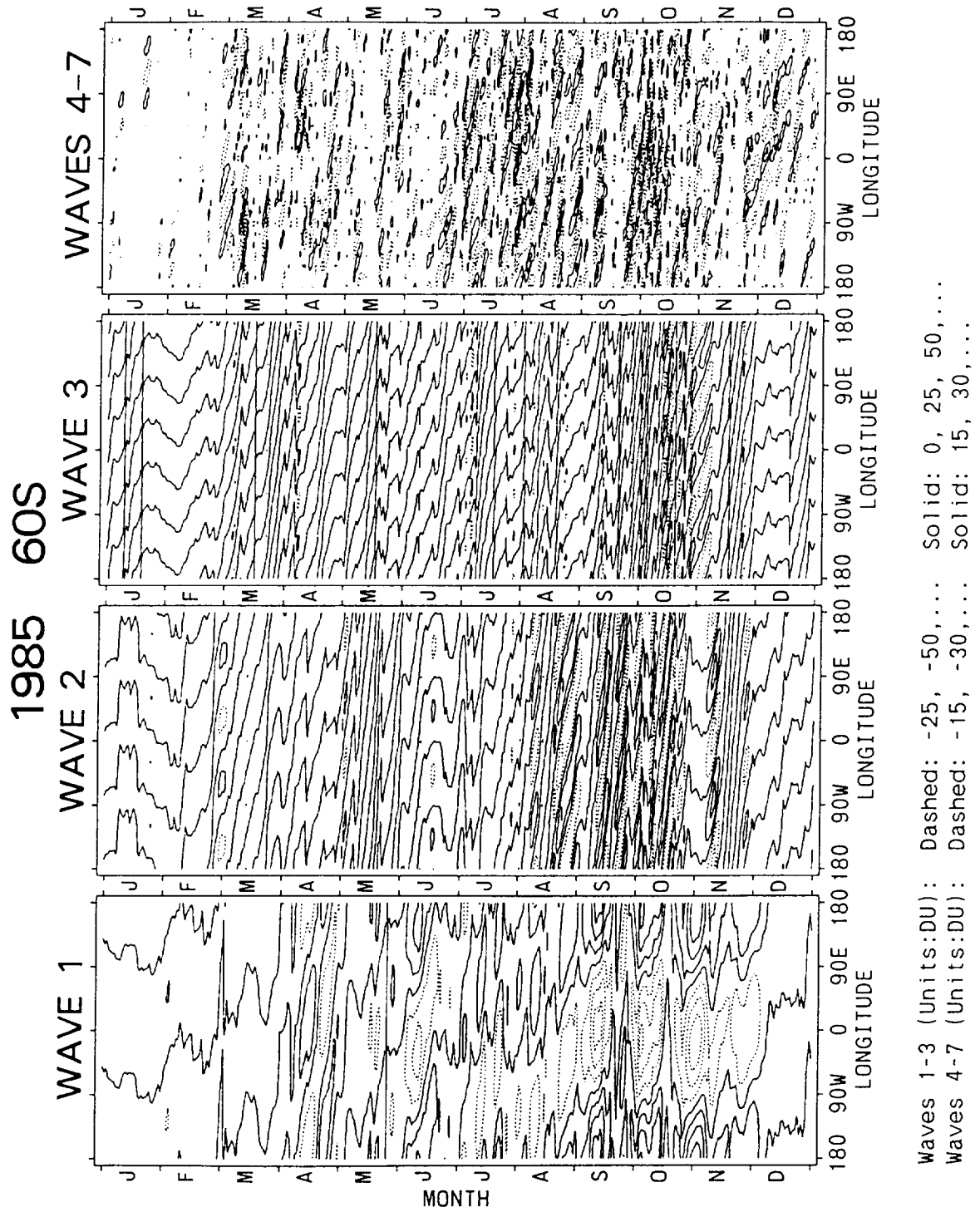


Figure 6. (continued)

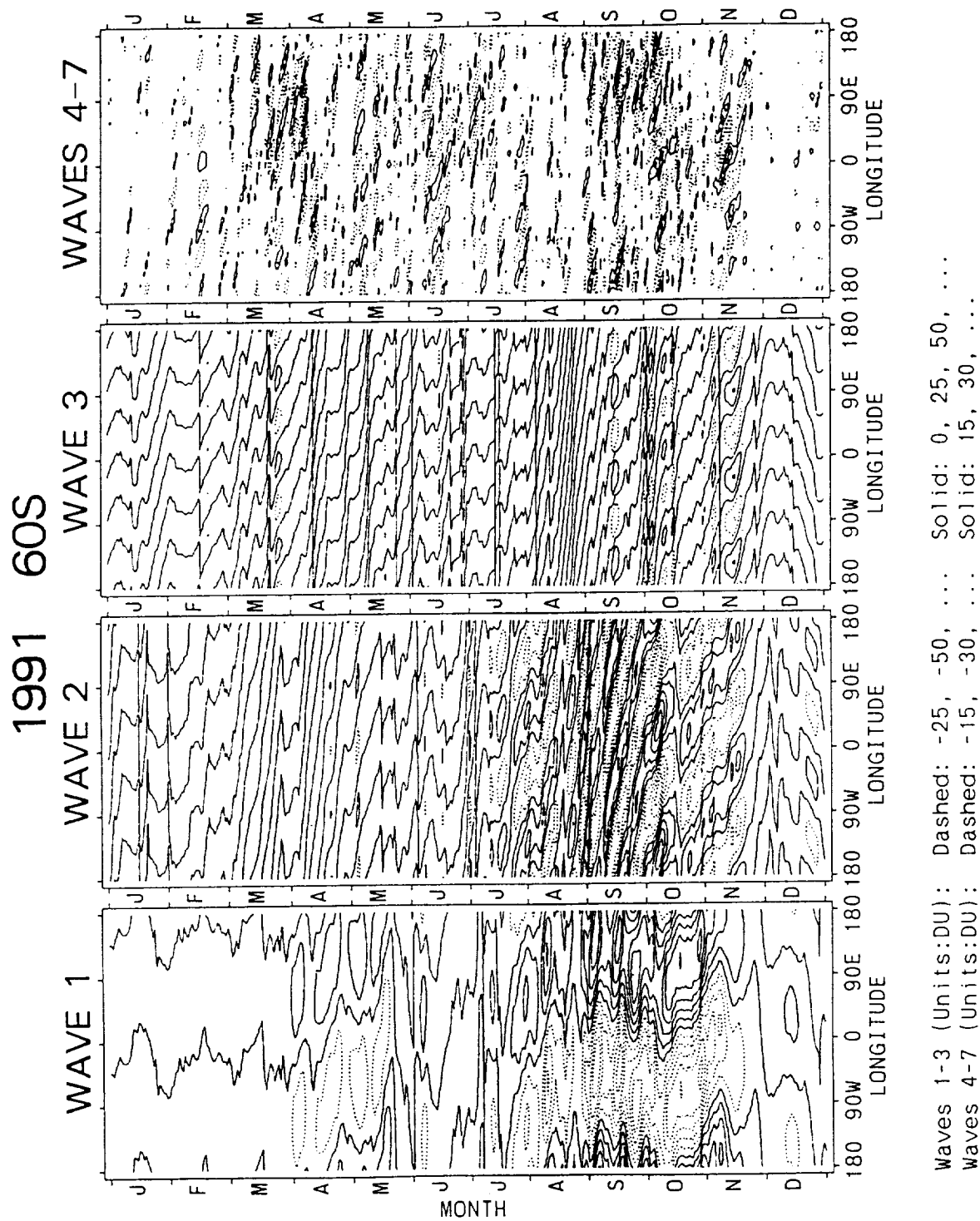


Figure 6. (continued)

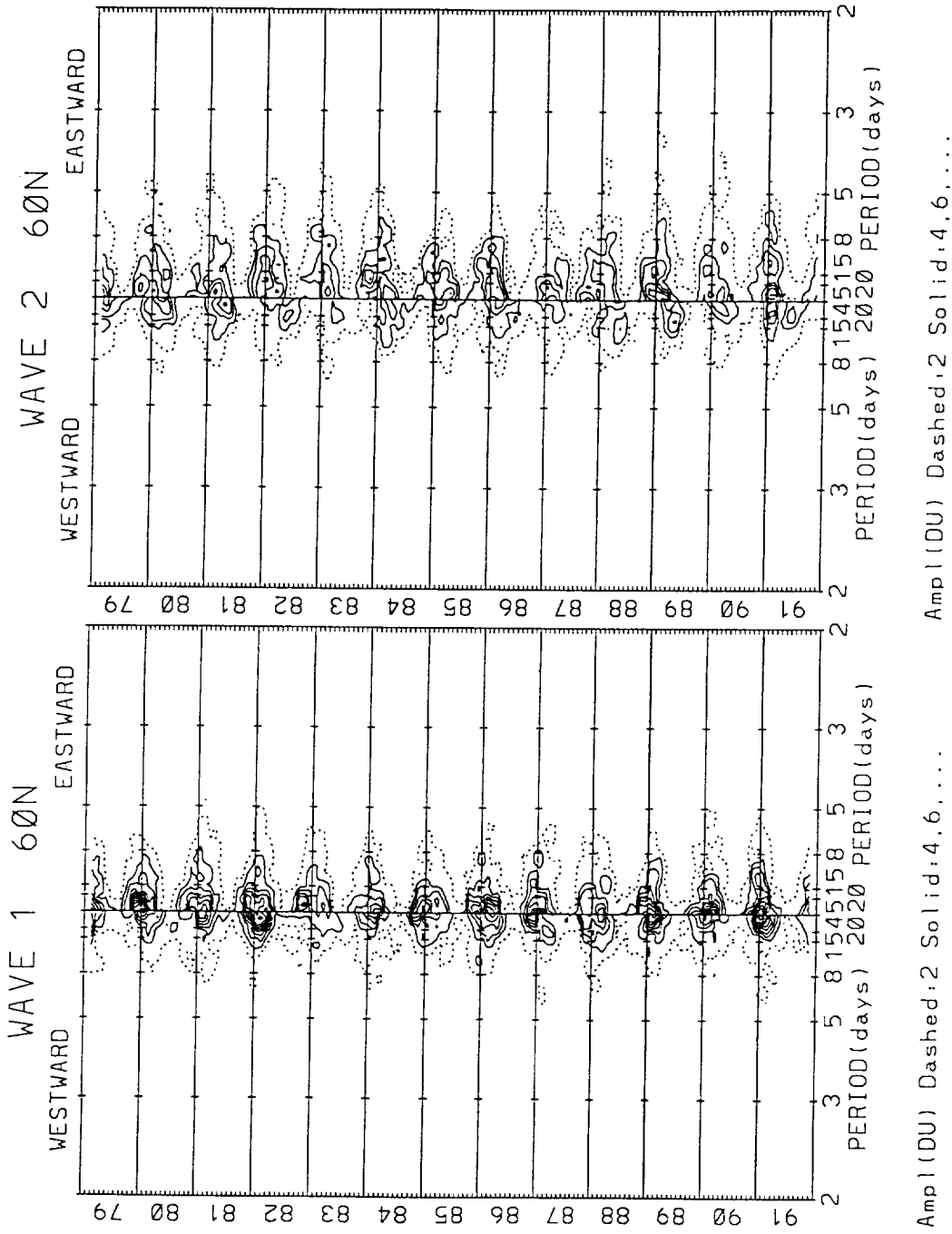


Figure 7. Time vs. frequency (periods in days shown) westward/eastward spectral amplitudes for waves 1, 2, 3, and 4–7 at latitudes 60° S to 60° N (15° increment). Units: DU. A 90-day window using a one month increment was employed. Temporal span: 1 January 1979–31 December 1991. Dashed and solid contour values are indicated under each frame.

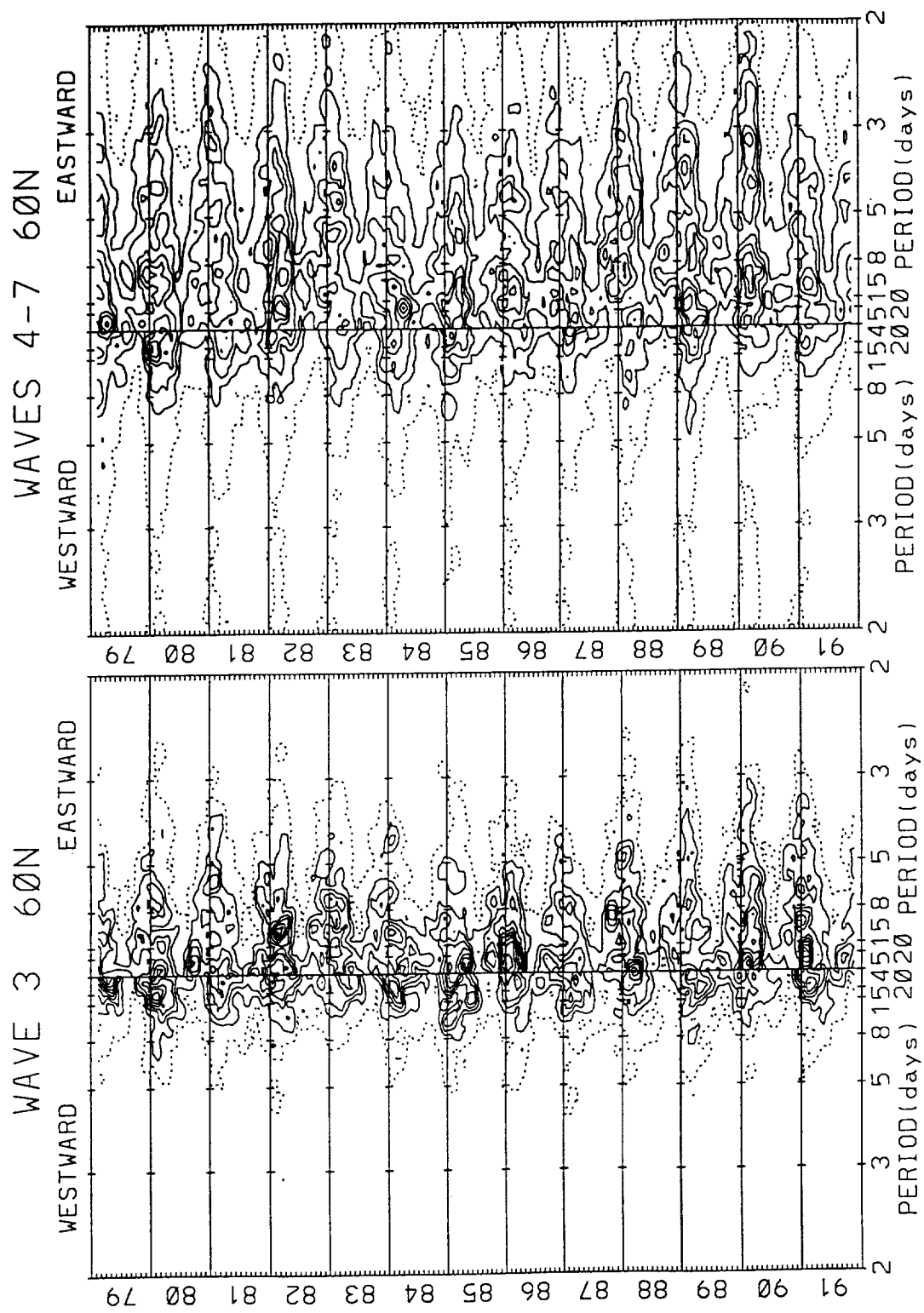


Figure 7. (continued)

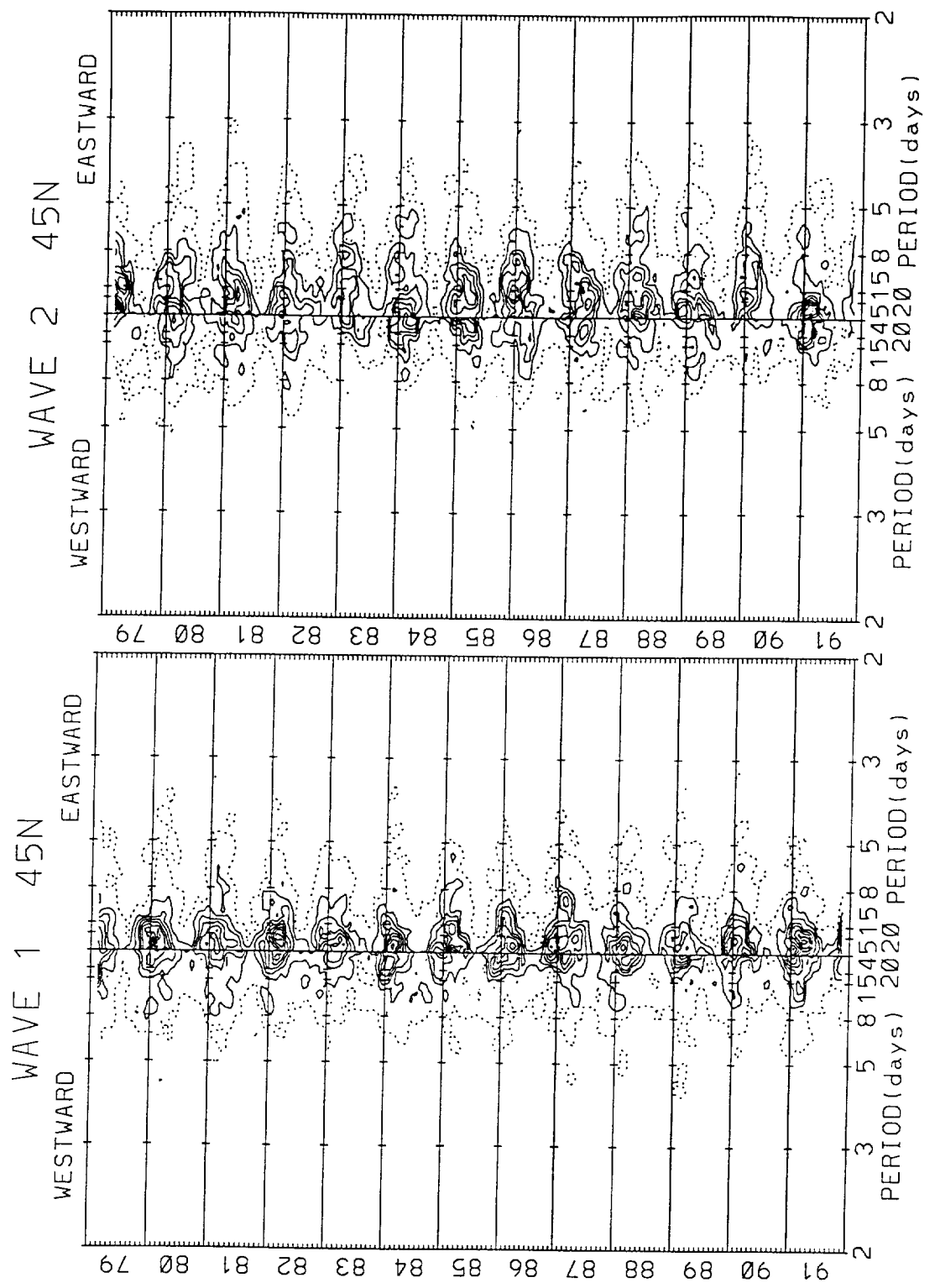
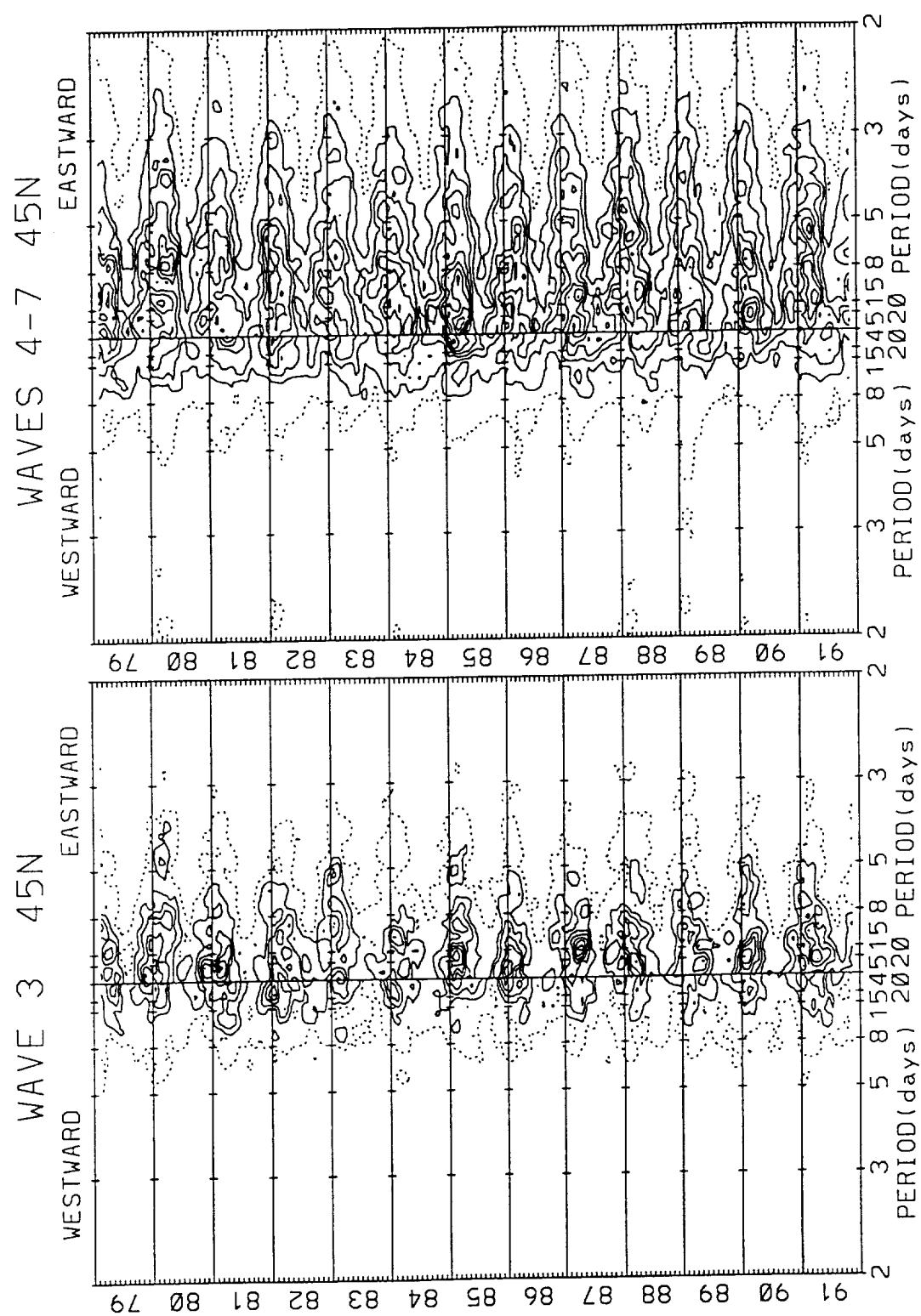


Figure 7. (continued)



Amp (DU) Dashed, 1 Solid, 2, 3, ...
2 3 5 8 15 45 58 200 PERIOD (days)

Figure 7. (continued)

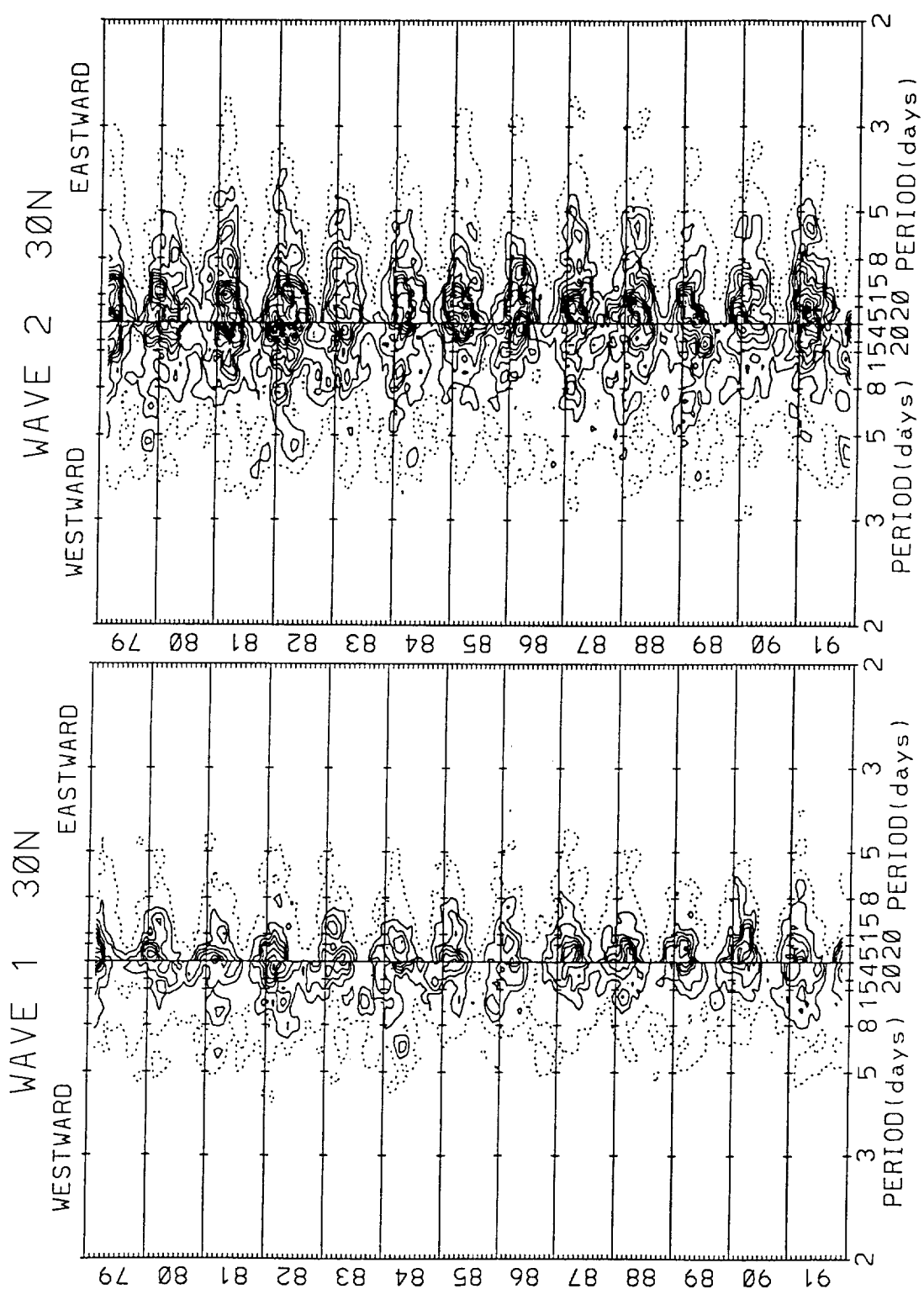


Figure 7. (continued)

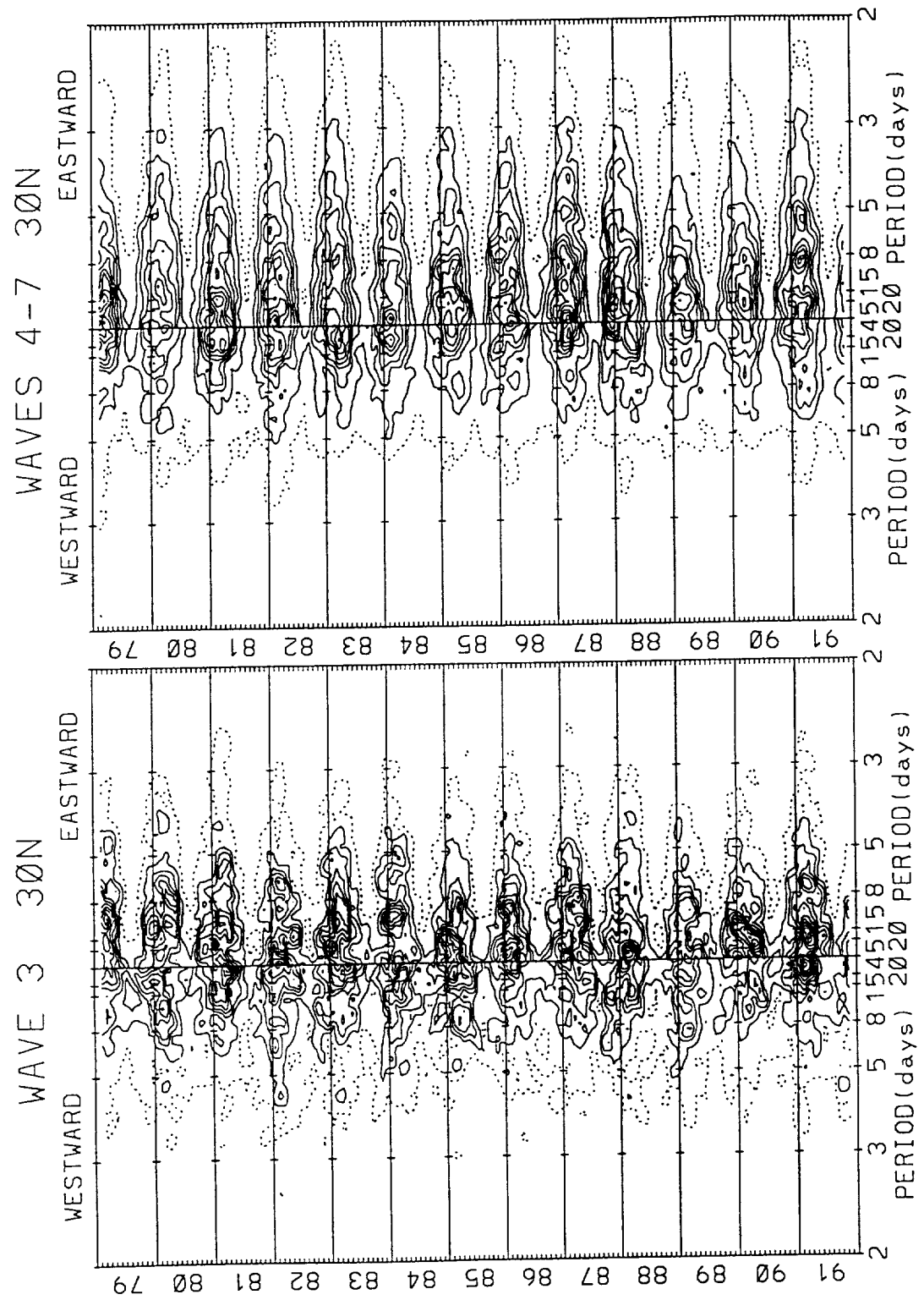


Figure 7. (continued)

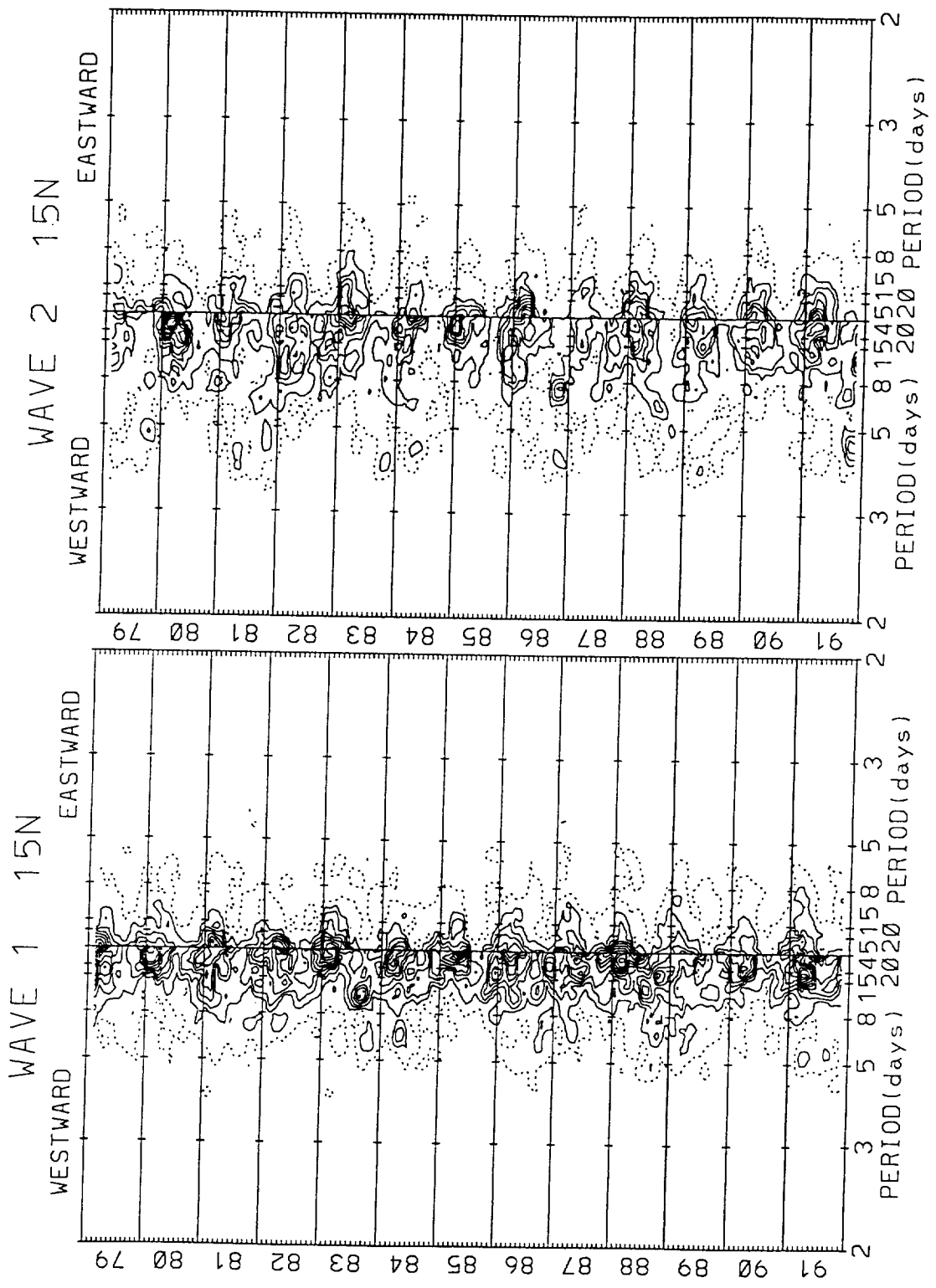


Figure 7. (continued)

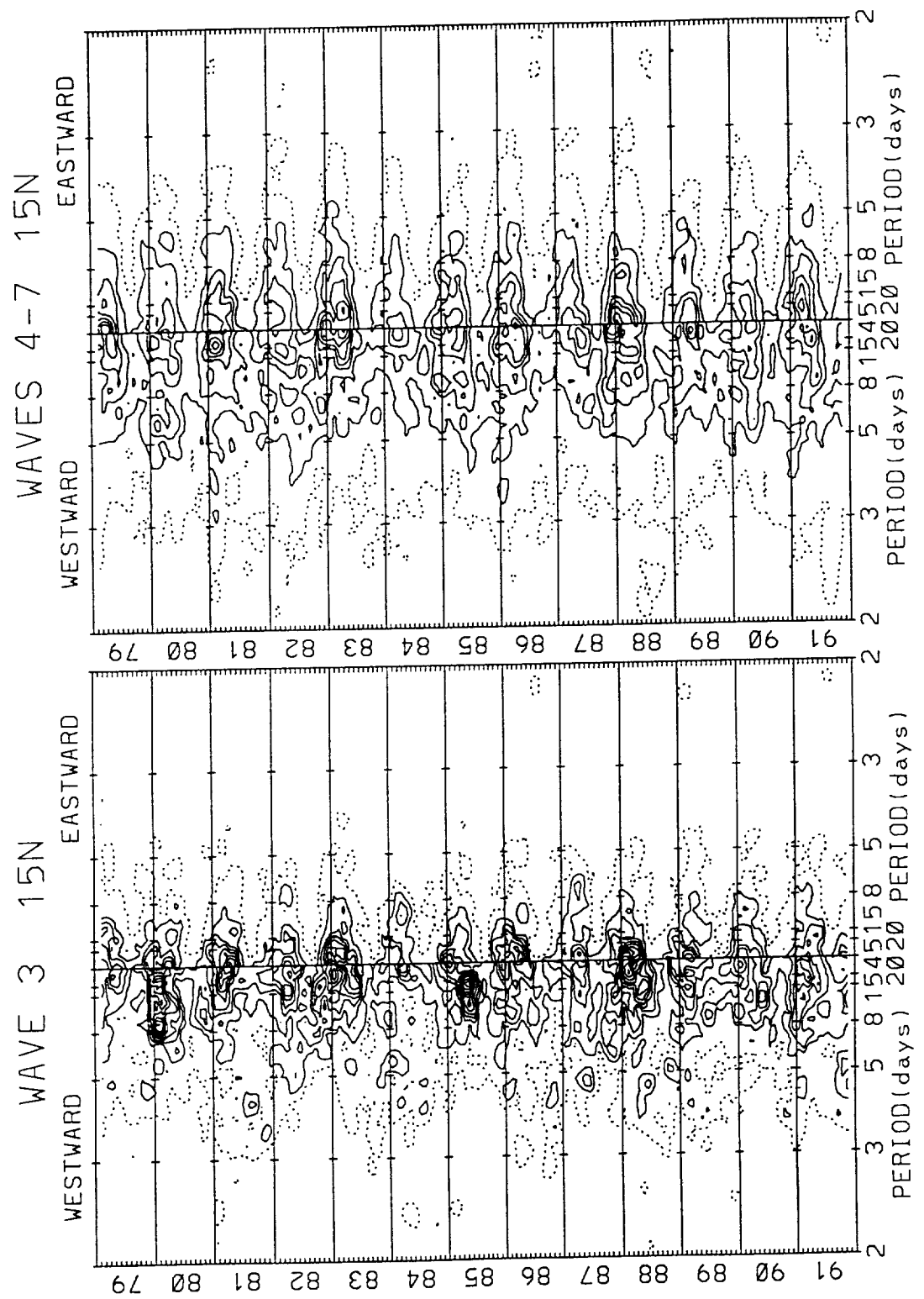


Figure 7. (continued)

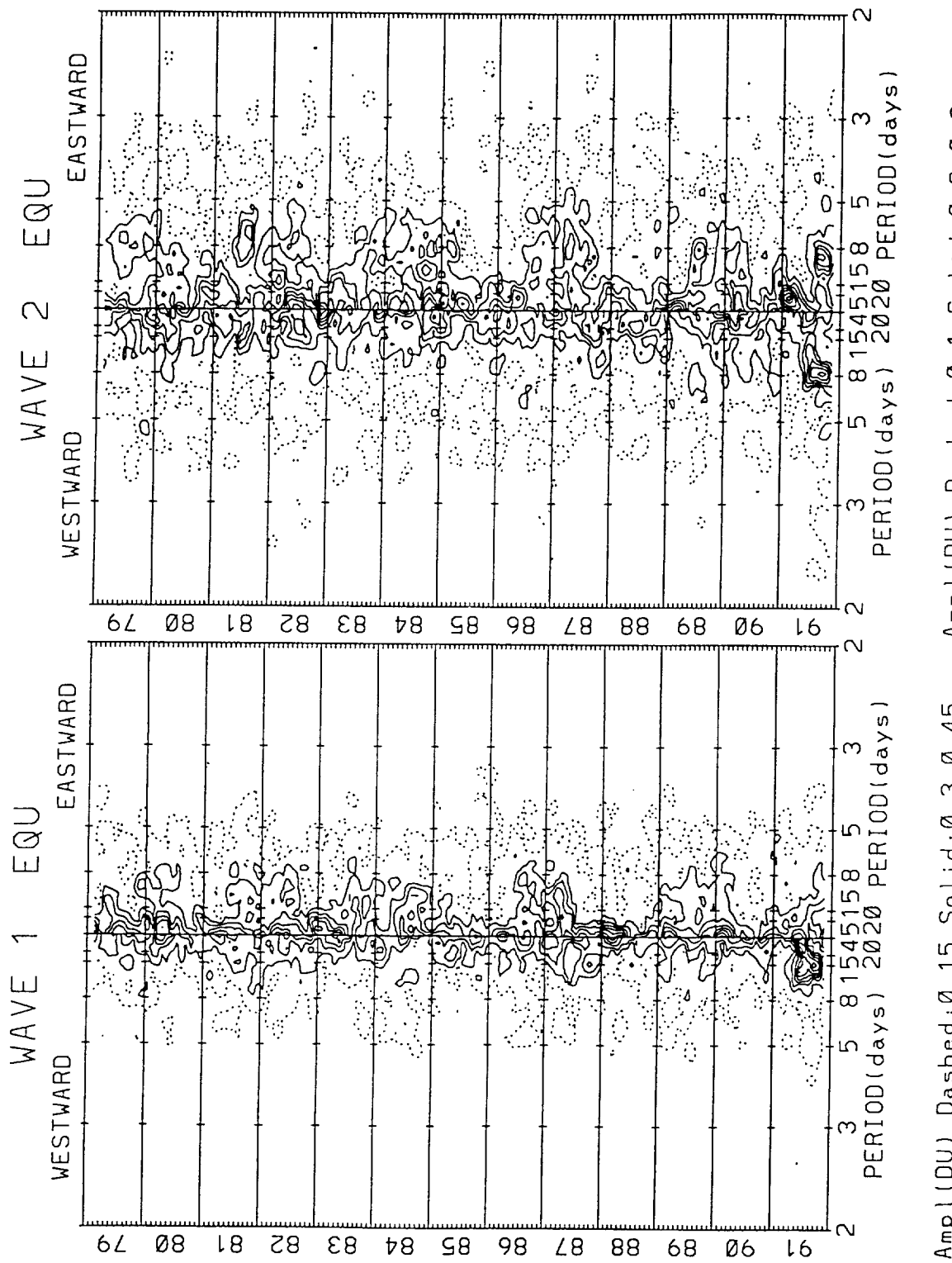


Figure 7. (continued)

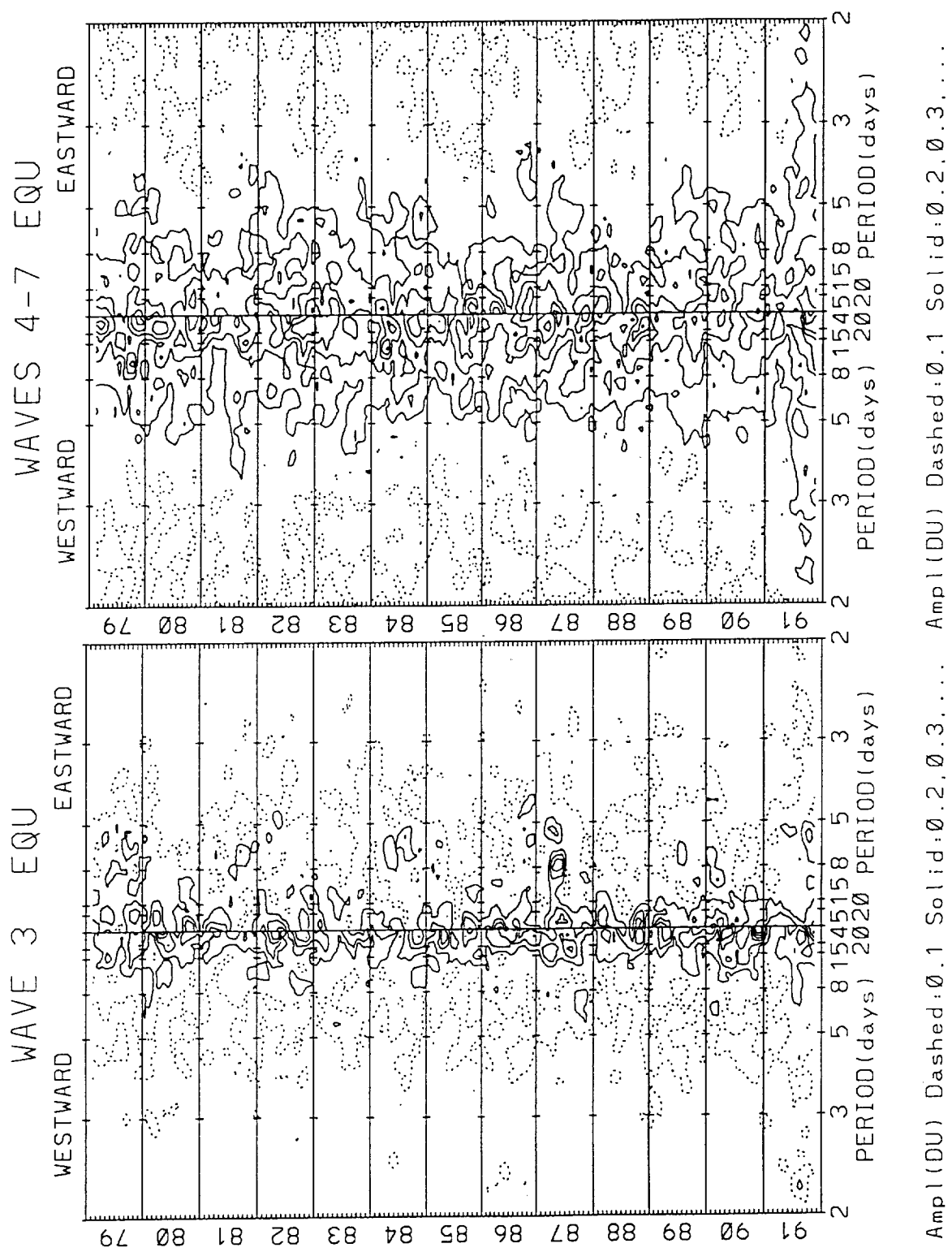
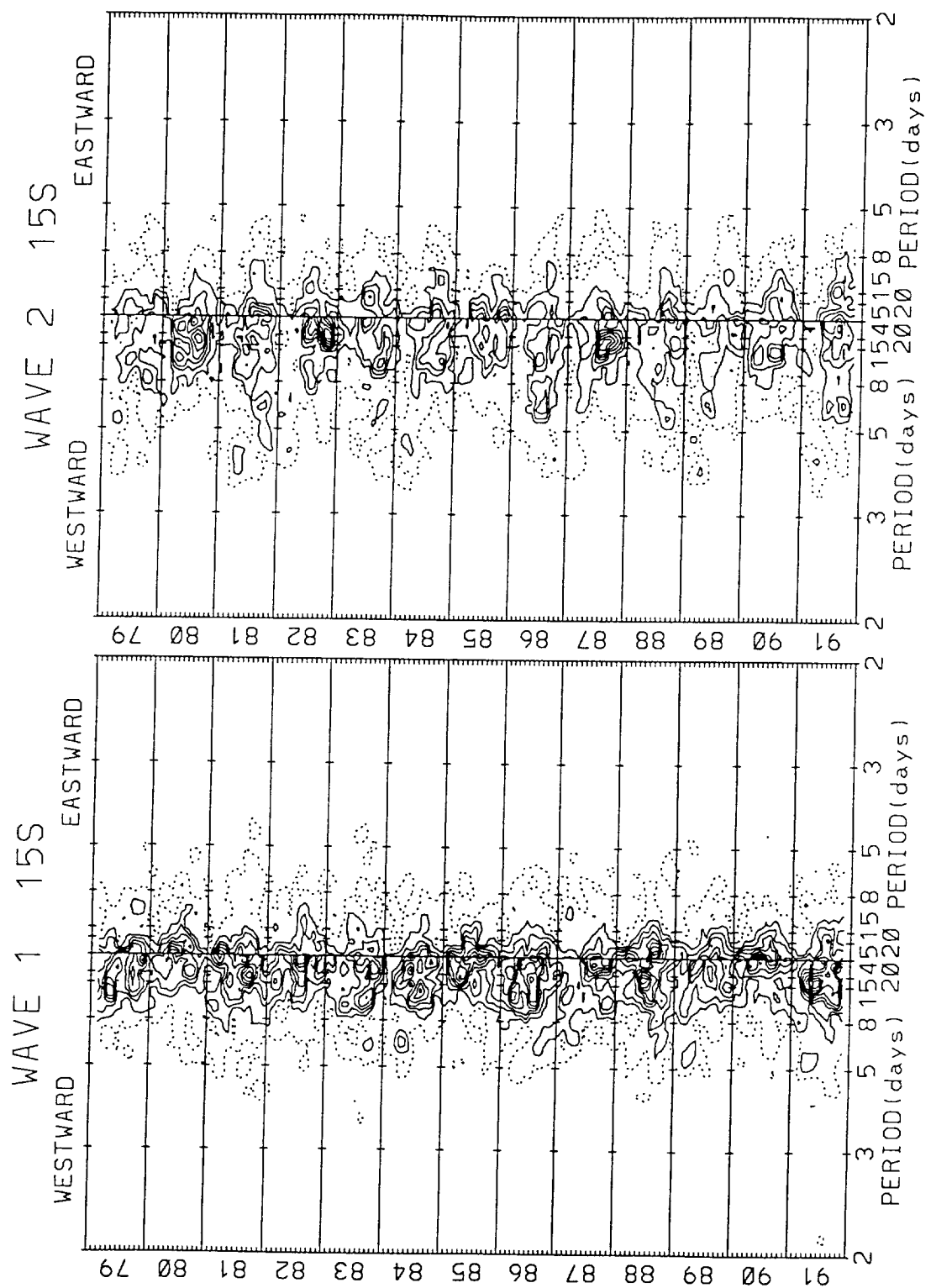
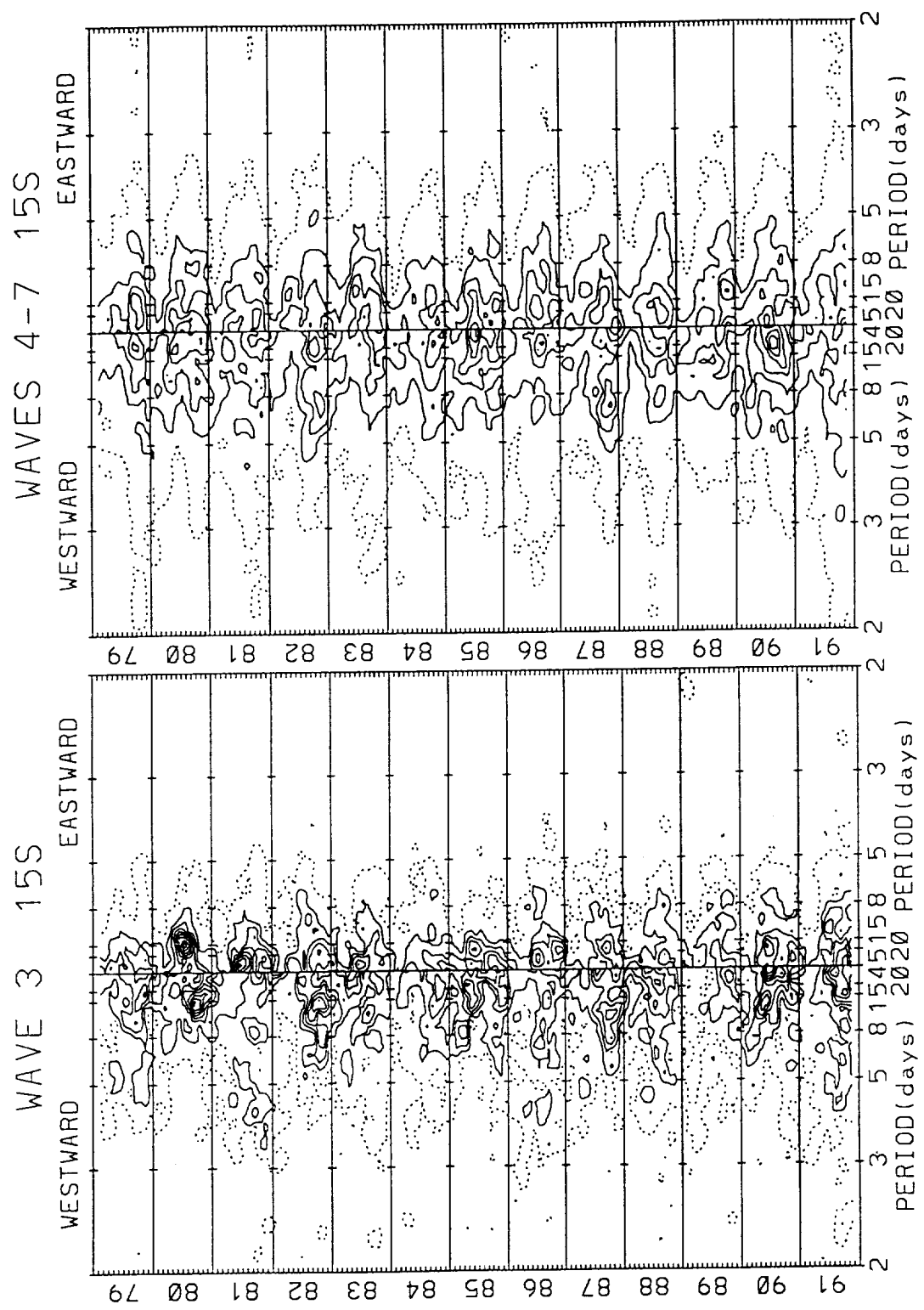


Figure 7. (continued)



Ampl (DU) Dashed: 0.2 Solid: 0.4, 0.6, ... Ampl (DU) Dashed: 0.2 Solid: 0.4, 0.6, ...

Figure 7. (continued)



Ampl (DU) Dashed: 0.15 Solid: 0.3, 0.45, ... Ampl (DU) Dashed: 0.2 Solid: 0.4, 0.6, ...

Figure 7. (continued)

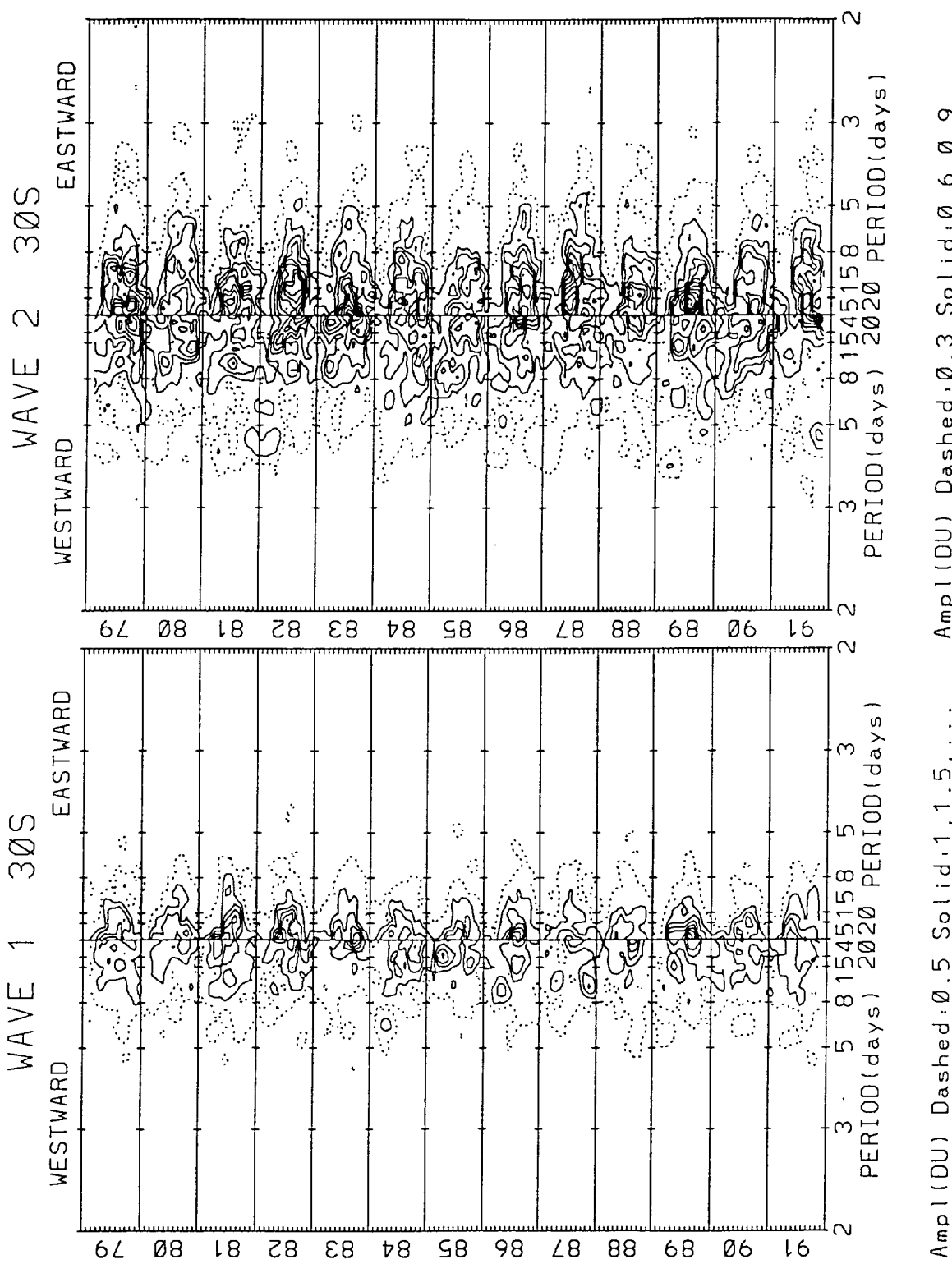


Figure 7. (continued)

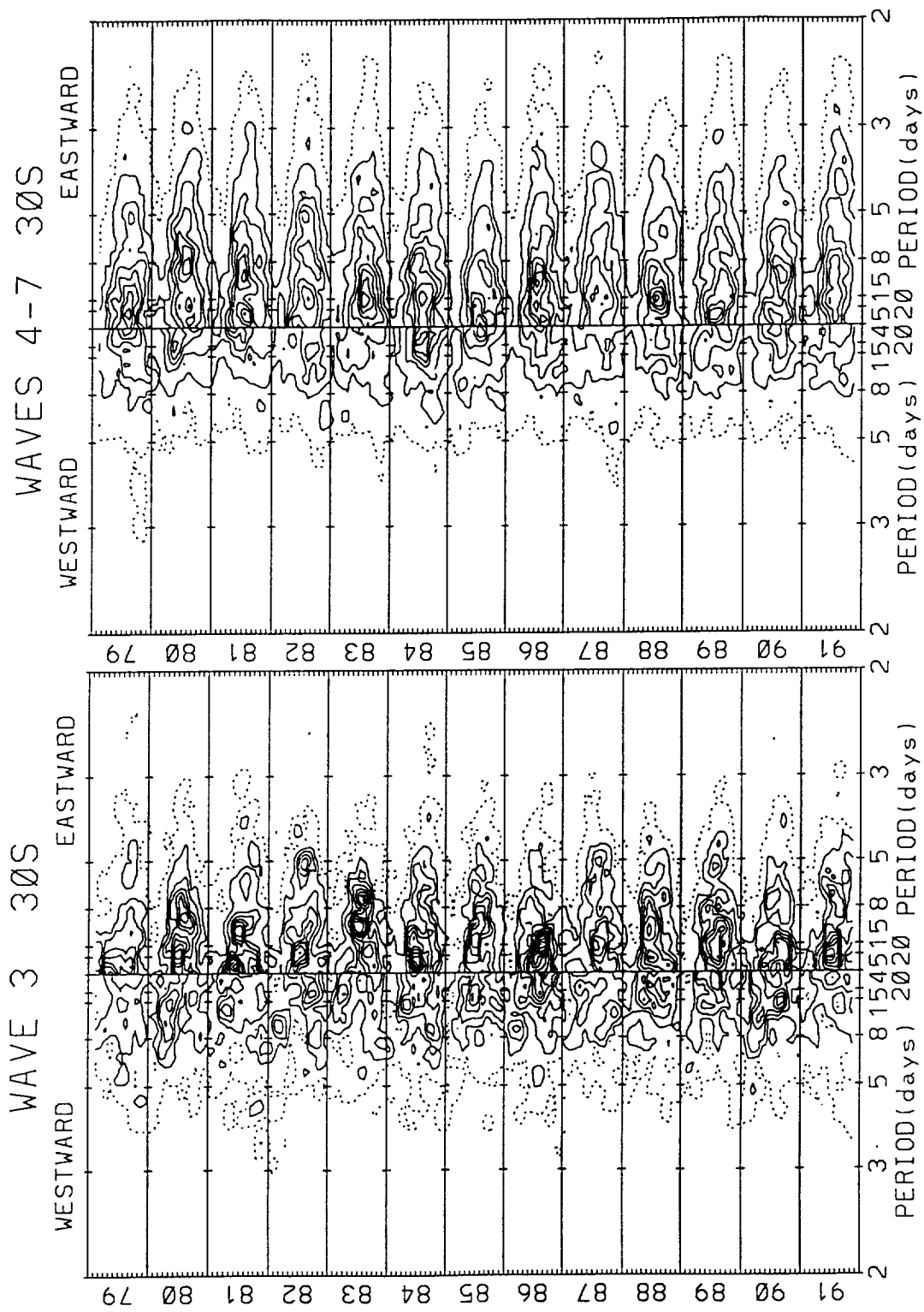


Figure 7. (continued)

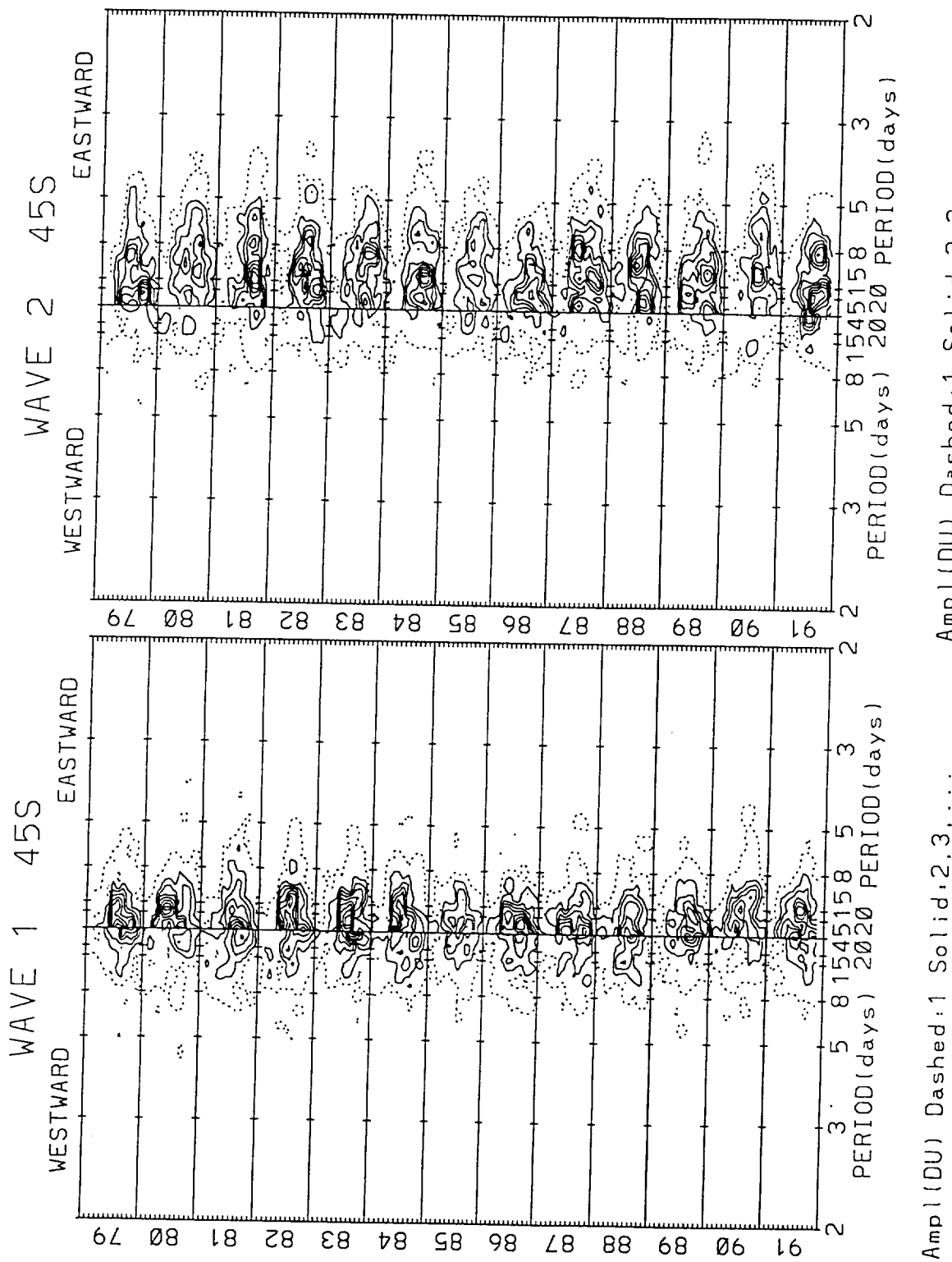


Figure 7. (continued)

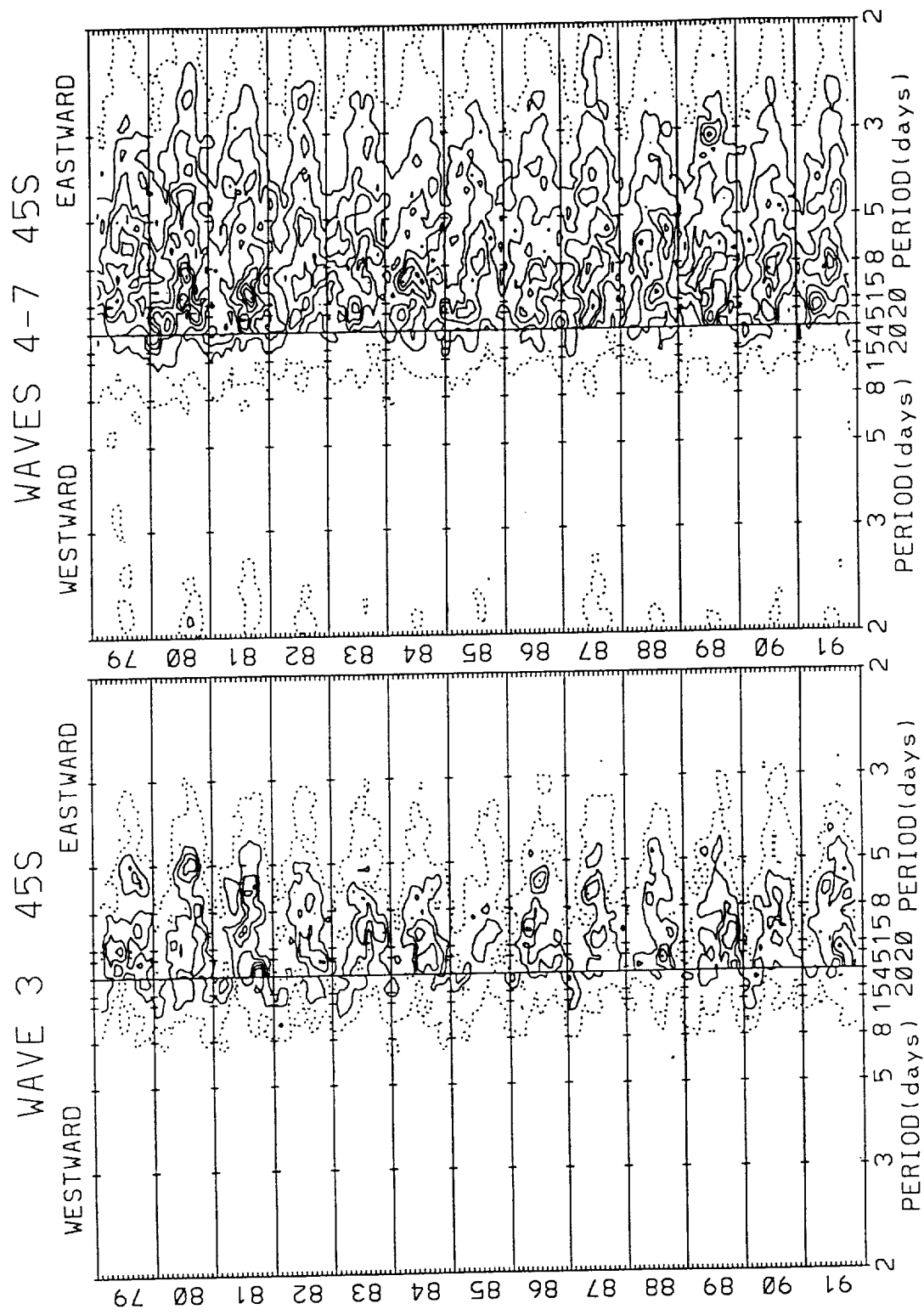


Figure 7. (continued)

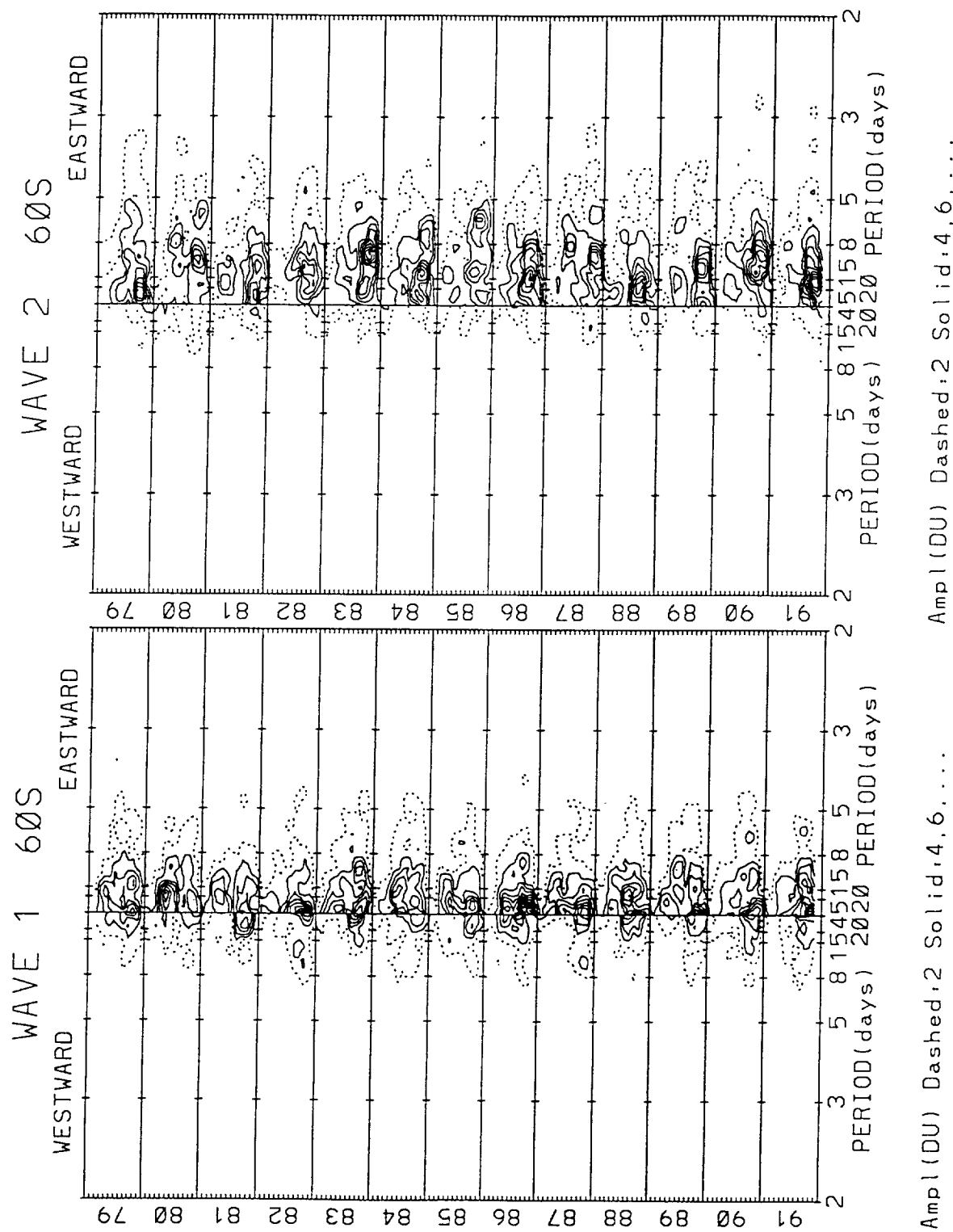


Figure 7. (continued)

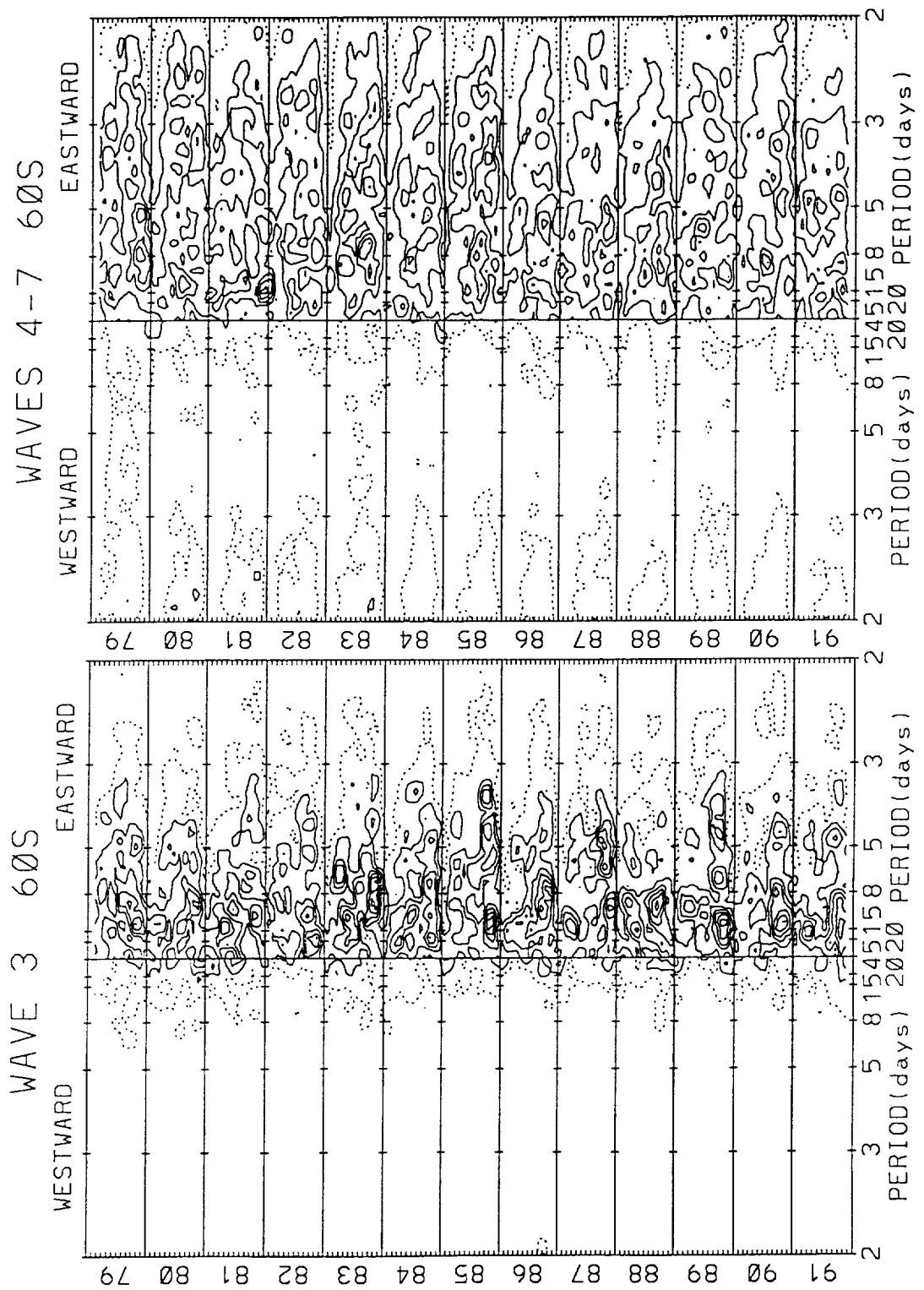


Figure 7. (continued)

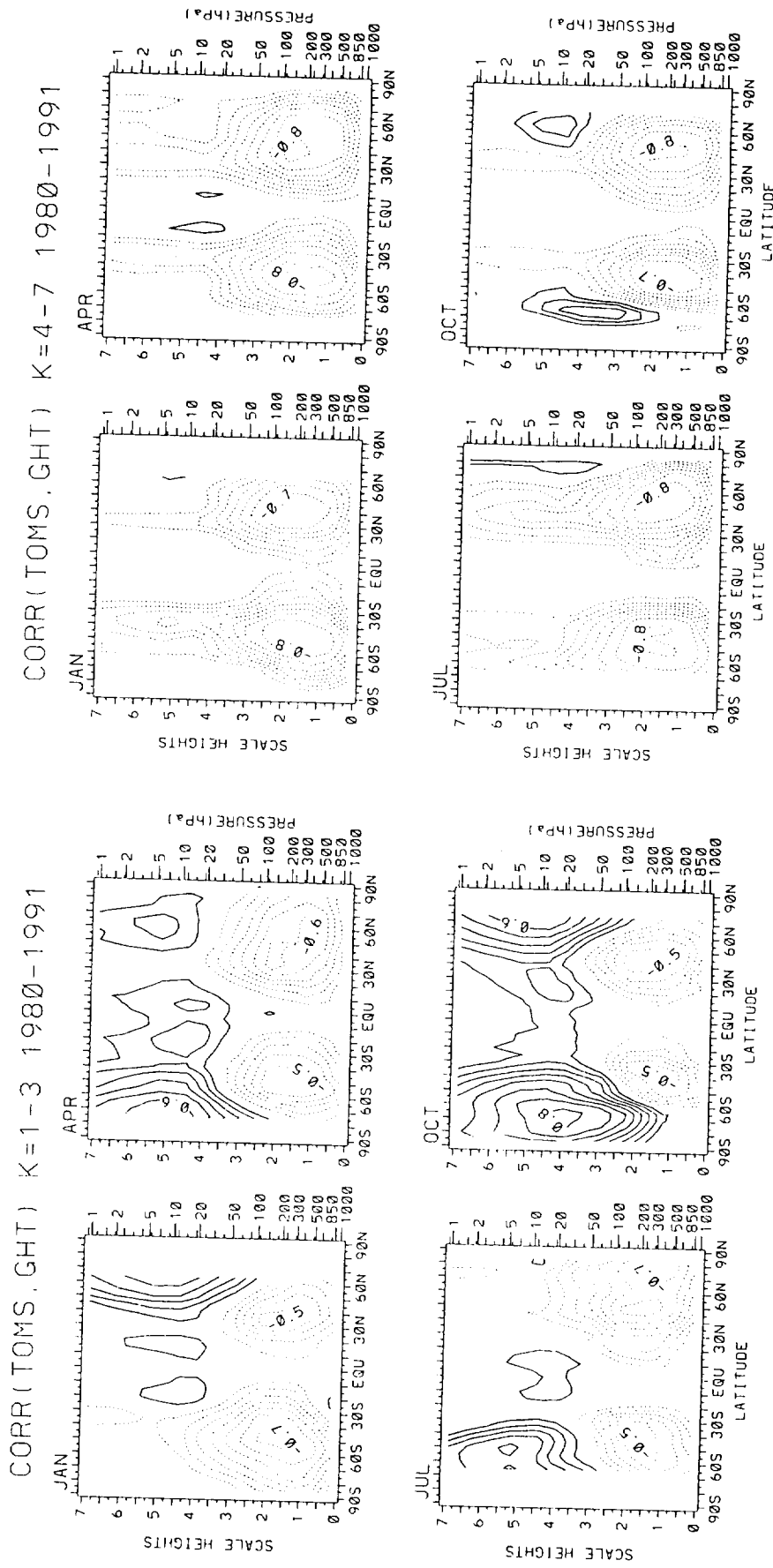


Figure 8. Zonally averaged climatological cross-correlations between 3D (latitude, longitude, pressure) geopotential heights and 2D (latitude, longitude) TOMS total ozone. Dashed (solid) contour values are 0.1, 0.2, ..., 0.9 (-0.1, -0.2, ..., -0.9). Left: waves 1-3 in TOMS and BMO heights. Right: waves 4-7. Monte Carlo results are (see text for methodology): critical correlation magnitudes 0.27, 0.38, 0.51, and 0.56 correspond to significance levels $\alpha=5$, 0.5, 0.01, and 0.001%, respectively.

REFERENCES

- Bowman, K. P., and A. J. Krueger, 1985, A global climatology of total ozone from the Nimbus-7 Total Ozone Mapping Spectrometer, *J. Geophys. Res.*, *90*, pp. 7967–7976.
- Fiedler, M., H. Frank, T. Gomer, M. Hausmann, K. Pfeilsticker, and U. Platt, 1993, The “minihole” event on 6 Feb. 1990: Influence of mie-scattering on the evaluation of spectroscopic measurements, *Geophys. Res. Lett.*, *20*, pp. 959–962.
- Herman, J. R., R. Hudson, R. McPeters, R. Stolarski, Z. Ahmad, X.-Y. Gu, S. Taylor, and C. Wellemeyer, 1991, A new self-calibration method applied to TOMS and SBUV backscattered ultraviolet data to determine long-term global ozone change, *J. Geophys. Res.*, *98*, pp. 12,783–12,793.
- Hirota, I., M. Shiotani, T. Sakuri, and J. Gille, 1991, Kelvin waves near the equatorial stratopause as seen in SBUV ozone data, *J. Meteorol. Soc. Jpn.*, *69*, pp. 179–186.
- Hofmann, D. J., and T. Deshler, 1990, Balloon borne measurements of polar stratospheric clouds and ozone at -93° C in the Arctic in February 1990, *Geophys. Res. Lett.*, *17*, pp. 2185–2188.
- Krueger, A., M. Schoeberl, P. Newman, and R. Stolarski, 1992, The 1991 Antarctic ozone hole; TOMS observations, *Geophys. Res. Letts.*, *19*, pp. 1215–1218.
- McPeters, R. D., A. J. Krueger, P. K. Bhartia, J. R. Herman, A. Oaks, Z. Ahmad, R. F. Cebula, B. M. Schlesinger, T. Swissler, S. L. Taylor, O. Torres, and C. Wellemeyer, 1993, *Nimbus-7 Total Ozone Mapping Spectrometer (TOMS) Data Products User's Guide*, NASA RP-1323.
- Randel, W. J., 1988, The seasonal evolution of planetary waves in the southern hemisphere stratosphere and troposphere, *Quart. J. R. Meteorol. Soc.*, *114*, pp. 1385–1409.
- Randel, W. J., and J. C. Gille, 1991, Kelvin wave variability in the upper stratosphere observed in SBUV ozone data, *J. Atmos. Sci.*, *48*, pp. 2336–2349.
- Rood, R. B., J. E. Nielsen, R. S. Stolarski, A. R. Douglass, J. A. Kaye, and D. J. Allen, 1992, Episodic total ozone minima and associated effects on heterogeneous chemistry and lower stratospheric transport, *J. Geophys. Res.*, *97*, pp. 7979–7996.
- Shiotani, M., 1992, Annual, quasi-biennial, and El Niño-Southern Oscillation (ENSO) time-scale variations in equatorial total ozone, *J. Geophys. Res.*, *97*, pp. 7625–7633.
- Shiotani, M., and F. Hasebe, 1994, Stratospheric ozone variations in the equatorial region as seen in Stratospheric Aerosol and Gas Experiment data, *J. Geophys. Res.*, *99*, pp. 14,575–14,584.

- Stanford, J. L., and J. R. Ziemke, 1993, Rossby-Gravity Waves in Tropical Total Ozone Data, 1993, *Geophys. Res. Lett.*, 20, pp. 2239-2242.
- Thompson, A. M., D. P. McNamara, K. E. Pickering, and R. D. McPeters, 1993, Effect of marine stratocumulus on TOMS ozone, *J. Geophys. Res.*, 98, pp. 23,051-23,057.
- Vaughan, G., and J. D. Price, 1991, On the relation between total ozone and meteorology, *Quart. J. R. Meteorol. Soc.*, 117, pp. 1281-1298.
- Ziemke, J. R., and J. L. Stanford, 1990, One-to-two month oscillations in the stratosphere during Southern winter, *J. Atmos. Sci.*, 47, pp. 1778-1793.
- Ziemke, J. R., and J. L. Stanford, 1994a, Kelvin waves in total column ozone, *Geophys. Res. Lett.*, 21, pp. 105-108.
- Ziemke, J. R., and J. L. Stanford, 1994b, Quasi-biennial oscillation and tropical waves in total ozone, *J. Geophys. Res.*, 99, pp. 23,041-23,056.

REPORT DOCUMENTATION PAGE

Form Approved
OMB No. 0704-0188

Public reporting burden for this collection of information is estimated to average 1 hour per response, including the time for reviewing instructions, searching existing data sources, gathering and maintaining the data needed, and completing and reviewing the collection of information. Send comments regarding this burden estimate or any other aspect of this collection of information, including suggestions for reducing this burden, to Washington Headquarters Services, Directorate for Information Operations and Reports, 1215 Jefferson Davis Highway, Suite 1204, Arlington, VA 22202-4302, and to the Office of Management and Budget, Paperwork Reduction Project (0704-0188), Washington, DC 20503.

1. AGENCY USE ONLY (Leave blank)			2. REPORT DATE April 1995		3. REPORT TYPE AND DATES COVERED Reference Publication		
4. TITLE AND SUBTITLE Spectral Analyses, Climatology, and Interannual Variability of Nimbus-7 TOMS Version 6 Total Column Ozone			5. FUNDING NUMBERS G - NAG5-1519 Code 916				
6. AUTHOR(S) J. L. Stanford, J. R. Ziemke, R. D. McPeters, A. J. Krueger, and P. K. Bhartia							
7. PERFORMING ORGANIZATION NAME(S) AND ADDRESS (ES) Goddard Space Flight Center Greenbelt, Maryland 20771			8. PERFORMING ORGANIZATION REPORT NUMBER 95B00045				
9. SPONSORING / MONITORING ADGENCY NAME(S) AND ADDRESS (ES) National Aeronautics and Space Administration Washington, DC 20546-0001			10. SPONSORING / MONITORING ADGENCY REPORT NUMBER NASA RP-1360				
11. SUPPLEMENTARY NOTES Stanford: Department of Physics and Astronomy, Iowa State University, Ames, Iowa; Ziemke: National Research Council, Goddard Space Flight Center, Greenbelt, Maryland; McPeters, Krueger, and Bhartia: Goddard Space Flight Center, Greenbelt, Maryland							
12a. DISTRIBUTION / AVAILABILITY STATEMENT Unclassified - Unlimited Subject Category 47 Availability: NASA CASI (301) 621-0390.			12b. DISTRIBUTION CODE				
13. ABSTRACT (Maximum 200 words) This reference publication presents selected results from space-time spectral analyses of 13 years of version 6 daily global ozone fields from the Total Ozone Mapping Spectrometer (TOMS). One purpose is to illustrate more quantitatively the well-known richness of structure and variation in total ozone. A second purpose is to provide, for use by modelers and for comparison with other analysts' work, quantitative measures of zonal waves 1, 2, 3, and medium-scale waves 4-7 in total ozone. Their variations throughout the year and at a variety of latitudes are presented, from equatorial to polar regions. The 13-year averages are given, along with selected individual years which illustrate year-to-year variability. The largest long-wave amplitudes occur in the polar winters and early springs of each hemisphere, and are related to strong wave amplification during major warming events. In low latitudes, total ozone wave amplitudes are an order of magnitude smaller than at high latitudes. However, TOMS fields contain a number of equatorial dynamical features, including Rossby-gravity and Kelvin waves.							
14. SUBJECT TERMS Total Ozone Mapping Spectrometer; Space-time spectra; Planetary waves; Medium scale waves; Rossby-gravity waves; Kelvin waves					15. NUMBER OF PAGES 90		
					16. PRICE CODE		
17. SECURITY CLASSIFICATION OF REPORT Unclassified		18. SECURITY CLASSIFICATION OF THIS PAGE Unclassified		19. SECURITY CLASSIFICATION OF ABSTRACT Unclassified		20. LIMITATION OF ABSTRACT UL	